MODELING AND CONTROL OF PROTON EXCHANGE MEMBRANE AND SOLID OXIDE FUEL CELLS AND SOLAR CELLS

by

GUN-HYUNG PARK

A dissertation submitted to the

Graduate School-New Brunswick

Rutgers, The State University of New Jersey

In partial fulfillment of the requirements

For the degree of

Doctor of Philosophy

Graduate Program in Electrical and Computer Engineering

Written under the direction of

Professor Zoran Gajić

And approved by

_____

_____

_____

_____

_____

New Brunswick, New Jersey

January, 2014

ABSTRACT OF THE DISSERTATION

Modeling and Control of Proton Exchange Membrane and Solid Oxide Fuel Cells and Solar Cells

by GUN-HYUNG PARK

Dissertation Director:
Professor Zoran Gajić

This dissertation addresses the modeling and control problems of proton exchange membrane fuel cells (PEMFCs) and solid oxide fuel cells (SOFCs), and solar cells in which the Cuk converter used for maximum power point tracking. Sliding mode control techniques are developed to keep pressures of oxygen and hydrogen at the desired values in PEMFCs and SOFCs and a jump parameter linear system controller is designed for the Cuk converter.

For PEMFCs, the sliding mode control strategy is applied to both the 5th-order linearized model and the corresponding nonlinear model. The well-known material balance model is linearized, and it is shown that it is asymptotically stable, controllable, and observable at the unique equilibrium point. Then the sliding surfaces for anode and cathode are designed, and sliding mode controllers are proposed for each sliding surface to make hydrogen and oxygen pressures close to each other and at the desired values despite of the abrupt fuel cell current changes. The sliding mode controller for nonlinear PEMFCs model is also designed. For SOFCs model, the sliding surface for anode side is the same as that for PEMFCs, but that of the cathode side is designed to force oxygen pressure to follow hydrogen pressure. The proposed controllers for fuel cells keep very precisely pressures of hydrogen and oxygen at the require values. Especially, the sliding mode controller for SOFCs makes the pressure difference between hydrogen and oxygen

very small in both the transient mode and at steady state.

For the jump parameter linear system control technique applied to the Cuk converter, with an accelerated algorithm, we have found the optimal values by changing the duty cycle and applied this technique with the integral action to keep the output voltage of the Cuk converter at the desired value despite of a constant disturbance on the input. The proposed controller with integral action outperforms the averaged converter system that has been most commonly used for DC-DC converter model.

Acknowledgements

First and foremost I express my deepest and sincerest gratitude to my supervisor, Prof. Zoran Gajić, who has supported me thoughout my dissertation with his guidance and patience. His wide knowledge, constructive comments, and logical way of thinking have been of great value for me. Without his guidance and persistent help this thesis would not have been possible.

I would like to thank my committee members, Prof. Dario Pompili, Prof. Predrag Spasojevic, Prof. Jingang Yi, and Dr. Ehab Shoubaki. I also would like to thank faculty in Electrical and Computer Engineering Department for their help to get strong backgrounds for my research.

My deepest gratitude goes to my family for their unflagging love and support. My wife, daughter, and son as well as my family in Korea, have supported me for their love. This thesis is simply impossible without them.

Lastly, I offer my regards and blessings to all of those who supported me in any respect during the completion of the project.

Table of Contents

List of Tables

List of Figures

Chapter 1

Introduction

1.1 Introduction to Energy Systems

There are two main problems with continuing use of fossil fuels. The first one is fossil fuel depletion. According to the petroleum companies, the fossil fuels, petroleum, and natural gas will peak sometime in a short time and begin to decrease. The second one is that the use of fossil fuels causes environmental problems such as climate changes, global warming, pollution, and etc.

The development of new energy technologies should be mandatory. Among them, fuel cells and solar cells are promising energy technologies since they have sufficient efficiency and cause low environmental pollution. In this chapter, the principles for two fuel cells (the proton exchange membrane fuel cells and the solid oxide fuel cells) and for solar cells are reviewed.

1.1.1 Fuel Cells

Fuel cells are electrochemical (mechanical) devices that convert chemical energy into electricity without generating carbon dioxide (promising power generation with high efficiency and low environmental impact). Since combustion is avoided, fuel cells produce power with minimal pollution. Reactants and oxidants in fuel cells must be replenished for continuous operation. Even though, fuel cells use a variety of reactants and oxidants, the most interest fuel cells use common fuels or hydrogen as a reductant, and ambient air as the oxidant. Different types of fuel cell are represented in Table 1.1.

In the following, an overview of fuel cell technology is given using proton exchange membrane fuel cells (PEMFC, also called the polymer electrolyte membrane fuel cell),

Table 1.1: Comparisions of Fuel Cells

Fuel cell type	Mobile ion	Operating temp.	Applications and notes
Alkaline (AFC)	OH^-	50 - 200(°C)	Used in space vehicles, e.g. Apolo, Shuttle.
Proton exchange membrane (PEMFC)	H^+	30 - 100(°C)	Vehicles and mobile applications, and for lower power CHP (Combined Heat and Power) systems (-500kW)
Direct methanol (DMFC)	H^+	20 - 90(°C)	Portable electronic systems of low power, running for long times
Phosphoric acid (PAFC)	H^+	150 - 200(°C)	Large numbers of 200-kW CHP systems in use.
Molten carbonate (MCFC)	CO_3^{2-}	600 - 700(°C)	Medium- to large- scale CHP systems, up to MW capacity
Solid oxide(SOFC)	O^{2-}	500-1000(°C)	All sizes of CHP systems, 2kW to multi-MW

which are the most developed and the best understood fuel cells.

PEMFC is a simple triode. It is represented in Figure 1.1. At the anode side of PEMFC, the hydrogen gas ionises, releasing electrons and creating protons (H^+ ions) according to the following reaction

$$2H_2 \rightarrow 4H^+ + 4e^- \tag{1.1}$$

At the cathode side, oxygen reacts with H^+ ions taken from the electrolyte and electrons coming to the air to form water according to the chemical reaction

$$O_2 + 4H^+ + 4e^- \rightarrow 2H_2O \tag{1.2}$$

It should be noted that the electrolyte only allows H^+ ions to pass through it, while the

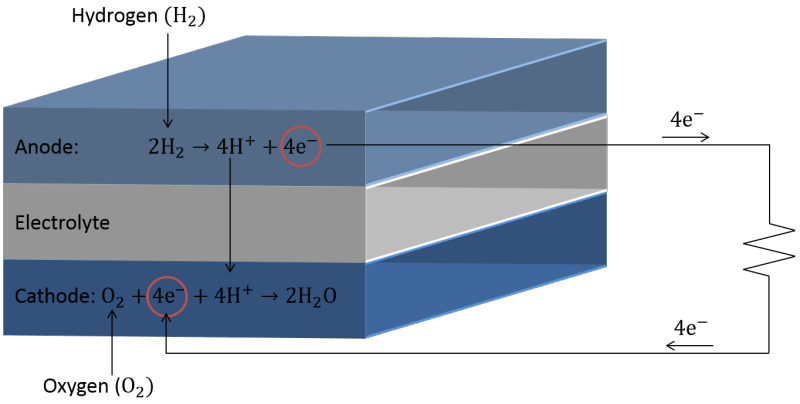

Figure 1.1: PEM fuel cell

electrons are collected and utilized as electricity by an outside electrical circuit before they reach the cathode side, see Figure 1.1.

The voltage of a fuel cell is quite small, about 0.7V. The voltage-current density characteristics is represented in Figure 1.3. To produce a higher voltage, many cells have to be connected in series forming a 'stack' represented in Figure 1.2. The output stack voltage V_{st} is defined as a function of the stack current (I), reactant partial pressures (P_{O_2}, P_{H_2}), fuel cell temperature (T) and membrane humidity (h) as

$$V_{fc} = f_v(P_{O_2}, P_{H_2}, T, h, I_{fc}) \tag{1.3}$$

The stack current is given by $I_{st} = I_{fc} = I = \frac{NV_{st}}{R_{load}}$, where N is the number of fuel cells in a stack and R_{load} is the load. V_{st} is given by

$$V_{st} = E - V_{activation} - V_{ohmic} - V_{concentration} \tag{1.4}$$

where E is the open-loop stack voltage given by the Nernst formula, $V_{activation}$ is the voltage needed to break and form chemical bonds at the anode and cathode, V_{ohmic} is the ohmic voltage drop due to the resistance of proton flow in the electrolyte, and $V_{concentration}$ is the voltage loss due to lack of current carriers, especially at high current

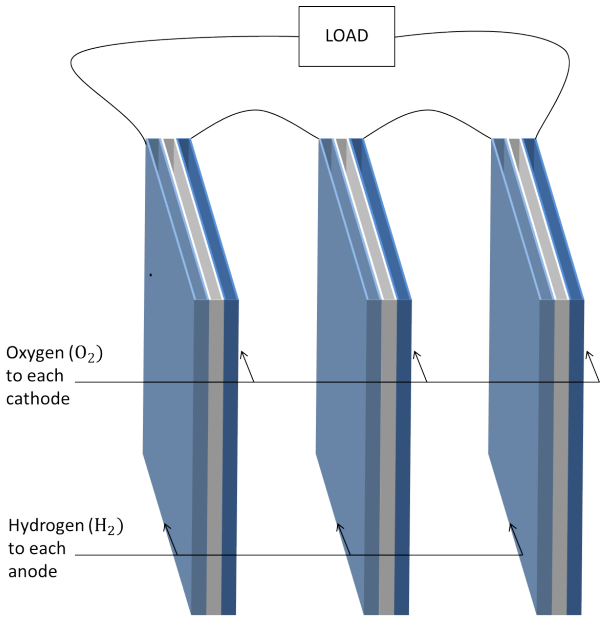

Figure 1.2: Simple edge connection of three cells in series

densities. Their formulas and approximation values are as follows

$$\begin{aligned} E &= N\left[V_0 + \frac{RT}{2F}\left(\frac{P_{H_2}\sqrt{P_{O_2}}}{P_{H_2C}}\right)\right] \approx 1V \\ V_{activation} &= N\frac{RT}{2\alpha F}\ln\left(\frac{I_{fc}+I_n}{I_0}\right) \leq 0.25V \\ V_{ohmic} &= NI_{fc}R_{ohm} \leq 0.15V \\ V_{concentration} &= Nl\exp^{mI_{fc}} \leq 0.6V \end{aligned} \tag{1.5}$$

where V_0 is open-cell voltage, R is the universal gas constant, F is the Faraday constant, T is fuel cell temperature, α is a charge transfer coefficient, I_0 is the exchange current density, I_n is the internal current density, and l, m are constants in the mass transfer voltage.

One of methods for cell interconnection is to use a 'bipolar plate'. The bipolar plate serves as a means of feeding fuel to the anode side and oxygen to the cathode side. At the same time, this makes connections all over the surface of the cathode and the anode of the next cell, which prevents the problem of the current collection point at the edge. Figure 1.4 shows a three-cell stack using bipolar plates.

A control oriented model of a fuel cell is derived by using the ideal gas law as follows

$$pV = nRT \tag{1.6}$$

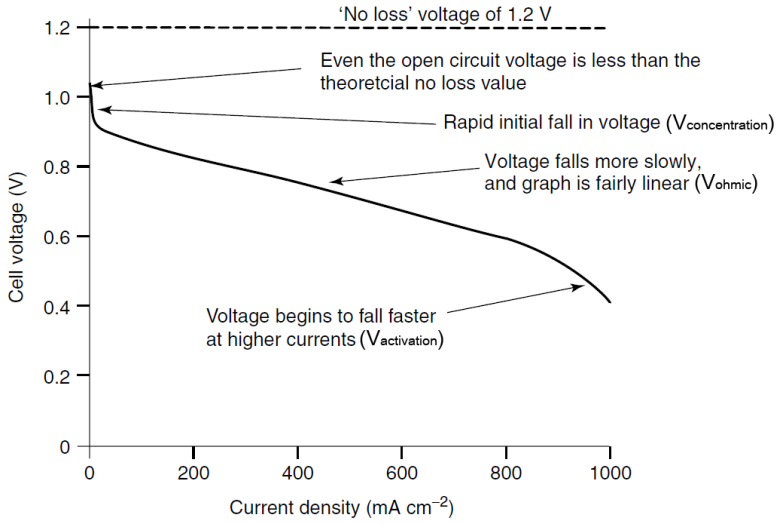

Figure 1.3: The voltage for a typical low temp., air pressure, fuel cell

where p is pressure, V is volume, n is the number of moles, R is the universal gas constant, and T is temperature. We assume that V and T are constant. Using (1.6), we get

$$\frac{dp}{dt} = \frac{RT}{V}\frac{dn}{dt} = \frac{RT}{V}(W_{in} - W_{out}) \tag{1.7}$$

where W_{in} and W_{out} are input and output mass flow rates.

In 2004, a simple 3^{rd} order model of PEMFC schematically represented in Figure 1.5, was developed by El-Sharkh et al. [1] as follows

$$\begin{aligned}
\frac{dP_{H_2}}{dt} &= \frac{RT}{V_a}(q_{H_2}^{in} - q_{H_2}^{out} - q_{H_2}^{reacted}) = \frac{RT}{V_a}q_{H_2}^{in} - \frac{RT}{V_a}K_{H_2}P_{H_2} - \frac{RT}{V_a}2K_rI \\
\frac{dP_{O_2}}{dt} &= \frac{RT}{V_c}(q_{O_2}^{in} - q_{O_2}^{out} - q_{O_2}^{reacted}) = \frac{RT}{V_c}q_{O_2}^{in} - \frac{RT}{V_c}K_{O_2}P_{O_2} - \frac{RT}{V_c}K_rI \\
\frac{dP_{H_2O}}{dt} &= \frac{RT}{V_c}(-q_{H_2O}^{out} - q_{H_2O}^{reacted}) = -\frac{RT}{V_c}K_{H_2O}P_{H_2O} - \frac{RT}{V_c}K_rI
\end{aligned} \tag{1.8}$$

where q stands for a molar mass flows.

With the time constants defined as $\tau_{H_2} = \frac{V_a}{RTK_{H_2}}$, $\tau_{O_2} = \frac{V_c}{RTK_{O_2}}$, and $\tau_{H_2O} = \frac{V_c}{RTK_{H_2O}}$, equation (1.8) is expressed in state space form as

$$\begin{bmatrix} \dot{x}_1 \\ \dot{x}_2 \\ \dot{x}_3 \end{bmatrix} = \begin{bmatrix} -\frac{1}{\tau_{H_2}} & 0 & 0 \\ 0 & -\frac{1}{\tau_{O_2}} & 0 \\ 0 & 0 & -\frac{1}{\tau_{H_2O}} \end{bmatrix} \begin{bmatrix} x_1 \\ x_2 \\ x_3 \end{bmatrix} + \begin{bmatrix} \frac{1}{\tau_{H_2}K_{H_2}} & 0 \\ 0 & \frac{1}{\tau_{O_2}K_{O_2}} \\ 0 & 0 \end{bmatrix} \begin{bmatrix} u_1 \\ u_2 \end{bmatrix} + \begin{bmatrix} -\frac{2K_r}{\tau_{H_2}K_{H_2}} \\ -\frac{K_r}{\tau_{O_2}K_{O_2}} \\ \frac{2K_r}{\tau_{H_2O}K_{H_2O}} \end{bmatrix} \tag{1.9}$$

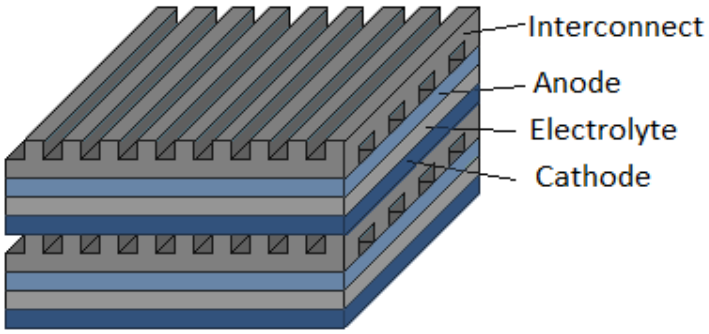

Figure 1.4: A three-cell stack using bipolar plates

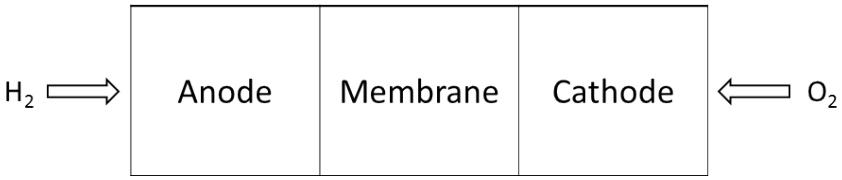

Figure 1.5: El-Sharkh et al. Model [1]

where $\begin{bmatrix} x_1 & x_2 & x_3 \end{bmatrix}^T = \begin{bmatrix} P_{H_2} & P_{O_2} & P_{H_2O} \end{bmatrix}^T$ and $\begin{bmatrix} u_1 & u_2 \end{bmatrix}^T = \begin{bmatrix} q_{H_2}^{in} & q_{O_2}^{in} \end{bmatrix}^T$.

In 2003, Gemmen considered the humidified air at the cathode side represented (see Figure 1.6 [2]). This model is also known as US DoE model. The model state equations

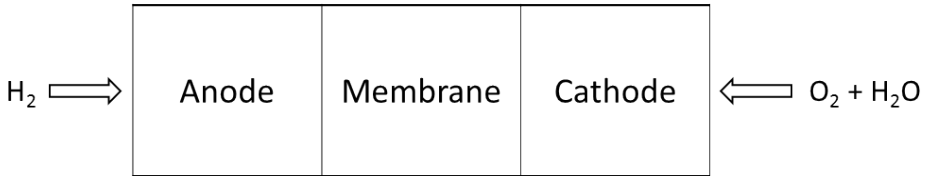

Figure 1.6: Gemmen's Model [2] (also Chiu's Model [3])

are

$$\begin{aligned} \frac{dP_{H_2}}{dt} &= \frac{RT}{V_a}(W_{H_2}^{in} - W_{H_2}^{out} - W_{H_2}^{used}) \\ \frac{dP_{O_2}}{dt} &= \frac{RT}{V_c}(W_{O_2}^{in} - W_{O_2}^{out} - W_{O_2}^{used}) \\ \frac{dP_{H_2O}}{dt} &= \frac{RT}{V_c}(W_{H_2O}^{in} - W_{H_2O}^{out} + W_{H_2O}^{produced}) \end{aligned} \tag{1.10}$$

where

$$\begin{aligned} W_{H_2}^{out} &= (Anode_{in} - 2K_rI)F_{H_2} \\ W_{O_2}^{out} &= (Cathode_{in} - K_rI)F_{O_2} \\ W_{H_2O}^{out} &= (Cathode_{in} + 2K_rI)F_{H_2} \end{aligned} \tag{1.11}$$

In the US Department of Energy model proposed by Gemmen [2], the pressure fraction rates are taken as

$$\begin{aligned} F_{H_2} &= \frac{P_{H_2}}{P_{op}} \\ F_{O_2} &= \frac{P_{O_2}}{P_{op}} \\ F_{H_2O} &= \frac{P_{H_2O}}{P_{op}} \end{aligned} \tag{1.12}$$

where P_{op} is the anode and cathode operating pressure at steady state (assumed to be identical).

In 2004, Chiu et al. [3], considered the water at the anode side. They used the same

state equations of (1.10) - (1.12) with the following formulas for pressure factors

$$\begin{aligned} F_{H_2} &= \frac{P_{H_2}}{P_{H_2} + P_{H_2O_A}} \\ F_{O_2} &= \frac{P_{O_2}}{P_{H_2} + P_{O_2} + P_{H_2O_C}} \\ F_{H_2O} &= \frac{P_{H_2O}}{P_{H_2} + P_{O_2} + P_{H_2O_C}} \end{aligned} \tag{1.13}$$

where $P_{H_2O_A}$ and $P_{H_2O_C}$ are pressures of pumped water at the anode and cathode sides. The state space system is as follows

$$\begin{aligned} \dot{x}_1 &= \frac{RT}{V_a}\big(u_1 - (u_1 + W^{in}_{H_2O_A} - 2K_rI)\frac{x_1}{x_1 + P_{H_2O_A}} - 2K_rI\big) \\ \dot{x}_2 &= \frac{RT}{V_c}\big(u_2 - (u_2 + u_3 + W^{in}_{N_2} - K_rI)\frac{x_2}{x_2 + x_3 + P_{N_2}} - K_rI\big) \\ \dot{x}_3 &= \frac{RT}{V_c}\big(u_3 - (u_2 + u_3 + W^{in}_{N_2} + 2K_rI)\frac{x_3}{x_2 + x_3 + P_{N_2}} + 2K_rI\big) \end{aligned} \tag{1.14}$$

where

$$\begin{aligned} \begin{bmatrix} x_1 & x_2 & x_3 \end{bmatrix}^T &= \begin{bmatrix} P_{H_2} & P_{O_2} & P_{H_2O_C} \end{bmatrix}^T \\ \begin{bmatrix} u_1 & u_2 & u_3 \end{bmatrix}^T &= \begin{bmatrix} W^{in}_{H_2} & W^{in}_{O_2} & W^{in}_{H_2O_A} \end{bmatrix}^T \end{aligned} \tag{1.15}$$

This model performs better than the US Department of Energy model but it is complex, especially for the obtained accuracy with respect to the experimental data. Also, $P_{H_2O_A}$, P_{N_2}, $W^{in}_{H_2O_A}$, $W^{in}_{N_2}$ should be treated as constant parameters otherwise the system is a time-varying nonlinear system that is difficult to study. Na and Gou have established 5th order model [4] since Chiu et al. indicated a need for using higher-order dimensional models studying dynamics of $H_2O^{in}_A$ and N^{in}_2 (see Figure 1.7).

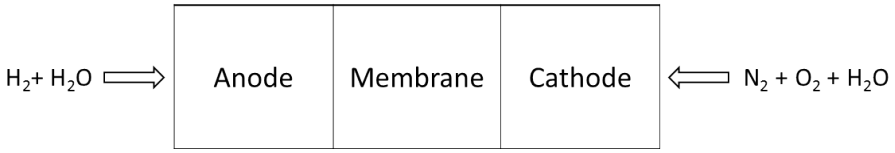

Figure 1.7: Na and Gou Model [4]

The state equations for the model of [4] are as follows

$$\begin{aligned}
\frac{dP_{H_2}}{dt} &= \frac{RT}{V_a}(W_{H_2}^{in} - W_{H_2}^{out} - W_{H_2}^{used}) \\
\frac{dP_{H_2O_A}}{dt} &= \frac{RT}{V_a}(W_{H_2O_A}^{in} - W_{H_2O_A}^{out} - W_{H_2O_A}^{membrane}) \\
\frac{dP_{O_2}}{dt} &= \frac{RT}{V_c}(W_{O_2}^{in} - W_{O_2}^{out} - W_{O_2}^{used}) \\
\frac{dP_{N_2}}{dt} &= \frac{RT}{V_c}(W_{N_2}^{in} - W_{N_2}^{out}) \\
\frac{dP_{H_2O_C}}{dt} &= \frac{RT}{V_c}(W_{H_2O_C}^{in} - W_{H_2O_C}^{out} + W_{H_2O_C}^{produced} - W_{H_2O_C}^{membrane})
\end{aligned} \tag{1.16}$$

where $W_{H_2O_A}^{membrane}$ and $W_{H_2O_C}^{membrane}$ represent the water vapor used to humidify the membrane from the anode and cathode sides, respectively. The state variables in this model represent respectively pressures of hydrogen and water vapor at the anode side and pressures of oxygen, nitrogen, and water vapor at the cathode side, that is

$$x(t) = \begin{bmatrix} P_{H_2}(t) & P_{H_2O_A}(t) & P_{O_2}(t) & P_{N_2}(t) & P_{H_2O_C}(t) \end{bmatrix}^T \tag{1.17}$$

The state space model is given by

$$\begin{aligned}
\dot{x}_1 =& \frac{RT\lambda_{H_2}}{V_a}\left(Y_{H_2} - \frac{x_1}{x_1+x_2}\right)k_a u_a + \frac{RTC_1}{V_a}\left(\frac{x_1}{x_1+x_2} - 1\right)I \\
\dot{x}_2 =& \frac{RT\lambda_{H_2}}{V_a}\left(\frac{\varphi_a P_{vs}}{x_1+x_2-\varphi_a P_{vs}} - \frac{x_2}{x_1+x_2}\right)k_a u_a + \frac{RTC_1}{V_a}\left(\frac{x_2}{x_1+x_2} - 1\right)I \\
\dot{x}_3 =& \frac{RT\lambda_{air}}{V_c}\left(Y_{O_2} - \frac{x_3}{x_3+x_4+x_5}\right)k_c u_c + \frac{RTC_1}{2V_c}\left(\frac{x_3}{x_3+x_4+x_5} - 1\right)I \\
\dot{x}_4 =& \frac{RT\lambda_{air}}{V_c}\left(Y_{N_2} - \frac{x_3}{x_3+x_4+x_5}\right)k_c u_c \\
\dot{x}_5 =& \frac{RT\lambda_{air}}{V_c}\left(\frac{\varphi_a P_{vs}}{x_3+x_4+x_5-\varphi_a P_{vs}} - \frac{x_3}{x_3+x_4+x_5}\right)k_c u_c \\
&+ \frac{RTC_1}{V_c}\left(\frac{C_2}{C_1}\left(1 - \frac{x_3}{x_3+x_4+x_5}\right) - 1 - \frac{x_3}{x_3+x_4+x_5}\right)I
\end{aligned} \tag{1.18}$$

where C_1, C_2 are known constants [4, 6], φ_a, φ_c are the relative humidity constants, P_{vs} is the saturation pressure, λ_{H_2} and λ_{air} are stoichiometric constants, and $Y_{H_2} = 0.99$, $Y_{O_2} = 0.21$, $Y_{N_2} = 0.79$, are reactant fractions. I is the cell current, and it is considered as a disturbance.

The model output variables are defined by [4, 6]

$$y(t) = \begin{bmatrix} P_{H_2}(t) \\ P_{O_2}(t) \end{bmatrix} = \begin{bmatrix} x_1(t) \\ x_3(t) \end{bmatrix} \tag{1.19}$$

The system control input is given by $u(t) = \begin{bmatrix} u_a(t) & u_c(t) \end{bmatrix}^T$ where

$$u_a(t) = \frac{1}{k_a}\big(H_{2in}(t) + H_2O_{Ain}(t)\big) \tag{1.20}$$

$H_{2in}(t)$ and $H_2O_{Ain}(t)$ represent inlet flow rates of the anode side hydrogen and water vapor with k_a being a known constant, and

$$u_c(t) = \frac{1}{k_c}\big(O_{2in}(t) + N_{2in}(t) + H_2O_{Cin}(t)\big) \tag{1.21}$$

$O_{2in}(t)$, $N_{2in}(t)$ and $H_2O_{Cin}(t)$ represent respectively inlet flow rates of the cathode oxygen, nitrogen, and water vapor with k_c being a known constant.

The model of (1.18) will play an important (central) roll in this dissertation. Other higher-order dimensional model of PEMFC can be found in [7].

1.1.2 Solar Cells

The solar cell is also a promising candidate for many applications that requires electric energy. The photovoltaic (PV), another common name used for solar cells, has received much attention with many feasible applications. A PV array is a p-n junction semiconductor, that convert solar energy into electricity. When the incoming energy exceeds the band-gap energy of the module, photons are absorbed by materials to generate electricity. The equivalent electric circuit of a solar cell is shown in Figure 1.8 [8].

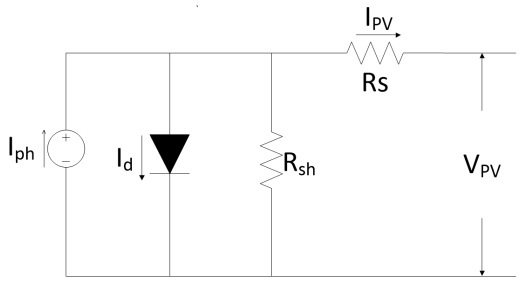

Figure 1.8: Equivalent circuit model of PV

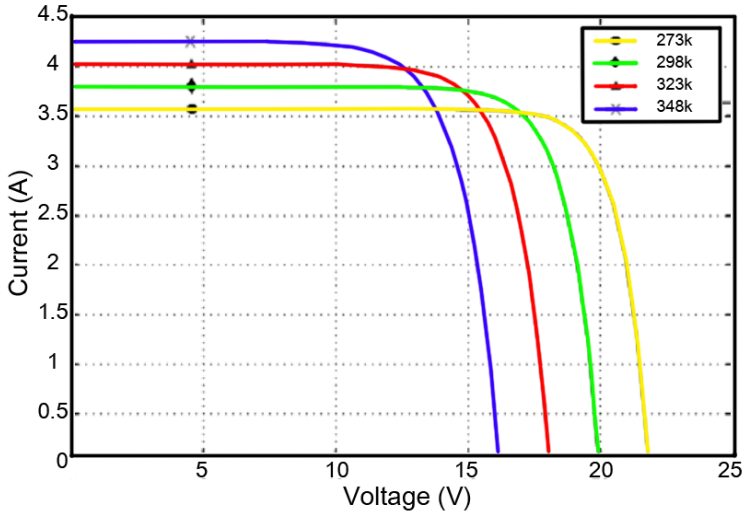

Figure 1.9: Characteristic under different temperature

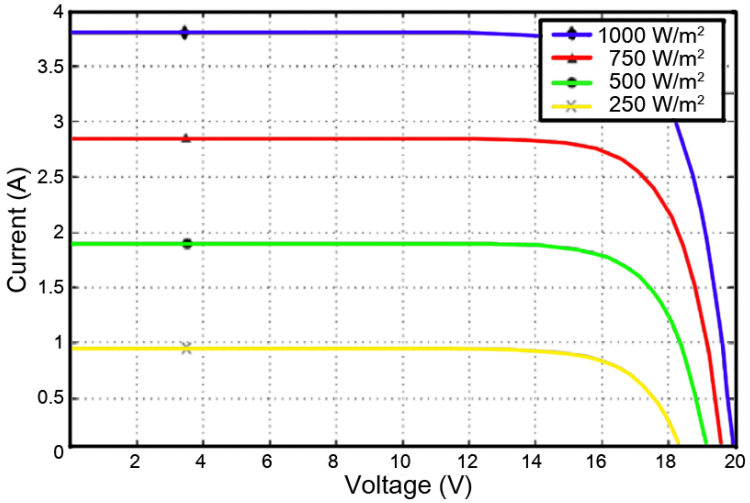

Figure 1.10: Characteristic under different irradiance levels

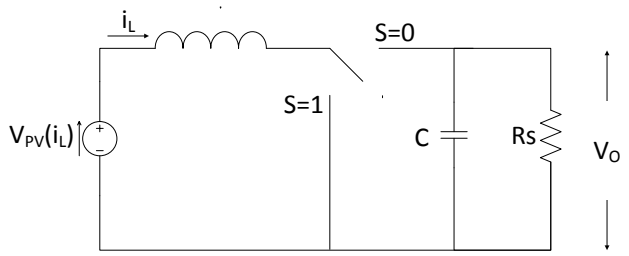

Figure 1.11: Maximum power point tracking schematic

The system is expressed as follow

$$\begin{aligned} I_{PV} &= I_{ph} - I_d\left[\exp\Big(\frac{q}{k_b T A}V\Big) - 1\right] \\ I_{ph} &= S[I_{scr} + k_i(T - T_r)] \\ I_d &= I_{rr}\left(\frac{T}{T_r}\right)^3 \exp\left(\frac{qE_g}{k_b Q A}\Big[\frac{1}{T_r} - \frac{1}{T}\Big]\right) \end{aligned} \tag{1.22}$$

where I_{PV} is the output current, V_{PV} is the output voltage, T is the cell temperature, S is the solar irradiance, I_{ph} is the light-generated current, I_d is the PV saturation current, I_{rr} is the saturation current at T_r, I_{scr} is the short-circuit current at reference conditions, T_R is the reference temperature, k_i is the short-circuit temperature coefficient, q is the charge of an electron, k_b is Boltzmann's constant, E_g is the energy band-gap of the material, Q is the total electron charge, and A is the ideality factor. The performance of PV depends on solar insolation, ambient temperature, and load impedance. Figures 1.9 and 1.10 show the PV characteristics under different temperature and under different irradiance levels, respectively. The system equivalent electrical circuit for maximum power point tracking is shown in Figure 1.11. Its nonlinear system can be written as follows

$$\begin{aligned} \frac{di_L}{dt} &= \frac{V_{PV}(i_L)}{L} - \frac{V_0}{L} + \frac{V_0}{L}\delta \\ \frac{dV_0}{dt} &= \frac{i_L}{C} - \frac{V_0}{CR_L} - \frac{i_L}{C}\delta \end{aligned} \tag{1.23}$$

where C is the capacity, L is the inductance, R_L is the resistive load, V_0 is the output voltage, i_L is the inductor current, and $\delta \in \begin{bmatrix} 0 & 1 \end{bmatrix}$ is the duty ration, that is also the

control input. The system (1.23) is expressed as

$$\dot{x} = (1-\delta)\dot{x}_1 + \delta\dot{x}_2 = f(x) + g(x)\delta \tag{1.24}$$

where $\dot{x}_1 = \begin{bmatrix} \dot{i}_{L_1} & \dot{V}_{0_1} \end{bmatrix}^T$ and $\dot{x}_2 = \begin{bmatrix} \dot{i}_{L_2} & \dot{V}_{0_2} \end{bmatrix}^T$ depending on the position of switch S.

1.2 Control Strategies for Energy Systems

There are many control design tools for linear and nonlinear systems. For example, PI or PID controllers, feedback linearization, backstepping, and sliding mode control. Also, depending on the model, certain requirements of the transient response or certain constraints on the control input exist. We need to design different controllers to optimize these requirements or constraints - issues of robustness or model uncertainties. In this chapter, some useful control strategies will be presented including sliding mode control, integral control, feedback linearization, and optimal control of jump linear systems. Most of them will be used in the follow up chapters of this dissertation.

1.2.1 Sliding Mode Control for Linear and Nonlinear Systems

Literature Review of Sliding Mode Control for Energy Systems

Since most of energy systems are nonlinear, sliding mode control techniques are good strategies that yields to reduce system uncertainties and exogenous disturbances. In this section, we only consider the problem of sliding mode controller design that can be used for various energy and power systems. The review is divided into four main parts: applications to fuel cells, solar cells, solar plants; wind and tidal energy, and electric power systems including power electronics. Due to a large number of published papers, the review of the corresponding journal papers is mostly limited to the last few years.

In the last few years, several control strategies for PEMFC are proposed. Especially, the sliding mode control technique that is robust against disturbances has been recently considered in several papers, [9–17]. A second-order sliding mode controller is designed for the breathing (oxidation) subsystem of a PEMFC stack in [10], where the authors have focused on the chattering phenomenon. The model used in [10] is nonlinear of

order six, which is derived based on the work of Pukrushpan et al., [7]. Talj et al., [9] have first simplified and reduced the ninth-order model of [7] to a fourth-order highly nonlinear model and experimentally justified such a procedure. Then, they designed the corresponding sliding mode controller using as the sliding variable the difference between the actual and nominal angular air compressor speeds. The oxygen flow problem with real time implementation of a sliding mode controller has been considered for the first-order model that is obtained from the process input/output data in [14]. In [15], a hybrid controller composed of an internal mode control based PID controller and an adaptive sliding mode controller has been designed. The first controller is used to control the hydrogen reformer and the second controller is used to control the PEMFC based on the work of El-Shark [1]. A sliding mode control scheme is proposed for the DC/DC buck converter which guarantees a low and stable output voltage given transient variations in the output voltage of a PEMFC in [16]. A fuzzy sliding mode current controller of a hybrid fuel cell/energy-storage systems is considered in [12]. The controller is presented for designing controllers for DC/DC and DC/AC converters. In [13], Hajizadeh and his coworkers used the fuel cell model of [13] coupled with a simple second-order model for the hydrogen reformer and a linear super capacitor model to design a sliding mode controller for active power under unbalanced voltage sag conditions. A sliding mode controller of DC/DC converters for a simplified dynamic model for fuel cells is used in [11]. Li has presented rapid-convergent sliding mode for the temperature control system of PEMFC stack [17]. In this dissertation, we study control of processes in PEMFC, and we did not consider the fuel cell connection to an electric grid [11–13, 16], but the model has included state space variables that represent the fuel cell temperature [17].

Recent applications to solar energy are summarized in journal papers [8, 18–25]. Sliding mode control has been applied to a solar air conditioning systems [18] as well as to a photovoltaic water-pumping system [19]. In [20], a predictive sliding mode controller is designed to control temperature in a field of solar collectors (solar plant). To track the power peak in a solar cell (they have a nonlinear current-voltage characteristics so that the power voltage characteristic looks like a parabolic function with clearly

distinguished the maximal power value) sliding mode control has been used in [8]. Stability and robustness of the corresponding sliding mode controller are considered in the same paper. Sliding mode control of the output power of a hybrid stand-alone solar/wind generation system has been studied in [21]. A wind/solar generation system has been considered also in [22] with emphasis on the chattering phenomenon. Sun tracking control such that the solar (photovoltaic) cell faces the sun in a way that it captures maximum irradiation is designed in [23]. A model of a three-phase grid connected photovoltaic system has been presented in [24]. In addition, in the same paper, a robust maximum power point tracker has been designed using a sliding mode controller. An improved solar energy based Cuk inverter with sliding mode control is presented in [25].

The recent wind energy application journal papers are [26–32], and the tidal power generation journal papers are [33, 34]. Sliding mode control for a wind turbines has been presented in [26] where uncertainties have been also considered. Sliding mode control strategy is presented in [27] to optimize the power conversion efficiency of a wind energy conversion system and in [28] to maximize the volume of water pumped based on the optimization of the wind energy capture. Another application of a wind turbine is presented in [29] for optimization of a wind energy conversion system efficiency and frequency shaping sliding mode control for vibration suppression of the shaft equipped with a wind turbine is proposed in [30] where a sliding mode control is implemented to adjust the turbine speed to extract maximum power from the wind. Spindle position regulation for wind power generators via the method of singular perturbations (multiple time scale technique) has been presented in [30]. In [31], sliding mode control of active and reactive power of a grid-connected doubly fed induction generator (DFIG) of wind turbines has been considered. Kim et al. [32] designed an adaptive observer to estimate a wind generation system parameters. In [33], a second-order robust sliding mode controller has been used to control a marine current turbine that generates tidal energy. Higher-order sliding mode controller for the same system has been designed by the same authors in [34].

There is a large number of applications of the sliding mode control technique to

electrical power generation systems, and especially to power electronics. In this brief section, we mention only a few of them published several years ago. A new discrete-time sliding mode controller for load-frequency control, in the control areas of a power system for hydro and thermal power plants is presented in [35]. In [36], a sliding mode controller of a power system comprising a single synchronous generator connected to an infinite bus with local load is designed using singular perturbation concepts. A sliding mode controller for a variable speed constant frequency energy conversion system is considered in [37]. Even though, some applications of sliding mode controls to the energy and power systems have been considered in these papers, energy efficiencies and uncertainties have not been completely addressed in the papers. A new active and reactive power control for the three-phase grid connected DC/AC connectors via a sliding mode control technique is considered in [38]. The sliding surface is chosen such that the DC/AC convertors track the predefined (set-point) active and reactive power values. A robust fuzzy sliding mode controller has been designed in [39] for a buck-boost DC/DC power supply converter that can be used for vehicles. In an interesting educational paper, [40], on control of an embedded system (DC servo system) via internet, in addition to a classical PI controller design, a more complex sliding mode controller design is presented. As the sliding surface, a linear combination of the position and speed errors is selected in [40]. A sliding mode observer has been designed in [41] for speed control of sensorless DC induction motor drives, and the corresponding energy optimizing sliding mode controller has been designed in [42]. The power factor correction problem for boost converters has been considered in [43] via feedback linearization using sliding mode control. The feedback linearization technique via a sliding mode control approach has been presented in [44] and [45] and applied to different power electronics devices. Low frequency current ripple control for power conditioning in DC/DC and DC/AC converters (connected to either fuel or solar cells) via sliding mode control is considered in [46]. The sliding surface is chosen in [46] as a sum of the tracking error and its integral.

The literature review given in this section is presented at a conference [47].

Continuous-Time Sliding Mode Control for Linear Systems

Continuous-time sliding mode control has been recognized as a robust control approach, which yields to reject matched disturbances (control subspace covers the disturbance subspace) and system uncertainties. The design of sliding mode control is achieved in two steps. Firstly, a sliding surface is described which ensures the system to remain on a plane after reaching it from any initial conditions in a finite time. Secondly, discontinuous control is designed to render a sliding mode.

Consider the following single input linear system [48].

$$\begin{bmatrix} \dot{x}_1(t) \\ \dot{x}_2(t) \end{bmatrix} = \begin{bmatrix} 0 & 1 \\ \alpha & \beta \end{bmatrix} \begin{bmatrix} x_1(t) \\ x_2(t) \end{bmatrix} + \begin{bmatrix} 0 \\ 1 \end{bmatrix} u(t) \tag{1.25}$$

If $x_2(t) = -\lambda x_1(t)$, where $\lambda > 0$, then $x_1(t)$ and $x_2(t)$ are asymptotically stable because (1.25) yields $\dot{x}_1(t) = -\lambda x_1(t)$. Define a line as follows

$$s(t) = x_2(t) + \lambda x_1(t),\ \lambda > 0 \tag{1.26}$$

Figure 1.12 shows a sliding line in the state space. The control objectives are to design

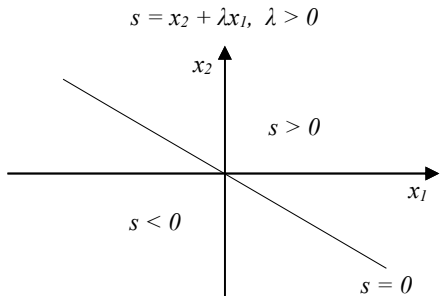

Figure 1.12: A sliding line $s(t) = 0$

$u(t)$ to ensure that the system reaches the sliding line from any initial condition in a finite time and stay on the line after reaching it. The conditions to achieve these objectives are called reaching and sliding conditions. The reaching condition provides that the system state reaches the sliding surface in a finite time, whereas the sliding condition facilitates that the system state slides on the sliding line towards the origin.

The reaching condition is described as [49, 50]

$$\dot{s}(t) = -\delta \text{sgn}(s(t)),\ \delta > 0 \tag{1.27}$$

where the signum function $\text{sgn}(s(t))$ is defined by

$$\text{sgn}(s(t)) = \begin{cases} +1 \text{ if } s(t) > 0 \\ 0 \text{ if } s(t) = 0 \\ -1 \text{ if } s(t) < 0 \end{cases} \tag{1.28}$$

which yields to the following condition [48]

$$\dot{s}(t)s(t) < 0 \tag{1.29}$$

The equivalent control $u_{eq}(x(t))$ is obtained when the system remains on the sliding mode, that is $\dot{s}(t) = 0$. From (1.26), we have

$$\dot{s}(t) = \alpha x_1(t) + (\beta + \lambda)x_2(t),\ \lambda > 0 \tag{1.30}$$

For $\dot{s}(t) = 0$, it follows

$$u_{eq}(t) = -\alpha x_1(t) - (\beta + \lambda)x_2(t),\ \lambda > 0 \tag{1.31}$$

Therefore, the control law to satisfy the reaching condition (1.27) is

$$u(t) = u_{eq}(t) - \delta \text{sgn}(s(t)),\ \delta > 0 \tag{1.32}$$

The following sliding condition [50]

$$\lim_{s(t)\to 0^+} \dot{s}(t) < 0,\ \lim_{s(t)\to 0^-} \dot{s}(t) > 0 \tag{1.33}$$

is sufficient and local.

Constructing Sliding Surfaces of MIMO System

There are several method to design sliding surfaces. Utkin and Young proposed a method for linear systems [51]. Consider a continuous-time linear system which is given by

$$\dot{x}(t) = Ax(t) + Bu(t) \tag{1.34}$$

where $x(t) \in \mathbf{R}^n$, $u(t) \in \mathbf{R}^m$, and A, B are constant matrices of appropriate dimensions, and B has full rank.

There exists a similarity transformation defined by [51]

$$q(t) = Hx(t) \tag{1.35}$$

with

$$H = \begin{bmatrix} N & B \end{bmatrix}^T \tag{1.36}$$

and columns of the $n \times (n-m)$ matrix N composed of basis vectors of the null space of B^T, which puts (1.34) into the form

$$\dot{q}(t) = \bar{A}q(t) + \bar{B}u(t) \tag{1.37}$$

with $\bar{A} = HAH^{-1}$ and $\bar{B} = HB = \begin{bmatrix} 0 \\ \bar{B}_r \end{bmatrix}$. Equation (1.37) is decomposed as follows

$$\begin{bmatrix} \dot{q}_1(t) \\ \dot{q}_2(t) \end{bmatrix} = \begin{bmatrix} \bar{A}_{11} & \bar{A}_{12} \\ \bar{A}_{21} & \bar{A}_{22} \end{bmatrix} \begin{bmatrix} q_1(t) \\ q_2(t) \end{bmatrix} + \begin{bmatrix} 0 \\ \bar{B}_r \end{bmatrix} u(t) \tag{1.38}$$

where $q_1(t) \in \mathbf{R}^{n-m}$, $q_2(t) \in \mathbf{R}^m$, and $\bar{B}_r$ is an $m \times m$ nonsingular matrix.

Equation (1.38) yields

$$\dot{q}_1(t) = \bar{A}_{11}q_1(t) + \bar{A}_{12}q_2(t) \tag{1.39}$$

and

$$\dot{q}_2(t) = \bar{A}_{21}q_1(t) + \bar{A}_{22}q_2(t) + \bar{B}_r u(t) \tag{1.40}$$

$q_2(t)$ is treated as a control input to the system (1.39) and a state feedback gain K, which makes the system stable, is defined by

$$q_2(t) = -Kq_1(t). \tag{1.41}$$

For the system (1.39), [51] has shown that $(\bar{A}_{11}, \bar{A}_{12})$ is controllable if and only if (A, B) is controllable [52].

On the sliding surface, the system trajectory in the $(q_1(t), q_2(t))$ coordinates is expressed as

$$\begin{bmatrix} K & I_m \end{bmatrix} \begin{bmatrix} q_1(t) \\ q_2(t) \end{bmatrix} = 0 \tag{1.42}$$

or

$$s(t) = Gx(t) = \begin{bmatrix} K & I_m \end{bmatrix} Hx(t) = 0 \tag{1.43}$$

in the original coordinates.

Variable Structure Control Law Design

Three major types of discontinuous (switching) control exist: variable structure type, signum function, and unit control.

The first method is called variable structure type. Consider a single-input system [49]

$$\begin{aligned} \dot{x}_i(t) &= \dot{x}_{i+1}(t),\ i = 1, \ldots, n-1 \\ \dot{x}_n(t) &= -\sum_{i=1}^{n} a_i(t) x_i(t) + u(t) \end{aligned} \tag{1.44}$$

where a_i are time-varying parameters and $u(t)$ is $m \times 1$ vector. This system has the sliding surface as

$$s(t) = x_n(t) + c_{n-1}(t)x_{n-1}(t) + \cdots + c_1(t)x_1(t) = 0 \tag{1.45}$$

The control law is described as

$$u(t) = -\sum_{i=1}^{n-1} \Psi_i x_i(t) - \delta \mathrm{sgn}(s(t)) \tag{1.46}$$

where δ is a small positive number and the feedback gains are

$$\Psi_i = \begin{cases} \alpha_i \text{ if } x_i s(t) > 0 \\ \\ \beta_i \text{ if } x_i s(t) < 0 \end{cases} \tag{1.47}$$

Another method is based on the use of a signum function. Consider a multi input system with a disturbance $d(t)$

$$\dot{x}(t) = Ax(t) + Bu(t) + Ed(t) \tag{1.48}$$

where $x(t) \in \mathbf{R}^n$, $u(t) \in \mathbf{R}^m$, $d(t) \in \mathbf{R}^l$ and A, B, E are constant matrices of appropriate dimensions, B and E have full rank. The sliding mode of (1.48) can be described as

$$s(t) = Gx(t) = 0 \tag{1.49}$$

where G is a $m \times n$ matrix. The sliding variable dynamics controls can be chosen by considering

$$\dot{s}(t) = G\dot{x}(t) = GAx(t) + GBu(t) + GEd(t) \tag{1.50}$$

Introduce a new variable $\bar{s}(t)$ to decouple the control input

$$\bar{s}(t) = (GB)^{-1}s(t) \tag{1.51}$$

From equations (1.50) and (1.51), the new sliding dynamics is obtained

$$\begin{aligned}\dot{\bar{s}}(t) &= (GB)^{-1}GAx(t) + u(t) + (GB)^{-1}GEd(t) \\ &= \begin{bmatrix} f_1(x(t)) + u_1(t) + d_1(t) \\ f_2(x(t)) + u_2(t) + d_2(t) \\ \vdots \\ f_m(x(t)) + u_m(t) + d_m(t) \end{bmatrix}\end{aligned} \tag{1.52}$$

such that each control law can be designed separately as [53]

$$\begin{aligned} u_1(t) &= -f_1(x(t)) - (d_1(t) + \sigma_1)\text{sgn}(\bar{s}_1(t)) \\ u_2(t) &= -f_2(x(t)) - (d_2(t) + \sigma_2)\text{sgn}(\bar{s}_2(t)) \\ &\vdots \\ u_m(t) &= -f_m(x(t)) - (d_m(t) + \sigma_m)\text{sgn}(\bar{s}_m(t)) \end{aligned} \tag{1.53}$$

Unit control of [51] also can be used. Consider the same system as on (1.48)

$$\dot{x}(t) = Ax(t) + Bu(t) + Ed(t) \tag{1.54}$$

with the same sliding variable dynamics such as

$$\dot{s}(t) = G\dot{x}(t) = GAx(t) + GBu(t) + GEd(t) \tag{1.55}$$

The control law which satisfies the reaching condition directly can be chosen as [51]

$$u(t) = -(GB)^{-1}GAx(t) - (GB)^{-1}(\gamma + \sigma)(\frac{s(t)}{||s(t)||}) \tag{1.56}$$

where

$$\gamma = ||GE||d_{max} \tag{1.57}$$

The Invariance Condition for Linear Systems with Exogenous Disturbances

Consider a multi input system with a disturbance $d(t)$ [54]

$$\dot{x}(t) = Ax(t) + Bu(t) + Ed(t) \tag{1.58}$$

where $x(t) \in \mathbf{R}^n$, $u(t) \in \mathbf{R}^m$, $d(t) \in \mathbf{R}^l$ and A, B, E are constant matrices of appropriate dimensions, B and E have full rank. The sliding mode of (1.58) can be described as

$$s(t) = Gx(t) = 0, \tag{1.59}$$

where $G(t)$ is a $m \times n$ matrix. Equation (1.58) is invariant to $d(t)$ in the sliding mode if and only if

$$\operatorname{rank}\begin{bmatrix} B & | & E \end{bmatrix} = \operatorname{rank}\begin{bmatrix} B \end{bmatrix} \tag{1.60}$$

1.2.2 Integral Control

Integral Control for Linear Systems

Consider a system as follows

$$\begin{aligned} \dot{x}(t) &= Ax(t) + Bu(t) + Gd(t) \\ y(t) &= Cx(t) \end{aligned} \tag{1.61}$$

where $x(t) \in \mathbf{R}^n$ is the state variables, $u(t) \in \mathbf{R}^m$ is the control input, $y(t) \in \mathbf{R}^p$ is the system output, and d is a *constant disturbance*. The objective is to regulate $y(t)$ to the desired value y_{ref} despite of $d(t)$ at steady state. Introduce the tracking error

$$e(t) = y(t) - y_{ref}(t) \tag{1.62}$$

and define a new variable

$$\sigma(t) = \int_0^t e(\tau)\,\mathrm{d}\tau \tag{1.63}$$

and form the augmented system as follows

$$\begin{aligned} \begin{bmatrix} \dot{x}(t) \\ \dot{\sigma}(t) \end{bmatrix} &= \begin{bmatrix} A & 0 \\ C & 0 \end{bmatrix} \begin{bmatrix} x(t) \\ \sigma \end{bmatrix} + \begin{bmatrix} B \\ 0 \end{bmatrix} u(t) + G \begin{bmatrix} d \\ 0 \end{bmatrix} - \begin{bmatrix} 0 \\ y_{ref} \end{bmatrix} \\ &= \mathcal{A} \begin{bmatrix} x(t) \\ \sigma \end{bmatrix} + \mathcal{B}u(t) + G \begin{bmatrix} d \\ 0 \end{bmatrix} - \begin{bmatrix} 0 \\ y_{ref} \end{bmatrix} \end{aligned} \tag{1.64}$$

Suppose now that (A, B) is controllable (stabilizable) and

$$\text{rank} \begin{bmatrix} A & B \\ C & 0 \end{bmatrix} = n + p \tag{1.65}$$

Then, $(\mathcal{A}, \mathcal{B})$ is controllable (stabilizable). Since the augmented system is controllable,

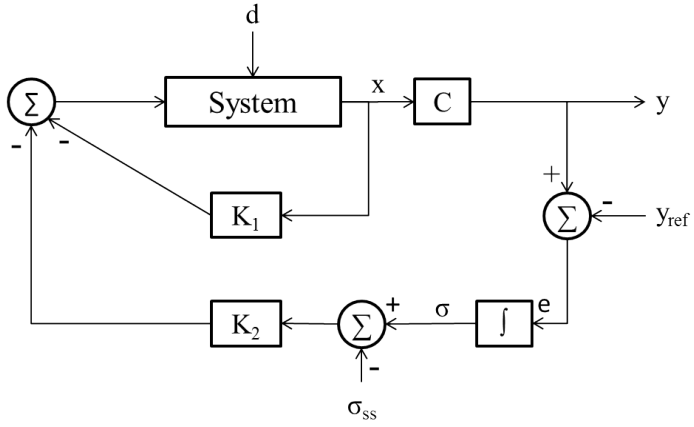

Figure 1.13: Integral Control Diagram for Linear Systems

we can find a linear feedback control law as follows

$$u = -K \begin{bmatrix} x \\ \sigma \end{bmatrix} = -K_1 x - K_2 \sigma \tag{1.66}$$

such that $(\mathcal{A}, \mathcal{B})$ is asymptotically stable. At the steady state

$$\begin{aligned} x(t) &\to x_{ss} \\ y(t) &\to y_{ss} = y_{ref} \\ \sigma(t) &\to \sigma_{ss} = const \end{aligned} \tag{1.67}$$

The corresponding block diagram is given in Figure 1.13

1.3 Contributions of the Dissertation

The contributions of the dissertation are summarized in the following:

- In Chapter 2, the sliding mode controllers are proposed for the fifth-order PEM-FCs pressure model. We have linearized the system and proved the uniqueness of steady state variables, asymptotic stability, controllability, and observability of

the system. Then, we have designed the control laws for the linearized system and nonlinear system. The sliding mode technique copes very well with the cell current changes I(t) which can be considered as a disturbance, and keeps very precisely the pressures of hydrogen and oxygen at the desired (required) values.

- The sliding mode control of SOFCs is proposed in Chapter 3. Even though, the material balance model is considered with temperature, the control input to keep pressures at the desired value does not depend on temperature. Assuming uncertainties of state variables, we do not need to design a nonlinear observer since the control input is only dependent on sliding surfaces, which are designed using only the system output.

- In Chapter 4, we have applied the optimal jump parameter control technique to the Cuk converter used in solar cells. The optimal values are obtained by changing the duty cycle and they are are almost insensitive to the value of the duty cycle δ. We have modified and accelerated algorithm of [55] and applied the optimal jump parameter control technique with integral action to the Cuk converter. The simulation result shows considerable smaller ripple than the averaged Cuk converter system that has been most commonly used.

1.4 Organization of the Dissertation

In Chapter 2, the modeling and control of PEMFCs are presented and those of SOFCs are presented in Chapter 3. Especially, the temperature modeling and control of SOFCs are found in Chapter 3. Optimal control via a jump parameter of the Cuk converter used in solar cells is followed in Chapter 4. The conclusions and future works are presented in Chapter 5.

Chapter 2

Modeling and Control of Proton Exchange Membrane Fuel Cells

2.1 Introduction

Fuel cells are electrochemical energy devices that convert the chemical energy, during a hydrogen-oxygen reaction, into electricity, heat, and water. As a renewable energy source, fuel cells are one of the promising energy technologies with high efficiency and low environmental impact. Proton exchange membrane fuel cells are the most developed and popular type of fuel cells, using hydrogen as the fuel. PEMFC represents a nonlinear, multiple-input and multiple-output dynamic system [56].

Third-order models of PEMFC can be found in [1] (linear model), [2] (bilinear model), and [3] (nonlinear model). Na and Gou have derived a fifth-order nonlinear model [4] since Chiu et al. [3] indicated a need for using higher-order dimensional models of anode water (needed for membrane humidification) and cathode nitrogen, see Figure 2.1. A nonlinear ninth-order model of PEMFC was derived in [7]. The model of [7] and its simplified fourth and sixth-order variants were considered in [9, 10].

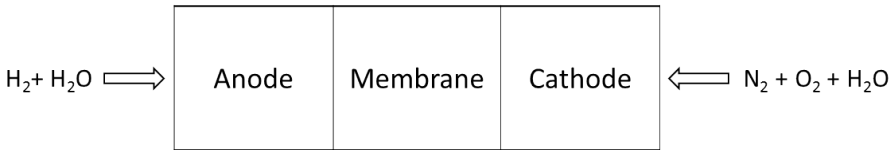

Figure 2.1: Na and Gou 2008 Model Schematic [4]

In the last few years, several control strategies for PEMFC are proposed. The sliding mode control technique that is robust against disturbances has been recently considered in several papers, [9–17]. A second-order sliding mode controller is designed

for the breathing subsystem of a PEMFC stack in [10], where the authors have focused on elimination of the chattering phenomenon. The model used in [10] is a nonlinear model of order six, which is derived from the work of Pukrushpan et al., [7]. Talj et al., [9] have first simplified and reduced the ninth-order model of [7] to a fourth-order highly nonlinear model and experimentally justified such a procedure. Then, they designed the corresponding sliding mode controller using as the sliding variable the difference between the actual and nominal angular air compressor speeds. The oxygen flow problem with real time implementation of a sliding mode controller has been considered for the first-order model that is obtained from the process input/output data in [14]. In [15], a hybrid controller composed of an internal mode control based PID controller and an adaptive sliding mode controller has been designed. The first controller is used to control the hydrogen reformer and the second controller is used to control the PEMFC model based on the work of [1]. A sliding mode control scheme is proposed for the DC/DC buck converter that guarantees a low and stable output voltage given transient variations in the output voltage of a PEMFC in [16]. A fuzzy sliding mode current controller of a hybrid fuel cell/energy-storage systems is considered in [12]. The method is presented for designing controllers for DC/DC and DC/AC converters. In [13], Hajizadeh and his coworkers used the fuel cell model of [57] coupled with a simple second-order model for the hydrogen reformer and a linear super capacitor model to design a sliding mode controller for active power under unbalanced voltage sag conditions. A sliding mode controller of DC/DC converters for a simplified dynamic model for fuel cells is used in [11]. Li et al. have presented a rapid-convergent sliding mode controller for the temperature control system of PEMFC stack [17]. That paper did not consider the fuel cell connection to an electric grid [11–13, 16], but the model has included state variables that represent the fuel cell temperature [17].

In this chapter, we propose a sliding mode controller design for the fifth-order nonlinear model of PEMFC developed in [4], see also [6]. It will be seen from the simulation results that the sliding mode controller proposed in this paper outperforms the feedback linearization-based controller proposed in [4]. The state variables in this model represent respectively the pressures of hydrogen and water at the anode side and the

pressures of oxygen, nitrogen, and water at the cathode side, that is

$$\begin{aligned} x(t) &= \begin{bmatrix} P_{H_2}(t) & P_{H_2O_A}(t) & P_{O_2}(t) & P_{N_2}(t) & P_{H_2O_C}(t) \end{bmatrix}^T \\ &= \begin{bmatrix} x_1(t) & x_2(t) & x_3(t) & x_4(t) & x_5(t) \end{bmatrix}^T \end{aligned} \tag{2.1}$$

The state space model is given by

$$\begin{aligned} \dot{x}_1 =& \frac{RT\lambda_{H_2}}{V_A}\left(Y_{H_2} - \frac{x_1}{x_1+x_2}\right)k_a u_a + \frac{RTC_1}{V_A}\left(\frac{x_1}{x_1+x_2} - 1\right)I \\ \dot{x}_2 =& \frac{RT\lambda_{H_2}}{V_A}\left(\frac{\varphi_a P_{vs}}{x_1+x_2-\varphi_a P_{vs}} - \frac{x_2}{x_1+x_2}\right)k_a u_a + \frac{RTC_1}{V_A}\left(\frac{x_2}{x_1+x_2} - 1\right)I \\ \dot{x}_3 =& \frac{RT\lambda_{air}}{V_C}\left(Y_{O_2} - \frac{x_3}{x_3+x_4+x_5}\right)k_c u_c + \frac{RTC_1}{2V_C}\left(\frac{x_3}{x_3+x_4+x_5} - 1\right)I \\ \dot{x}_4 =& \frac{RT\lambda_{air}}{V_C}\left(Y_{N_2} - \frac{x_4}{x_3+x_4+x_5}\right)k_c u_c \\ \dot{x}_5 =& \frac{RT\lambda_{air}}{V_C}\left(\frac{\varphi_a P_{vs}}{x_3+x_4+x_5-\varphi_a P_{vs}} - \frac{x_5}{x_3+x_4+x_5}\right)k_c u_c \\ &+ \frac{RTC_1}{V_C}\left(\frac{C_2}{C_1}\left(1 - \frac{x_5}{x_3+x_4+x_5}\right) - 1 - \frac{x_5}{x_3+x_4+x_5}\right)I \end{aligned} \tag{2.2}$$

where R is the universal gas constant, T is temperature, V_A, V_C and are anode and cathode volumes. C_1, C_2 are known constants [4, 6], φ_a, φ_c are the relative humidity constants, P_{vs} is the saturation pressure, λ_{H_2}, λ_{air} and are stoichiometric constants, $Y_{H_2} = 0.99$, $Y_{O_2} = 0.21$, $Y_{N_2} = 0.79$, are reactant fractions. I is the cell current, and it is considered as a disturbance since it changes as V_{fc}/R_L, where V_{fc} is the produced fuel cell voltage and R_L is the load of active users, which changes randomly.

The model output variables are defined by [4, 6]

$$y(t) = \begin{bmatrix} P_{H_2}(t) \\ P_{O_2}(t) \end{bmatrix} = \begin{bmatrix} x_1(t) \\ x_3(t) \end{bmatrix} \tag{2.3}$$

The system control input is given by $u(t) = \begin{bmatrix} u_a(t) & u_c(t) \end{bmatrix}^T$ where

$$u_a(t) = \frac{1}{k_a}\big(H_{2in}(t) + H_2O_{Ain}(t)\big) \tag{2.4}$$

$H_{2in}(t)$ and $H_2O_{Ain}(t)$ represent inlet flow rates of the anode side hydrogen and water vapor with k_a being a known constant, and

$$u_c(t) = \frac{1}{k_c}\big(O_{2in}(t) + N_{2in}(t) + H_2O_{Cin}(t)\big) \tag{2.5}$$

$O_{2in}(t)$, $N_{2in}(t)$ and $H_2O_{Cin}(t)$ represent respectively inlet flow rates of the cathode oxygen, nitrogen, and water with k_c being a known constant.

2.2 Linearization Of PEM Fuel Cell Dynamic Model

Using MATLAB Symbolic Math Toolbox, we obtain a unique equilibrium point for the given system (2.2) as

$$\begin{aligned}
\bar{x}_1 &= \frac{\varphi_{11}}{\varphi_{12}}\varphi_a P_{vs} \\
\bar{x}_2 &= \frac{\varphi_{21}}{\varphi_{22}}\varphi_a P_{vs} \\
\bar{x}_3 &= \frac{\varphi_{31}}{\varphi_{32}}\varphi_c P_{vs} \\
\bar{x}_4 &= \frac{\varphi_{41}}{\varphi_{42}}\varphi_c P_{vs} \\
\bar{x}_5 &= \frac{\varphi_{51}}{\varphi_{52}}\varphi_c P_{vs}
\end{aligned} \tag{2.6}$$

Functions φ_{ij} are given in Appendix A.1.

Using the Jacobian linearization technique [58, 59], the system (2.2) can be linearized at the equilibrium points. The Jacobian matrices at the equilibrium point defined by $\bar{x}$, $\bar{u}$, and $\bar{I}$, corresponding to system (2.2), and represented in general as $\dot{x} = f(x, u, I)$, are

$$\left.\frac{\partial f}{\partial x}\right|_{x=\bar{x},u=\bar{u},I=\bar{I}}, \ \left.\frac{\partial f}{\partial u}\right|_{x=\bar{x},u=\bar{u},I=\bar{I}}, \ \left.\frac{\partial f}{\partial I}\right|_{x=\bar{x},u=\bar{u},I=\bar{I}} \tag{2.7}$$

where

$$\begin{aligned}
x(t) &= \bar{x} + \delta_x(t) \\
u(t) &= \bar{u} + \delta_u(t) \\
x(I) &= \bar{I} + \delta_I(t)
\end{aligned} \tag{2.8}$$

The perturbations defined in (2.8) are assumed to be small, [58, 59]. The linearized system is defined by

$$\dot{\delta}_x(t) = A\delta_x(t) + B\delta_u(t) + G\delta_I(t) \tag{2.9}$$

with the constant matrices given by

$$\begin{aligned}
A &= \left.\frac{\partial f}{\partial x}\right|_{x=\bar{x},u=\bar{u},I=\bar{I}} \in \mathbf{R}^{5\times 5}, \\
B &= \left.\frac{\partial f}{\partial u}\right|_{x=\bar{x},u=\bar{u},I=\bar{I}} \in \mathbf{R}^{5\times 2}, \\
G &= \left.\frac{\partial f}{\partial I}\right|_{x=\bar{x},u=\bar{u},I=\bar{I}} \in \mathbf{R}^{5\times 1}
\end{aligned} \tag{2.10}$$

It has been found that the matrix A is given by

$$A = \frac{\partial f}{\partial x}\bigg|_{x=\bar{x},u=\bar{u},I=\bar{I}} = \begin{bmatrix} A_1 & 0_{2\times 3} \\ 0_{3\times 2} & A_2 \end{bmatrix}\bigg|_{x=\bar{x},u=\bar{u},I=\bar{I}} \tag{2.11}$$

where

$$A_1 = \begin{bmatrix} a_{11} & a_{12} \\ a_{21} & a_{22} \end{bmatrix},\ A_2 = \begin{bmatrix} a_{33} & a_{34} & a_{34} \\ a_{43} & a_{44} & a_{43} \\ a_{53} & a_{53} & a_{55} \end{bmatrix} \tag{2.12}$$

Elements a_{ij} are given in Appendix A.2.

The matrix B is similarly obtained as

$$B = \frac{\partial f}{\partial u}\bigg|_{x=\bar{x},u=\bar{u},I=\bar{I}} = \begin{bmatrix} b_{11} & 0 \\ b_{21} & 0 \\ 0 & b_{32} \\ 0 & b_{42} \\ 0 & b_{52} \end{bmatrix} \tag{2.13}$$

with elements b_{ij} given in Appendix A.3.

The matrix G is obtained as follows

$$G = \frac{\partial f}{\partial I}\bigg|_{x=\bar{x},u=\bar{u},I=\bar{I}} = \begin{bmatrix} g_1 \\ g_2 \\ g_3 \\ g_4 \\ g_5 \end{bmatrix} = \begin{bmatrix} \frac{RTC_1}{V_A}\left(\frac{\bar{x}_1}{\bar{x}_1+\bar{x}_2} - 1\right) \\ \frac{RTC_1}{V_A}\left(\frac{\bar{x}_2}{\bar{x}_1+\bar{x}_2} - 1\right) \\ \frac{RTC_1}{2V_C}\left(\frac{\bar{x}_3}{\bar{x}_3+\bar{x}_4+\bar{x}_5} - 1\right) \\ 0 \\ \frac{RTC_1}{V_C}\left(\frac{C_2}{C_1}\left(1 - \frac{\bar{x}_5}{\bar{x}_3+\bar{x}_4+\bar{x}_5}\right) - 1 - \frac{\bar{x}_5}{\bar{x}_3+\bar{x}_4+\bar{x}_5}\right) \end{bmatrix} \tag{2.14}$$

2.3 Sliding Mode Controller Design of the Linearized PEM Fuel Cell Dynamic Model

Sliding mode control is a form of variable structure control [51], where sliding surfaces are designed such that systems trajectories exhibit desirable properties. A system using sliding mode control has been considered as a robust system, which yields to reduced system sensitivity to uncertainties and exogenous disturbances.

Sliding mode control systems have been studied in different set-ups by many researchers [51]. The controller is designed in two steps - finding the sliding surface and reaching the sliding mode. After finding sliding surfaces using the method of [51] for linear systems or the Lyapunov method for nonlinear systems [60], the design of sliding mode control is achieved as follows. Firstly, a sliding surface is defined which ensures that the system remains on a hyper-plane after reaching it from any initial condition in a finite time. Secondly, discontinuous control is designed to render a sliding mode. Approaches [48, 51, 54, 60] can be used for continuous-time sliding mode control which has been recognized as a robust control approach, which yields to reject matched disturbances and system uncertainties. The matching condition [54], provided the control input makes the system asymptotically stable, assures robustness against parametric uncertainties and exogenous disturbances.

One can use the technique in (1.34) - (1.57) where the disturbance matching condition, [54], is given by

$$\text{rank}(\begin{bmatrix} B & E \end{bmatrix}) = \text{rank}(\begin{bmatrix} B \end{bmatrix}) \tag{2.15}$$

For the state space model (2.2), our objective is to keep y_{ref} in a certain range, which means to keep $e = y - y_{ref}$ around 0. We can define a sliding surface as follows

$$s = y - y_{ref} \tag{2.16}$$

which yields

$$\dot{s} = \dot{y} - \dot{y}_{ref} = \dot{y} = \begin{bmatrix} \dot{x}_1 \\ \\ \dot{x}_3 \end{bmatrix} \tag{2.17}$$

The sliding mode control laws that satisfy $s\dot{s} < 0$ can be determined from (2.18) and (2.19), will be presented in the next section.

Several other more complicated techniques for designing sliding surfaces and sliding mode controllers can be found in the engineering literature, see for example, [61–63]. However, they are not needed for the purpose of this chapter, since with the already introduced two standard and simple sliding mode techniques we get excellent results. As it will be shown in the simulation results, the chattering phenomenon (the main problem in using sliding mode control) will be fully suppressed and the abrupt changes

of the fuel cell current (disturbance in a pretty broad range of 80A to 200A) will have no impact on hydrogen and oxygen pressures.

2.4 Linearized PEM Fuel Cell Dynamic Model and Its Control

2.4.1 Linearized Model

The numerical data taken from [4], used in this chapter, are presented in Table 2.1.

Table 2.1: Parameters Of Fuel Cell

Symbol	Parameter	Value [Unit]
R	Gas constant	0.08205 [L atm mol^{-1} K^{-1}]
T	Operating cell temperature	353 [K]
N	Number of cells	35
V_A	Anode volume	0.005 [m^3]
V_C	Cathode volume	0.010 [m^3]
k_a	Anode conversion factor	7.034×10^{-4} [mol s^{-1}]
k_c	Cathode conversion factor	7.036×10^{-4} [mol s^{-1}]
A	Fuel cell active area	232×10^{-4} [m^2]
F	Faraday constant	96,485 [A s mol^{-1}]
P_{vs}	Saturation pressure	0.3158 [atm]
Y_{O_2}	O_2 reactant factor	0.2095
Y_{N_2}	N_2 reactant factor	0.7808
Y_{H_2}	H_2 reactant factor	0.9999
$C1$	$N \cdot A/2F$	4.21×10^{-6} [m^2 mol A^{-1} s^{-1}]
$C2$	$1.2684N \cdot A/F$	1.07×10^{-5} [m^2 mol A^{-1} s^{-1}]
λ_{H_2}	H_2 stoichiometric constant	2
λ_{air}	Air stoichiometric constant	2.5
φ_a	Anode humidity constant	0.8
φ_c	Cathode humidity constant	0.9
H_{2in}	H_2 inlet flow rate	0.0611 [L s^{-1}]
H_2O_{Ain}	H_2O inlet flow rate (Anode)	0.0019 [L s^{-1}]
O_{2in}	O_2 inlet flow rate	4.5403 [L s^{-1}]
N_{2in}	N_2 inlet flow rate	0.1503 [L s^{-1}]
H_2O_{Cin}	H_2O inlet flow rate (Cathode)	0.0019 [L s^{-1}]
I	Cell current density	100 [A m^{-2}]

With the realistic numerical data in Table 2.1, we have found that the considered fuel cell system has a unique equilibrium point (steady state point) given by

$$\bar{x}(t) = \begin{bmatrix} 2.6509 & 0.0003 & 7.009 & 26.175 & 0.3390 \end{bmatrix}^T \tag{2.18}$$

The corresponding linearized system is

$$\begin{aligned}\dot{\delta}_x(t) = &\begin{bmatrix} -8.741\times10^{-7} & 0.00782 & 0 & 0 & 0 \\ -0.00102 & -0.00884 & 0 & 0 & 0 \\ 0 & 0 & -0.02767 & 0.00732 & 0.00732 \\ 0 & 0 & 0.02733 & -0.00767 & 0.02733 \\ 0 & 0 & 0.00005 & 0.00005 & -0.03508 \end{bmatrix} \delta_x(t) \\ &+ \begin{bmatrix} 9.5846\times10^{-8} & 0 \\ 8.5750\times10^{-4} & 0 \\ 0 & 2.0935\times10^{-6} \\ 0 & 2.9127\times10^{-3} \\ 0 & -6.3572\times10^{-6} \end{bmatrix} \delta_u(t) + \begin{bmatrix} 2.7255\times10^{-9} \\ -2.4384\times10^{-5} \\ -9.6493\times10^{-6} \\ 0 \\ 8.1233\times10^{-5} \end{bmatrix} \delta_I(t) \\ =&A\delta_x(t) + B\delta_u(t) + G\delta_I(t)\end{aligned} \tag{2.19}$$

By examining the eigenvalues of the matrix A we found that all of them are in the left half complex plane, so that this system is open-loop asymptotically stable. The output equation according to (2.3) has been already defined in the linear form in [4] and [6] as

$$y(t) = Cx(t) \tag{2.20}$$

with

$$C = \begin{bmatrix} 1 & 0 & 0 & 0 & 0 \\ 0 & 0 & 1 & 0 & 0 \end{bmatrix} \tag{2.21}$$

Having obtained matrices A, B, and C, we can examine the controllability and observability of the linearized system, [64]. The controllability can be examined by studying the rank of the controllability matrix defined by [64]

$$\mathbf{C_o} = \begin{bmatrix} B & AB & A^2B & A^3B & A^4B \end{bmatrix} \tag{2.22}$$

It was found that the rank of the controllability matrix is equal to 5, equal to the order of the system, $n = 5$, and hence this system is controllable. In order words, control inputs exist that can transfer the state of the system from any location in the state space to any desired location in the state space, [64]. The system observability is tested

by examining the rank of the observability matrix defined by [64]

$$\mathbf{O} = \begin{bmatrix} C \\ CA \\ CA^2 \\ CA^3 \\ CA^4 \end{bmatrix} \tag{2.23}$$

It was found that the rank of the observability matrix is equal to 5 (equal to the order of the system), and this system is also observable [64].

2.4.2 Sliding Mode Controller Design

The system in (2.19) can be divided into two subsystems as follow

$$\begin{aligned} \begin{bmatrix} \dot{\delta}_{x_1}(t) \\ \dot{\delta}_{x_2}(t) \end{bmatrix} =& \begin{bmatrix} -8.741 \times 10^{-7} & 0.00782 \\ -0.00102 & -0.00884 \end{bmatrix} \begin{bmatrix} \delta_{x_1}(t) \\ \delta_{x_2}(t) \end{bmatrix} \delta_x(t) \\ &+ \begin{bmatrix} 9.5846 \times 10^{-8} \\ 8.5750 \times 10^{-4} \end{bmatrix} \delta_{u_a}(t) + \begin{bmatrix} 2.7255 \times 10^{-9} \\ -2.4384 \times 10^{-5} \end{bmatrix} \delta_I(t) \\ =& A_1\delta_x(t) + B_1\delta_u(t) + G_1\delta_I(t) \end{aligned} \tag{2.24}$$

$$\begin{aligned} \begin{bmatrix} \dot{\delta}_{x_1}(t) \\ \dot{\delta}_{x_2}(t) \\ \dot{\delta}_{x_3}(t) \end{bmatrix} =& \begin{bmatrix} -0.02767 & 0.00732 & 0.00732 \\ 0.02733 & -0.00767 & 0.02733 \\ 0.00005 & 0.00005 & -0.03508 \end{bmatrix} \begin{bmatrix} \delta_{x_3}(t) \\ \delta_{x_4}(t) \\ \delta_{x_5}(t) \end{bmatrix} \\ &+ \begin{bmatrix} 2.0935 \times 10^{-6} \\ 2.9127 \times 10^{-3} \\ -6.3572 \times 10^{-6} \end{bmatrix} \delta_{u_c}(t) + \begin{bmatrix} -9.6493 \times 10^{-6} \\ 0 \\ 8.1233 \times 10^{-5} \end{bmatrix} \delta_I(t) \\ =& A_2\delta_x(t) + B_2\delta_u(t) + G_2\delta_I(t) \end{aligned} \tag{2.25}$$

The objective is to keep the pressure differences of hydrogen and oxygen in a certain range to protect the membrane damages. We have designed the controller to keep both pressures around 3 atm.

For the first subsystem of (2.24), there exists a nonsingular similarity transformation T_1 [51], which yields

$$\begin{aligned}\begin{bmatrix}\dot{q}_1(t)\\ \dot{q}_2(t)\end{bmatrix} &= \begin{bmatrix}-1.6346\times10^{-6} & -9.1207\\ 8.7110\times10^{-7} & -8.8370\times10^{-3}\end{bmatrix}\begin{bmatrix}q_1(t)\\ q_2(t)\end{bmatrix}\\ &+\begin{bmatrix}0\\ 7.3531\times10{-}7\end{bmatrix}(u_a(t)+dI(t))\end{aligned} \tag{2.26}$$

with $d=-2.8436\times10^{-2}$. The disturbance can be nullified using Drazenovic's invariance condition since rank($\begin{bmatrix}B_1 & G_1\end{bmatrix}$) = rank($\begin{bmatrix}B_1\end{bmatrix}$), [54, 65].

The pair $(\bar{A}_{1_{11}}, \bar{A}_{1_{12}})$ is controllable since the original system is controllable [51]. Hence, we can find a state feedback gain matrix K_1 such that $\bar{A}_{1_{11}} - K_1\bar{A}_{1_{12}}$ is asymptotically stable.

On the sliding surface [51], the system trajectory in the $(q_1(t), q_2(t))$ coordinates is expressed as

$$\begin{bmatrix}K_1 & 1\end{bmatrix}\begin{bmatrix}q_1(t)\\ q_2(t)\end{bmatrix} = \begin{bmatrix}-0.5482 & 1\end{bmatrix}\begin{bmatrix}q_1(t)\\ q_2(t)\end{bmatrix} = 0 \tag{2.27}$$

or

$$\begin{aligned}s_1(t) &= \begin{bmatrix}0.5482 & 1\end{bmatrix}T_1\begin{bmatrix}x_1(t)\\ x_2(t)\end{bmatrix} = G_1\begin{bmatrix}x_1(t)\\ x_2(t)\end{bmatrix}\\ &= 0.5482x_1(t) + 7.9622\times10^{-4}x_2(t) = 0\end{aligned} \tag{2.28}$$

in the original coordinates.

Starting with $\dot{s}_1(t) = 0$, we design the sliding mode control law for the sliding surface (2.28)

$$\dot{s}_1(t) = 0 = G_1\begin{bmatrix}\dot{x}_1\\ \dot{x}_2\end{bmatrix} = G_1A_1\begin{bmatrix}x_1(t)\\ x_2(t)\end{bmatrix} + G_1B_1(u_1(t)+dI(t)) \tag{2.29}$$

From (2.29) and using the result of (2.28), control $u_1(t)$ is obtained as

$$u_1(t) = -(G_1B_1)^{-1}G_1A_1\begin{bmatrix}x_1(t)\\ x_2(t)\end{bmatrix} - (G_1B_1)^{-1}(\gamma_1+\sigma_1)\frac{s_1(t)}{||s_1(t)||} \tag{2.30}$$

where

$$\gamma_1 = ||G_1B_1||dI_{max} \tag{2.31}$$

is required to overcome the disturbance $I(t)$ and $\sigma_1 > 0$ provides that

$$s_1(t)\dot{s}_1(t) < 0 \tag{2.32}$$

is satisfied

The second subsystem (2.25) does not satisfy Drazenovic's invariance condition. Instead of using Utkin and Young's method [51], we define the sliding surface for the second subsystem as

$$s_2(t) = y_2(t) - y_{2ref}(t) \tag{2.33}$$

similar with the method of Talj et al. [9]. Starting with $\dot{s}_2(t) = 0$, we design the sliding mode control law for the sliding surface defined in (2.33)

$$\dot{s}_2(t) = 0 = \dot{y}_2(t) = \dot{x}_3(t) = a_{33}x_3(t) + a_{34}x_4(t) + a_{34}x_5(t) + b_{32}u_c(t) + g_3I(t) \tag{2.34}$$

From (2.34), control $u_2(t)$ is obtained as

$$u_2(t) = -\frac{1}{b_{32}}(a_{33}x_3(t) + a_{34}x_4(t) + a_{34}x_5(t) + \sigma_2 + |g_3|I_{max})|s_2(t)| \tag{2.35}$$

where $\sigma_2 > 0$ is chosen to satisfy the condition

$$s_2\dot{s}_2 < 0 \tag{2.36}$$

Note that we can use the same procedure to find the sliding surface and the controller for the subsystem 1.

The simulation results are presented in Figures 2.2 and 2.3. The disturbance current waveform is presented in Figure 2.9.

In Figure 2.2, the sliding mode control law is from Utkin and Young's method [51] and in Figure 2.3, the control law is found by using $s = y_2 - y_{2ref}$. It can be noticed from Figures 2.2 and 2.3 that the pressures are kept around 3 atm after about 1 sec despite the current density changes during entire time internal of interest, from 0 to 5 seconds.

2.5 Nonlinear Sliding Mode Control for the Fifth-order PEMFC model

In the following we present the sliding mode control technique for the fifth-order nonlinear PEMFC model (2.2)-(2.3). We can rewrite the state space model (2.2) as follows

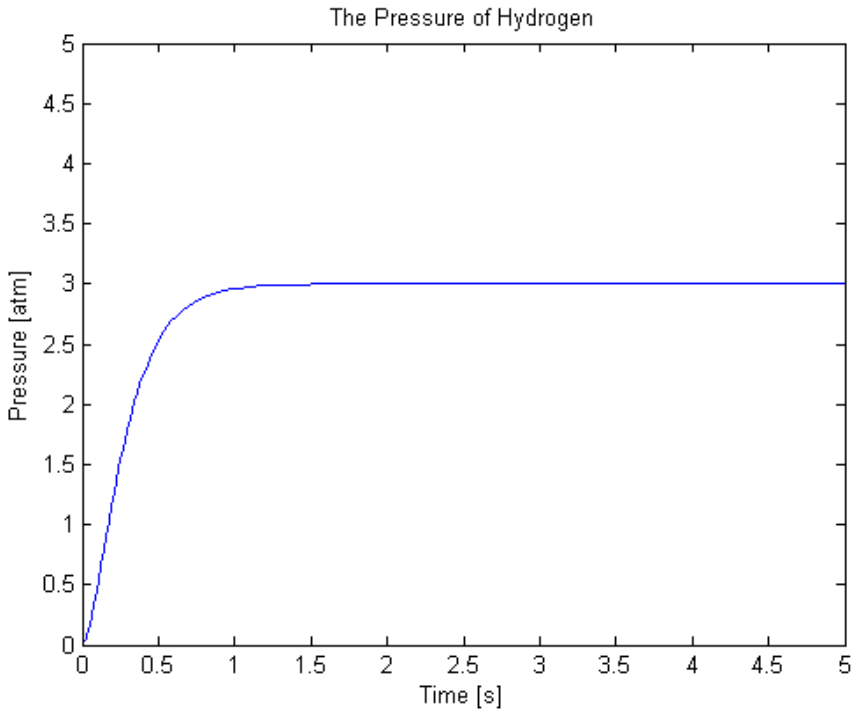

Figure 2.2: Pressure of hydrogen of the linearized system

$$\dot{x}(t) = f(x(t)) + g_1(x(t))u_a(t) + g_2(x(t))u_c(t) + p(x(t))I(t) \tag{2.37}$$

with the output equation

$$\begin{bmatrix} y_1(t) \\ y_2(t) \end{bmatrix} = \begin{bmatrix} h_1(x(t)) \\ h_2(x(t)) \end{bmatrix} = \begin{bmatrix} x_1(t) \\ x_3(t) \end{bmatrix} \tag{2.38}$$

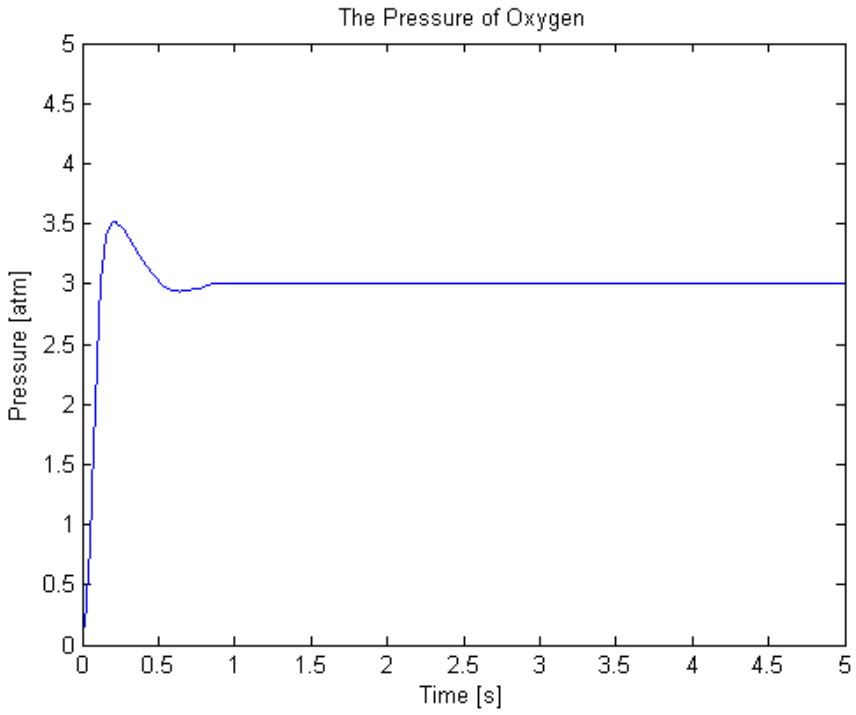

Figure 2.3: Pressure of oxygen of the linearized system

where

$$f(x(t)) = 0$$

$$g_1(x(t)) = \begin{bmatrix} \frac{RT\lambda_{H_2}}{V_A}\left(Y_{H_2} - \frac{x_1(t)}{x_1(t)+x_2(t)}\right)k_a \\ \frac{RT\lambda_{H_2}}{V_A}\left(\frac{\varphi_a p_{vs}}{x_1(t)+x_2(t)-\varphi_a p_{vs}} - \frac{x_2(t)}{x_1(t)+x_2(t)}\right)k_a \\ 0 \\ 0 \\ 0 \end{bmatrix} \tag{2.39}$$

$$g_2(x(t)) = \begin{bmatrix} 0 \\ 0 \\ \frac{RT\lambda_{air}}{V_C}\left(Y_{O_2} - \frac{x_3(t)}{x_3(t)+x_4(t)+x_5(t)}\right)k_c \\ \frac{RT\lambda_{air}}{V_C}\left(Y_{N_2} - \frac{x_4(t)}{x_3(t)+x_4(t)+x_5(t)}\right)k_c \\ \frac{RT\lambda_{air}}{V_C}\left(\frac{\varphi_a p_{vs}}{x_3(t)+x_4(t)+x_5(t)-\varphi_a p_{vs}} - \frac{x_5(t)}{x_3(t)+x_4(t)+x_5(t)}\right)k_c \end{bmatrix}$$

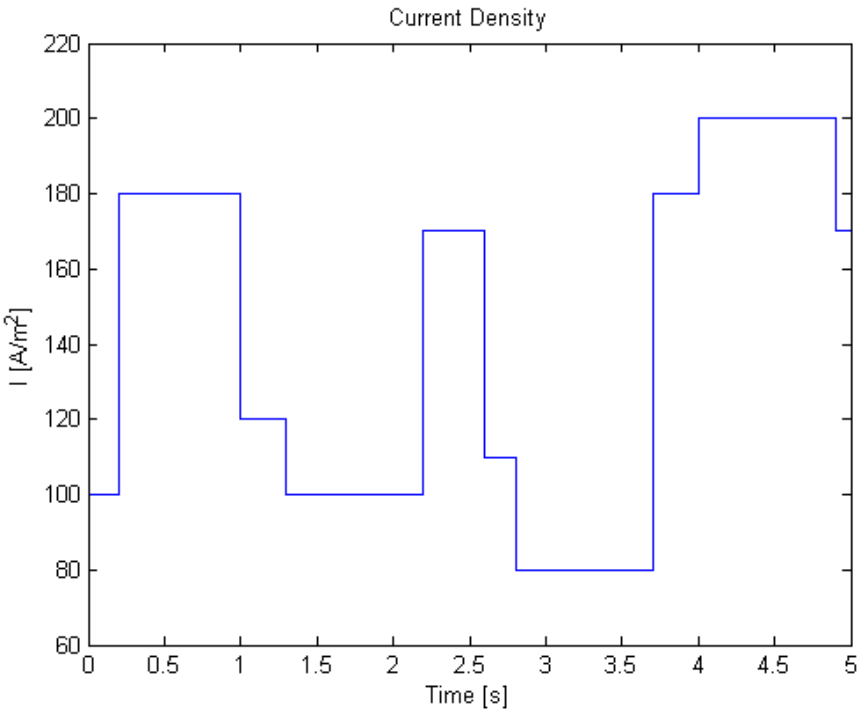

Figure 2.4: Current density changes

$$p(x(t)) = \begin{bmatrix} \frac{RTC_1}{V_A}\left(\frac{x_1(t)}{x_1(t)+x_2(t)} - 1\right) \\ \frac{RTC_1}{V_A}\left(\frac{x_2(t)}{x_1(t)+x_2(t)} - 1\right) \\ \frac{RTC_1}{2V_C}\left(\frac{x_3(t)}{x_3(t)+x_4(t)+x_5(t)} - 1\right) \\ 0 \\ \frac{RTC_1}{V_C}\left(\frac{C_2}{C_1}\left(1 - \frac{x_5(t)}{x_3(t)+x_4(t)+x_5(t)}\right) - 1 - \frac{x_5(t)}{x_3(t)+x_4(t)+x_5(t)}\right) \end{bmatrix}$$

Our goal is to design a sliding mode surface and find a control law such that the output $y(t)$ tracks a constant reference $y_{desired}$.

The sliding manifold is defined as follows since the relative degree of the system is [1 1] [59].

$$s(t) = \begin{bmatrix} s_1(t) \\ s_2(t) \end{bmatrix} = e(t) = y(t) - y_{ref} = 0 \tag{2.40}$$

$e_i(t)$ is the error between the output $y_i(t)$ and $y_{i_{desired}}$. In this definition, $s(x,t) = 0$ is a stable differential operator acting on the error between actual pressures and desired pressures of hydrogen and oxygen. Specifically, $s(t) = 0$ implies that the pressure error is zero. It can be shown that an expression for the control input appears in the equation

for $\dot{s}(t)$.

With the sliding surface defined in (2.40), we can find

$$\begin{aligned}\dot{s}(t) &= \begin{bmatrix}\dot{s}_1(t)\\ \dot{s}_2(t)\end{bmatrix} = \dot{y}(t) = \begin{bmatrix}\dot{x}_1(t)\\ \dot{x}_3(t)\end{bmatrix}\\ &= \begin{bmatrix}\frac{RT\lambda_{H_2}}{V_A}\big(Y_{H_2} - \frac{x_1(t)}{x_1(t)+x_2(t)}\big)k_a u_a(t) + \frac{RTC_1}{V_A}\big(\frac{x_1(t)}{x_1(t)+x_2(t)} - 1\big)I(t)\\ \frac{RT\lambda_{air}}{V_C}\big(Y_{O_2} - \frac{x_3(t)}{x_3(t)+x_4(t)+x_5(t)}\big)k_c u_c(t) + \frac{RTC_1}{2V_C}\big(\frac{x_3(t)}{x_3(t)+x_4(t)+x_5(t)} - 1\big)I(t)\end{bmatrix}\end{aligned} \tag{2.41}$$

Note that

$$\begin{aligned}Y_{H_2} - \frac{x_1(t)}{x_1(t)+x_2(t)} > 0\\ Y_{O_2} - \frac{x_3(t)}{x_3(t)+x_4(t)+x_5(t)} > 0\end{aligned} \tag{2.42}$$

since

$$\begin{aligned}Y_{H_2} = 0.99 \simeq 1 \geq \frac{p_{H_2}}{p_{H_2}+p_{H_2O_A}}\\ Y_{O_2} = 0.79 = \frac{p_{O_2}}{p_{O_2}+p_{N_2}} \geq \frac{p_{O_2}}{p_{O_2}+p_{N_2}+p_{H_2O_C}}\end{aligned} \tag{2.43}$$

We assume that the current change is in the region

$$0 < I_{min} < I(t) < I_{max} \tag{2.44}$$

We can design the control laws, satisfying $s_i(t)\dot{s}_i(t) < 0,\ i = 1, 2$, as follows (following the unit sliding mode control design of [51] taking into account constraint (2.44))

$$u_a(t) = \begin{cases} -\frac{C_1\big(\frac{x_1(t)}{x_1(t)+x_2(t)}-1\big)I_{min}}{\lambda_{H_2}\big(Y_{H_2}-\frac{x_1(t)}{x_1(t)+x_2(t)}\big)k_a} - \sigma_1 \mathrm{sat}\big(s_1(t)\big) & \text{if } s_1(t) > 0\\ -\frac{C_1\big(\frac{x_1(t)}{x_1(t)+x_2(t)}-1\big)I_{max}}{\lambda_{H_2}\big(Y_{H_2}-\frac{x_1(t)}{x_1(t)+x_2(t)}\big)k_a} - \sigma_2 \mathrm{sat}\big(s_1(t)\big) & \text{if } s_1(t) < 0\end{cases} \tag{2.45}$$

and

$$u_c(t) = \begin{cases} -\frac{C_1\big(\frac{x_3(t)}{x_3(t)+x_4(t)+x_5(t)}-1\big)I_{min}}{2\lambda_{air}\big(Y_{O_2}-\frac{x_3(t)}{x_3(t)+x_4(t)+x_5(t)}\big)k_c} - \sigma_3 \mathrm{sat}\big(s_2(t)\big) & \text{if } s_2(t) > 0\\ -\frac{C_1\big(\frac{x_3(t)}{x_3(t)+x_4(t)+x_5(t)}-1\big)}{2\lambda_{air}\big(Y_{O_2}-\frac{x_3(t)}{x_3(t)+x_4(t)+x_5(t)}\big)k_c} - \sigma_4 \mathrm{sat}\big(s_2(t)\big) & \text{if } s_2(t) < 0\end{cases} \tag{2.46}$$

where $\sigma_i > 0,\ i = 1, 2, 3, 4$ are used for adjusting the speed of reaching the sliding surfaces. σ_1 and σ_3 should provide $u_a(t) > 0$ and $u_c(t) > 0$ since $u_a(t)$ and $u_c(t)$ are the flow rates. σ_2 and σ_4 should be chosen according to the upper limits of $u_a(t)$ ($u_{a_{max}}$) and $u_c(t)$ ($u_{c_{max}}$).

The sliding mode control laws in (2.45) and (2.46) satisfy the following sliding mode condition [51]

$$s_i(t)\dot{s}_i(t) < 0,\ i = 1, 2 \tag{2.47}$$

This can be seen from

$$\dot{s}_1(t) = \begin{cases} \frac{RTC_1}{V_A}\big(1 - \frac{x_1(t)}{x_1(t)+x_2(t)}\big)\big(I_{min} - I(t)\big) \\ \qquad -\frac{RT\lambda_{H_2}}{V_A}\big(Y_{H_2} - \frac{x_1(t)}{x_1(t)+x_2(t)}\big)k_a\sigma_1\mathrm{sat}\big(s_1(t)\big) < 0 \quad \text{if } s_1(t) > 0 \\ \frac{RTC_1}{V_A}\big(1 - \frac{x_1(t)}{x_1(t)+x_2(t)}\big)\big(I_{max} - I(t)\big) \\ \qquad -\frac{RT\lambda_{H_2}}{V_A}\big(Y_{H_2} - \frac{x_1(t)}{x_1(t)+x_2(t)}\big)k_a\sigma_2\mathrm{sat}\big(s_1(t)\big) > 0 \quad \text{if } s_1(t) < 0 \end{cases}$$

$$\dot{s}_2(t) = \begin{cases} \frac{RTC_1}{2V_C}\big(1 - \frac{x_3(t)}{x_3(t)+x_4(t)+x_5(t)}\big)\big(I_{min} - I(t)\big) \\ \qquad -\frac{RT\lambda_{air}}{V_C}\big(Y_{O_2} - \frac{x_3(t)}{x_3(t)+x_4(t)+x_5(t)}\big)k_c\sigma_3\mathrm{sat}\big(s_2(t)\big) < 0 \quad \text{if } s_2(t) > 0 \\ \frac{RTC_1}{2V_C}\big(1 - \frac{x_3(t)}{x_3(t)+x_4(t)+x_5(t)}\big)\big(I_{max} - I(t)\big) \\ \qquad -\frac{RT\lambda_{air}}{V_C}\big(Y_{O_2} - \frac{x_3(t)}{x_3(t)+x_4(t)+x_5(t)}\big)k_c\sigma_4\mathrm{sat}\big(s_2(t)\big) > 0 \quad \text{if } s_2(t) < 0 \end{cases} \tag{2.48}$$

since

$$\begin{aligned} \frac{RTC_1}{V_A}\Big(\frac{x_1(t)}{x_1(t)+x_2(t)} - 1\Big)I &= -\frac{RTC_1}{V_A}\frac{x_2(t)}{x_1(t)+x_2(t)}I < 0 \\ \frac{RTC_1}{2V_C}\Big(\frac{x_3(t)}{x_3(t)+x_4(t)+x_5(t)} - 1\Big)I &= -\frac{RTC_1}{2V_C}\frac{x_4(t)+x_5(t)}{x_3(t)+x_4(t)+x_5(t)}I < 0 \end{aligned} \tag{2.49}$$

Note that $I(t) - I_{min} > 0$ and $I_{max} - I(t) > 0$.

The controllers in equations (2.45)-(2.46) use the state variables which are not known except for $x_1(t)$ and $x_3(t)$. Instead using nonlinear observer to observe the states, we can design the controller assuming $K_1 \le \frac{1-\frac{x_1(t)}{x_1(t)+x_2(t)}}{Y_{H_2}-\frac{x_1(t)}{x_1(t)+x_2(t)}} \le K_2$ and $K_3 \le \frac{1-\frac{x_3(t)}{x_3(t)+x_4(t)+x_5(t)}}{Y_{O_2}-\frac{x_3(t)}{x_3(t)+x_4(t)+x_5(t)}} \le K_4$.

The simplified control laws can be found as follows,

$$u_a(t) = \begin{cases} -\frac{K_1C_1I_{min}}{\lambda_{H_2}k_a} - \sigma_1\mathrm{sat}\big(s_1(t)\big) & \text{if } s_1(t) > 0 \\ -\frac{K_2C_1I_{max}}{\lambda_{H_2}k_a} - \sigma_2\mathrm{sat}\big(s_1(t)\big) & \text{if } s_1(t) < 0 \end{cases} \tag{2.50}$$

$$u_c(t) = \begin{cases} -\frac{K_3C_1I_{min}}{2\lambda_{air}k_c} - \sigma_3\mathrm{sat}\big(s_2(t)\big) & \text{if } s_2(t) > 0 \\ -\frac{K_4C_1I_{max}}{2\lambda_{air}k_c} - \sigma_4\mathrm{sat}\big(s_2(t)\big) & \text{if } s_2(t) < 0 \end{cases} \tag{2.51}$$

These *simplified* control laws (2.50)-(2.51) will be implemented in our simulation study.

Using formula (2.50), $\dot{s}_1(t)$ in equation (2.41) can be expressed as follows

$$\begin{aligned}\dot{s}_1(t) =&\frac{K_1RTC_1}{V_A}\big(Y_{H_2} - \frac{x_1(t)}{x_1(t)+x_2(t)}\big)I_{min} + \frac{RTC_1}{V_A}\big(\frac{x_1(t)}{x_1(t)+x_2(t)} - 1\big)I(t)\\ &- \frac{RT\lambda_{H_2}}{V_A}\big(Y_{H_2} - \frac{x_1(t)}{x_1(t)+x_2(t)}\big)k_a\sigma_1\text{sat}\big(s_1(t)\big)\\ =&\frac{RTC_1}{V_A}\Big(\big(Y_{H_2} - \frac{x_1(t)}{x_1(t)+x_2(t)}\big)K_1I_{min} - \big(1 - \frac{x_1(t)}{x_1(t)+x_2(t)}\big)I(t)\Big)\\ &- \frac{RT\lambda_{H_2}}{V_A}\big(Y_{H_2} - \frac{x_1(t)}{x_1(t)+x_2(t)}\big)k_a\sigma_1\text{sat}\big(s_1(t)\big) < 0\end{aligned} \tag{2.52}$$

when $s_1(t) > 0$, and

$$\begin{aligned}\dot{s}_1(t) =&\frac{K_2RTC_1}{V_A}\big(Y_{H_2} - \frac{x_1(t)}{x_1(t)+x_2(t)}\big)I_{max} + \frac{RTC_1}{V_A}\big(\frac{x_1(t)}{x_1(t)+x_2(t)} - 1\big)I(t)\\ &- \frac{RT\lambda_{H_2}}{V_A}\big(Y_{H_2} - \frac{x_1(t)}{x_1(t)+x_2(t)}\big)k_a\sigma_2\text{sat}\big(s_1(t)\big)\\ =&\frac{RTC_1}{V_A}\Big(\big(Y_{H_2} - \frac{x_1(t)}{x_1(t)+x_2(t)}\big)K_2I_{max} - \big(1 - \frac{x_1(t)}{x_1(t)+x_2(t)}\big)I(t)\Big)\\ &- \frac{RT\lambda_{H_2}}{V_A}\big(Y_{H_2} - \frac{x_1(t)}{x_1(t)+x_2(t)}\big)k_a\sigma_2\text{sat}\big(s_1(t)\big) > 0\end{aligned} \tag{2.53}$$

when $s_1(t) < 0$.

Similarly, condition (2.47) for $s_2(t)$ can be checked using formula (2.51) and equation (2.41).

For $s_2(t) > 0$, we have

$$\begin{aligned}\dot{s}_2(t) =&\frac{K_3RTC_1}{2V_C}\big(Y_{O_2} - \frac{x_3(t)}{x_3(t)+x_4(t)+x_5(t)}\big)I_{min}\\ &\qquad + \frac{RTC_1}{2V_C}\big(\frac{x_3(t)}{x_3(t)+x_4(t)+x_5(t)} - 1\big)I(t)\\ &- \frac{RT\lambda_{air}}{V_C}\big(Y_{O_2} - \frac{x_3(t)}{x_3(t)+x_4(t)+x_5(t)}\big)k_c\sigma_3\text{sat}\big(s_2(t)\big)\\ =&\frac{RTC_1}{2V_C}\Big(\big(Y_{O_2} - \frac{x_3(t)}{x_3(t)+x_4(t)+x_5(t)}\big)K_3I_{min}\\ &\qquad - \big(1 - \frac{x_3(t)}{x_3(t)+x_4(t)+x_5(t)}\big)I(t)\Big)\\ &- \frac{RT\lambda_{air}}{V_C}\big(Y_{O_2} - \frac{x_3(t)}{x_3(t)+x_4(t)+x_5(t)}\big)k_c\sigma_3\text{sat}\big(s_2(t)\big) < 0\end{aligned} \tag{2.54}$$

and for $s_2(t) < 0$, we obtain

$$\begin{aligned}\dot{s}_2(t) =& \frac{K_4 RTC_1}{2V_C}\big(Y_{O_2} - \frac{x_3(t)}{x_3(t)+x_4(t)+x_5(t)}\big) I_{max} \\ &+ \frac{RTC_1}{2V_C}\big(\frac{x_3(t)}{x_3(t)+x_4(t)+x_5(t)} - 1\big) I(t) \\ &- \frac{RT\lambda_{air}}{V_C}\big(Y_{O_2} - \frac{x_3(t)}{x_3(t)+x_4(t)+x_5(t)}\big) k_c \sigma_4 \text{sat}\big(s_2(t)\big) \\ =& \frac{RTC_1}{2V_C}\Big(\big(Y_{O_2} - \frac{x_3(t)}{x_3(t)+x_4(t)+x_5(t)}\big) K_4 I_{max} \\ &- \big(1 - \frac{x_3(t)}{x_3(t)+x_4(t)+x_5(t)}\big) I(t)\Big) \\ &- \frac{RT\lambda_{air}}{V_C}\big(Y_{O_2} - \frac{x_3(t)}{x_3(t)+x_4(t)+x_5(t)}\big) k_c \sigma_4 \text{sat}\big(s_2(t)\big) > 0\end{aligned} \tag{2.55}$$

K_1, K_2, K_3, and K_4 can be found explicitly from simulations using control laws of (2.45)-(2.46). Controls in (2.45), (2.46), (2.50), and (2.51) are applied to the linearized model.

2.6 Numerical Example

The numerical data taken from [4], used in this chapter, are presented in Table 2.1. The objective is to keep the pressure differences between hydrogen and oxygen in a certain range to protect the membrane damages with certain range of control inputs: 0 slpm[1] < input flow rate of hydrogen or oxygen ([slpm]) < 10 slpm. We have designed the controller to keep both pressures around 3 atm. We have also required that controller reduces the pressure differences between hydrogen and oxygen during the transient state.

With the realistic numerical data in Table 2.1, the simulation results using all state variables (formulas (2.45)-(2.46)) are presented in Figures 2.5 and 2.6 with the disturbance current waveform presented in Figure 2.9. It can be noticed from Figures 2.5 and 2.6 that pressures are kept around 3 atm after reaching desired values after about 19 seconds despite the current changes. Note that the PEMFC has a slow start (it takes some time to reach the steady state due to slow chemical processes) so that the fact that it takes about 19 seconds for pressures of hydrogen and oxygen to reach their

[1]slpm stands for the standard liter per minute unit.

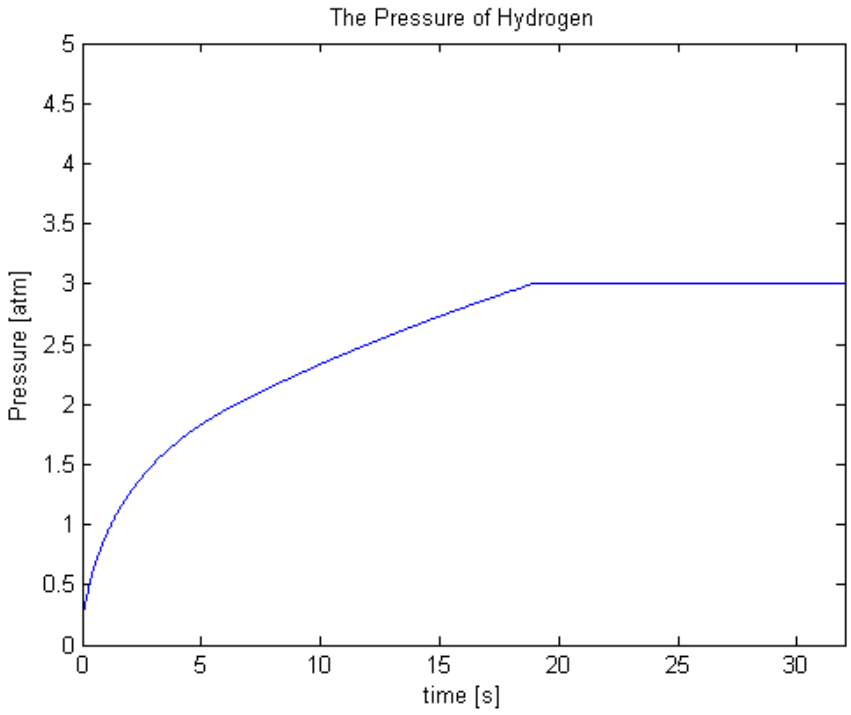

Figure 2.5: Pressure of hydrogen for the nonlinear system using (2.45)

steady state values has negligible impact on the fuel cell operation. The corresponding control laws are presented in Figures 2.7 and 2.8. After entering the sliding mode at about 19 seconds, (to keep pressures of hydrogen and oxygen at 3 atm) the flow rate changes are needed to make $s_i(t) = 0,\ i = 1, 2$, at some points as seen in the zoom-in of the plots in Figures 2.7 and 2.8.

Since we only know $x_1(t)$ and $x_3(t)$ from the output equation, using the simplified controllers in equations (2.50)-(2.51), the pressures of hydrogen and oxygen are regulated. The simulation results with $K_1 = 1.0003$, $K_2 = 1.2$, $K_3 = 1.3715$, and $K_4 = 1.3833$, are shown in Figures 2.10-2.13 that indicate pressures and controllers have very similar trajectories as those of Figures 2.5-2.8.

In the approach of [4], whenever changes of the stack current happen, the waveform looks like the one presented in Figure 2.14. For the actual simulation results of [4], see the corresponding Figures 9 and 10 from that paper. When the sliding mode control technique of this chapter is used, no ripples appear as evident from Figures 2.5, 2.6, 2.10, and 2.11. The sliding mode controller presented has a good feature to keep hydrogen

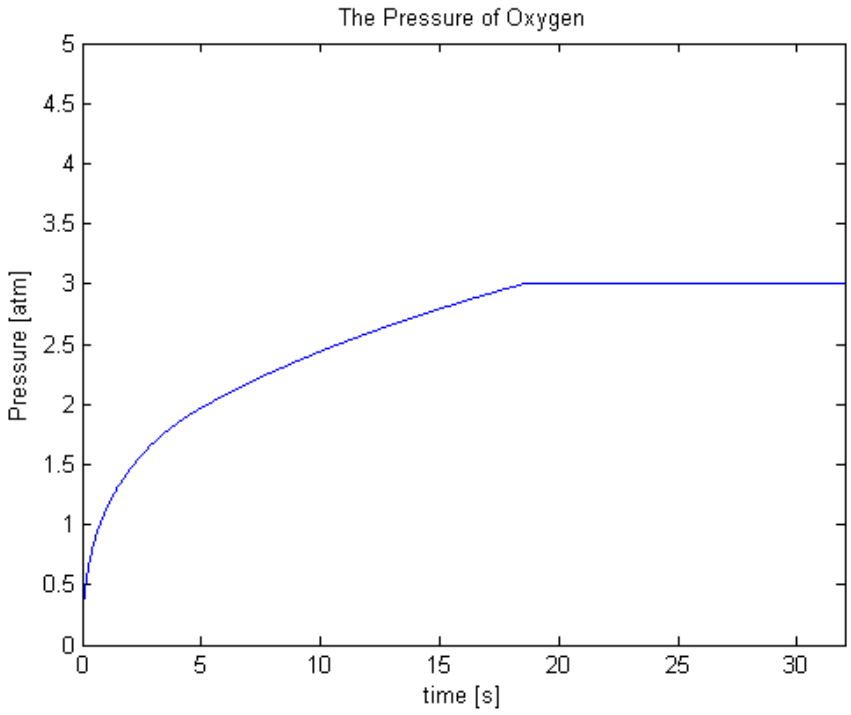

Figure 2.6: Pressure of oxygen for the nonlinear system using (2.46)

and oxygen pressures close to each other despite the current changes.

2.7 Conclusion

We have applied the sliding mode strategy for the linearized model of the well-known nonlinear model of the proton exchange membrane fuel cell obtained using the MATLAB Symbolic Tool Box. For this well defined model, which has uniqueness of steady state variables, asymptotic stability, controllability, and observability, the sliding mode technique copes very well with the cell current changes $I(t)$, and keeps very precisely the pressures of hydrogen and oxygen at the desired (required) values.

In the future, more accurate models of PEMFCs could be and should be developed since "the chemical kinetics in PEMFCs is fast, and the limiting factors in PEMFCs are water and heat transport. And, in the state space modeling in [4], the electro-chemical reactions in the catalysts layers and the species transport in the membrane electrolyte assembly are not considered." We believe that our approach with some modifications will be applicable to more complex modes of PEMFCs than the one derived in [4].

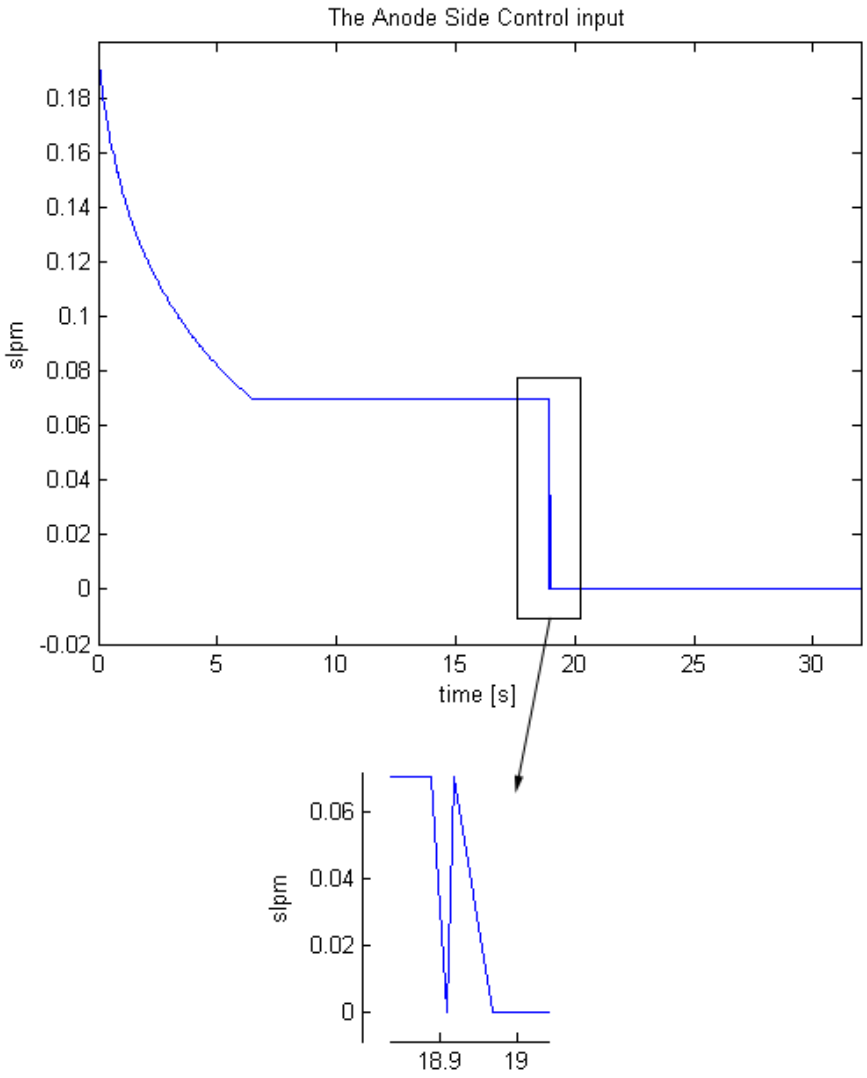

Figure 2.7: Control input at the anode side using (2.45)

The main results of this section (chapter) were reported by the author in [66, 67]

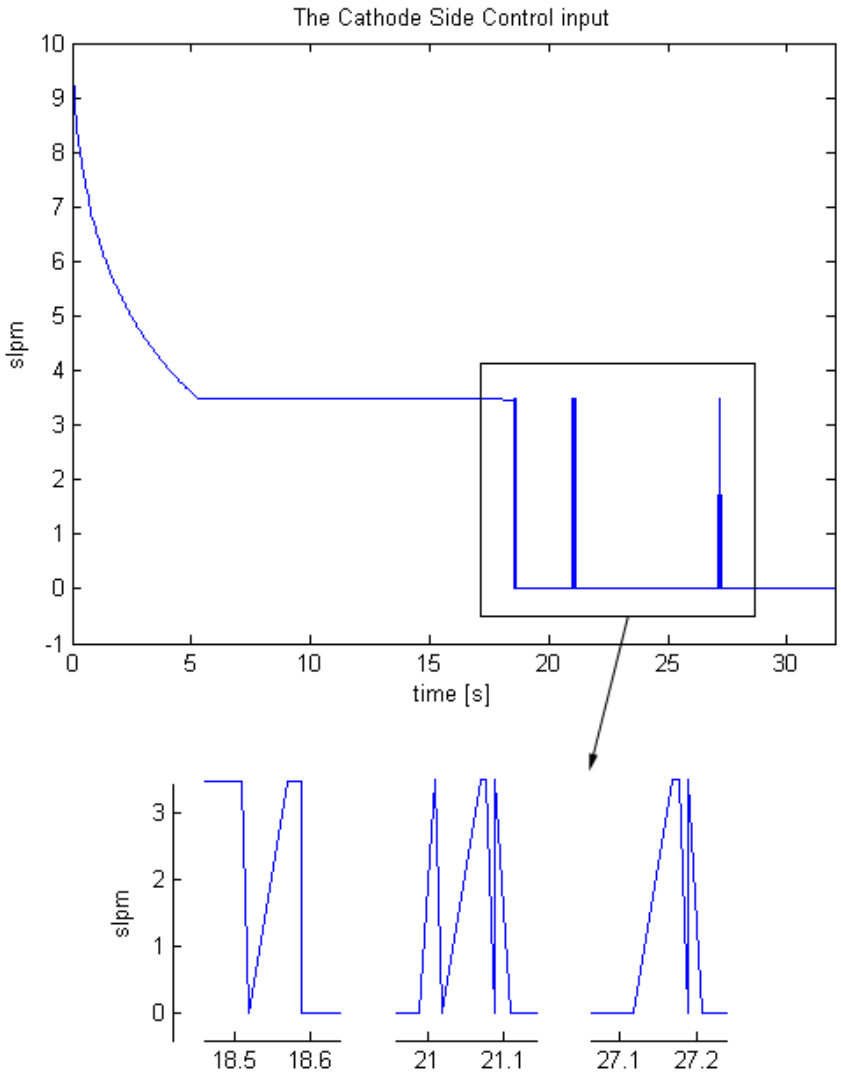

Figure 2.8: Control input at the cathode side using (2.46)

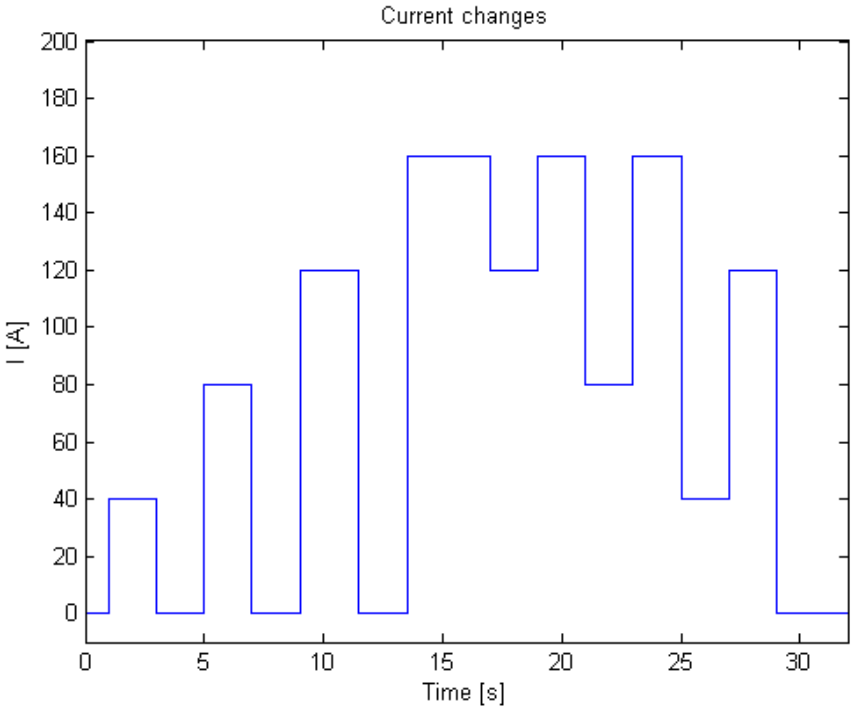

Figure 2.9: Current changes

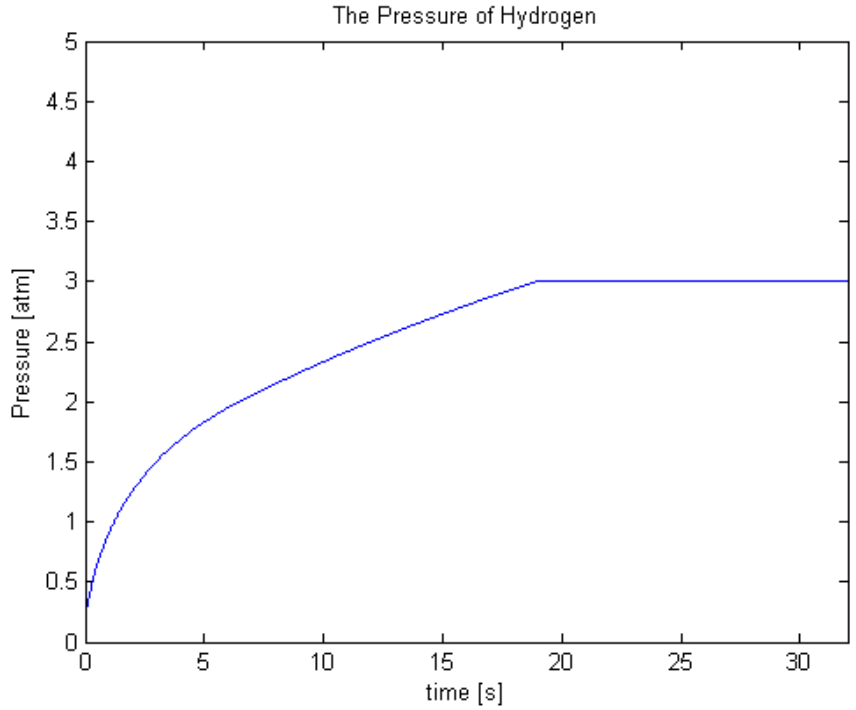

Figure 2.10: Pressure of hydrogen for the nonlinear system using (2.50)

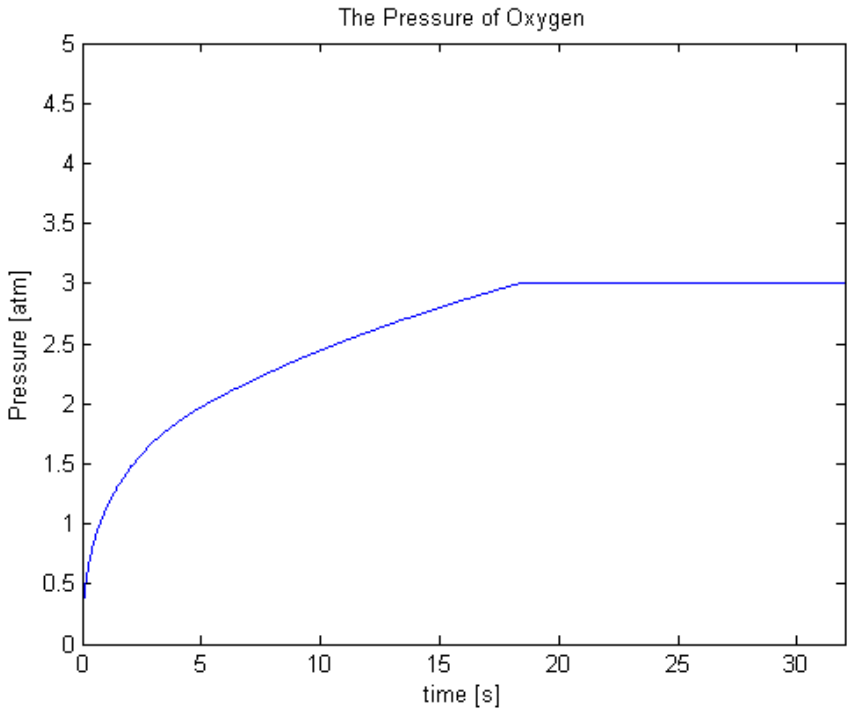

Figure 2.11: Pressure of oxygen for the nonlinear system using (2.51)

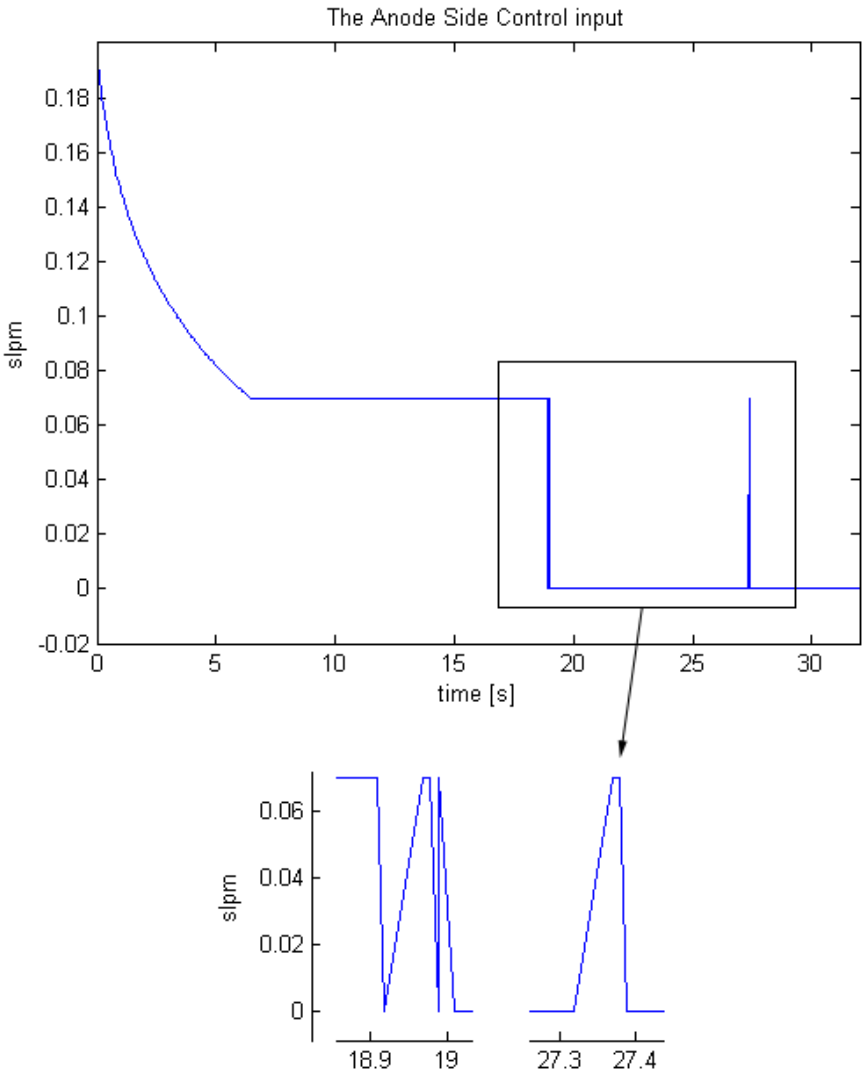

Figure 2.12: Control input at the anode side using (2.50)

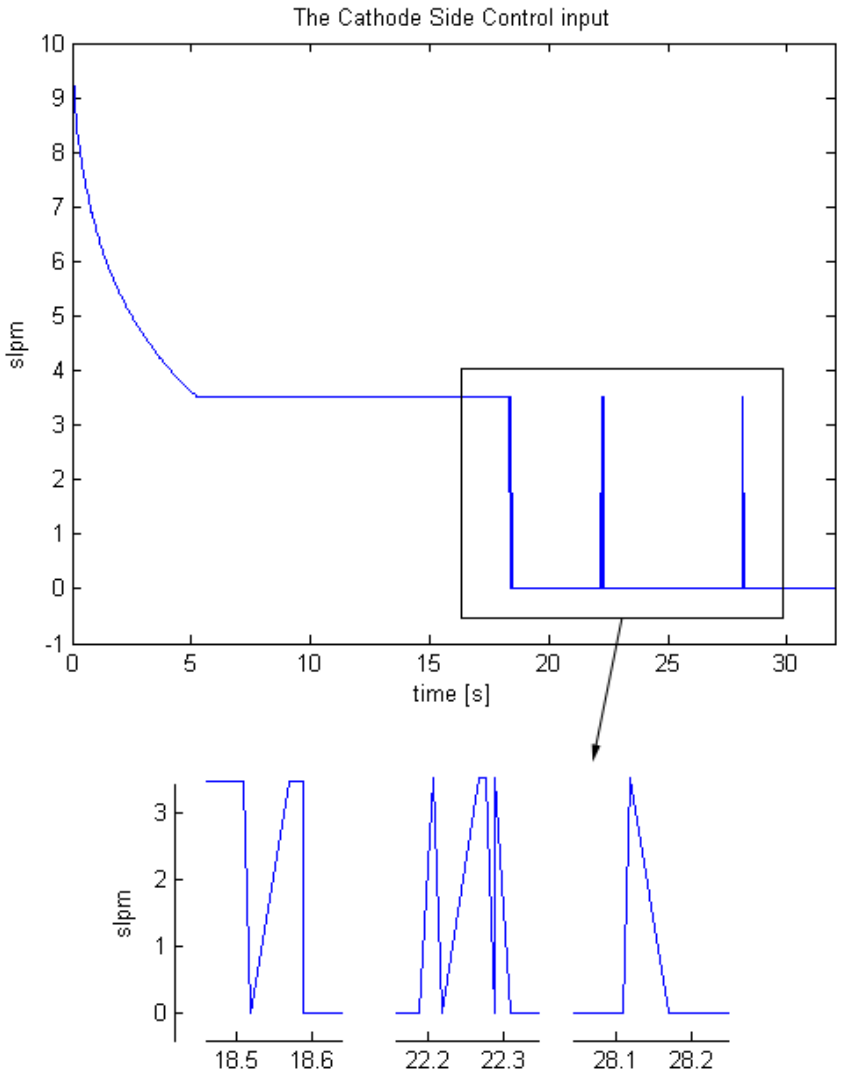

Figure 2.13: Control input at the cathode side using (2.51)

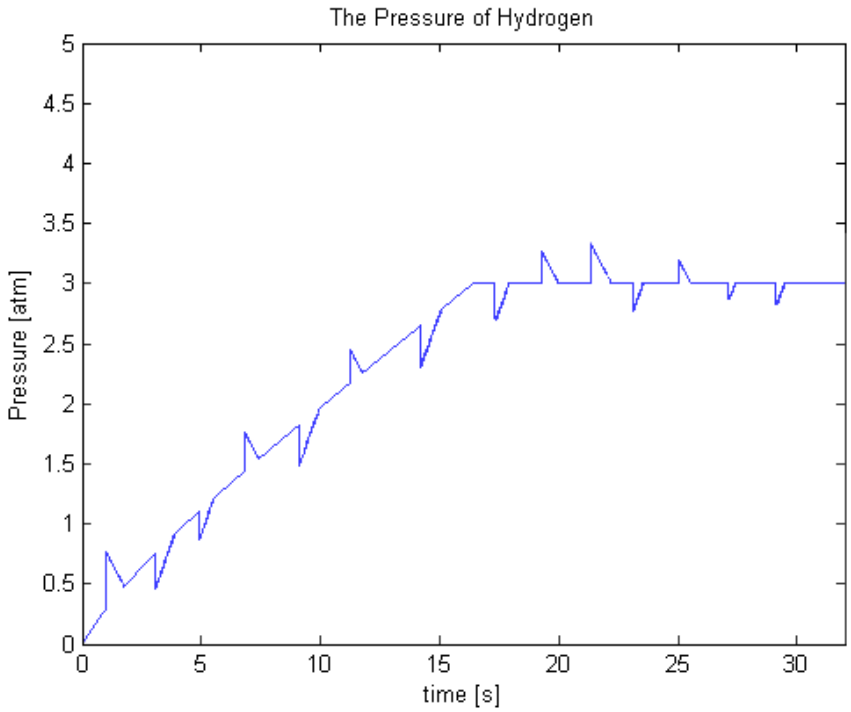

Figure 2.14: Example of pressure changes with ripples (using the method of [4])

Chapter 3

Modeling and Control of Solid Oxide Fuel Cells

3.1 Introduction

Fuel cells are electrochemical energy devices that convert chemical energy into electricity, heat, and water without generating carbon dioxide. Fuel cells are one of the most promising clean energy technologies among renewable energy sources since they have high efficiency and low environmental pollution. Among various fuel cells, the proton exchange membrane fuel cells (PEMFCs) and the solid oxide fuel cells (SOFCs) are identified as most significant fuel cells. Especially, PEMFCs are fully understood, and most developed, but SOFCs are not, since they have not become a mainstream power generation technology yet. SOFCs are very promising future energy sources for electric power distribution (commercial and industrial) since they can generate large amounts of electric power, and in addition provide a lot of heat ($1,000\,^{\circ}\mathrm{C}$) so that they can be used also for heating.

This chapter will focus on SOFCs. A large amount of literature of SOFCs has been published in the last decade, but most of them has focused on electrochemical characteristics such as cell components, new materials, reaction mechanisms, etc. This chapter will present a review of the dynamic characteristics of SOFCs for the purpose of dynamic simulation and control and the control strategies for temperature and pressure in fuel cell stacks are proposed.

3.2 SOFC Principles

SOFCs use a special solid oxide cermet, mostly yttria-stabilized zirconia (YSZ), as the electrolyte and work at intermediate temperature range, i.e. $600-1,000\,^{\circ}\mathrm{C}$ to maintain

ionic conductivity of the electrolyte. This temperature is used through turbine generators to get higher overall efficiency but not too harsh to materials. These characteristics will make SOFCS significant in the future for eigher million watts scale stationary power generation or kilo watts scale truck auxiliary power units (APU), including residential power and heat supply [68]. The efficiencies of stand-alone SOFCs are about $40-50\%$ and those of pressurized by hybrid gas turbine SOFCs are about $60-70\%$.

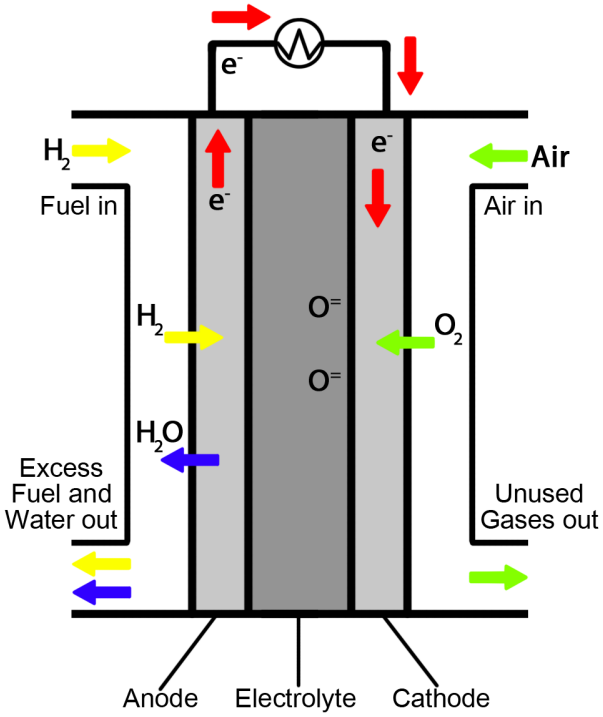

Figure 3.1: Solid Oxide Fuel Cell

A typical SOFC is a triode which is composed of anode, cathode, and electrolyte as shown in Figure 3.1. Hydrogen rich fuels and air are continuously fed into the anode side and the cathode side, respectively. The electrolyte only allows certain types of ions (O^{2-}) to pass through it, while the electrons are collected and generate electricity to an outside electrical circuit.

Besides the planar type of SOFC, a tubular type of SOFC has been developed, which is composed of several tubular SOFC stacks presented in Figures 3.2 and 3.3.

The chemical reactions inside the cell that converts chemical energy of fuel and

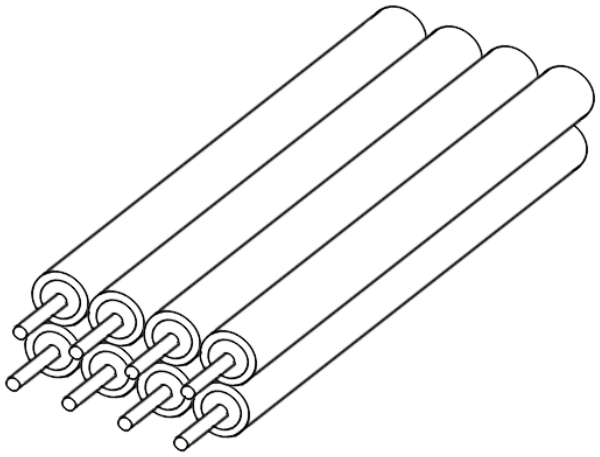

Figure 3.2: Tubular SOFC design of Siemens-Westinghouse

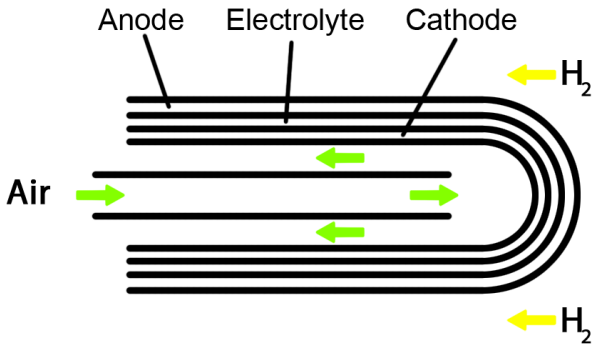

Figure 3.3: A Cell Cross-section in [5]

oxidant to electrical energy are as follow [68]

$$\begin{aligned} &\text{anode}: H_2 + O^{2-} \rightarrow H_2O + 2e^- \\ &\text{cathode}: \frac{1}{2}O_2 + 2e^- \rightarrow O^{2-} \end{aligned} \tag{3.1}$$

The difference of potential energy between anode and cathode is called electromotive force (EMF) or open circuit voltage (OCV). In the ideal situation, the OCV is defined using the Gibbs free energy released $\Delta\bar{g}_f = -2FE$, i.e.

$$E = -\frac{\Delta\bar{g}_f}{2F} \tag{3.2}$$

The OCV is well studied, both theoretically and experimentally, and defined using partial pressures and temperature through the Nernst equation [68]

$$E = E^0 + \frac{RT}{2F}\ln\left(\frac{P_{H_2}P_{O_2}^{0.5}}{P_{H_2O}}\right) \tag{3.3}$$

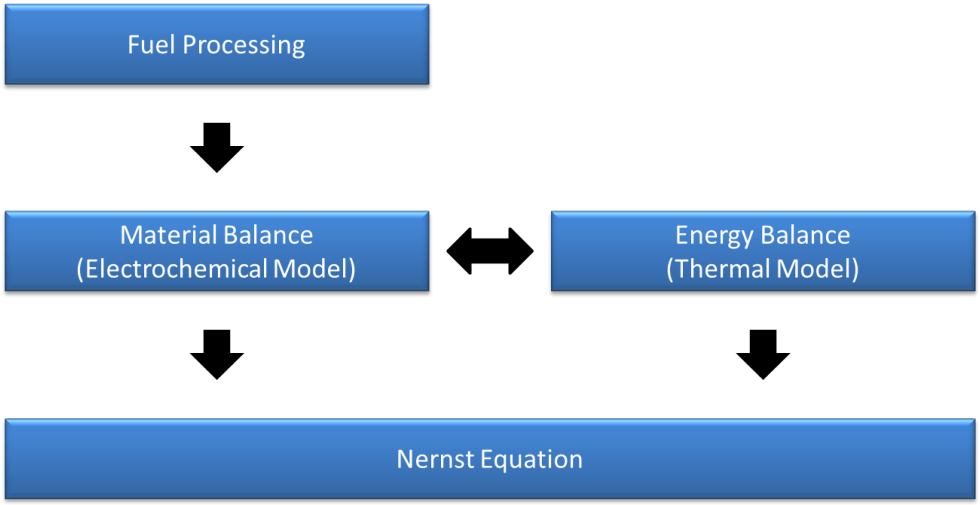

Figure 3.4: SOFC Modeling Block Diagram

When the fuel cells are connected through an external circuit, the relation between current and the fuel consumption rate are defined as follows [68]

$$i = 2FJ_{H_2} = 2FJ_{H_2O} = 4FJ_{O_2} \tag{3.4}$$

The output voltage modeled in the steady state form [68]

$$V = E - V_{activation} - V_{ohmic} - V_{concentration} \tag{3.5}$$

where $V_{activation}$ is activation loss, V_{ohmic} is ohmic loss, and $V_{concentration}$ is concentratino loss.

3.3 SOFC Modeling

The SOFC system includes a fuel processing unit or the reformer and a fuel stack. The SOFC system dynamic model can be derived using several sub-models such as fuel processing unit model, fuel cell stack model, and thermal model. An overview of a typical SOFC system is described in Figure 3.4.

3.3.1 Fuel Processing Unit Model

Even though H_2 is used for a main fuel, the fuel of SOFC can be Syngas, which is a mixture of CH_4, H_2, CO, H_2O, and CO_2 if a reforming/shilfting reaction is considered [69–73]. CH_4 and H_2O generate H_2 and CO which directly participate in the

electrochemical reaction thorough reforming/shifing reaction as follows

$$\begin{aligned} &\text{Reforming:} \quad \mathrm{CH_4 + H_2O \rightleftharpoons 3H_2 + CO} \\ &\text{Shifting:} \qquad \mathrm{CO + H_2O \rightleftharpoons H_2 + CO_2} \end{aligned} \tag{3.6}$$

A simple mathematical model of the reformer to generate hydrogen through reforming methane can be written [69, 70]

$$\frac{N_{H_2}^{in}}{N_f} = \frac{CV}{\tau_1 s + 1} \tag{3.7}$$

where $N_{H_2}^{in}$ is the gas flow rate of H_2, N_f is the natural gas flow rate, CV is the conversion factor, and τ_1 is the reformer time constants.

3.3.2 Material Balance: Electrochemical Model

From the perspective of control relevant models, Hall and Colclaser studied the transient behavior of SOFCs in 1999 [74]. In 2000, Padulles et al. [57] considered the dynamic performance of a SOFC stack. After the model of [57], SOFC stacks modes have been presented in [69, 75–87], based on the model of Padulles et al. [57]. The physical processes of SOFC via a block diagram are interpreted in [57]. The authors have considered partial pressures on the triple phase boundary in terms of current and fuel supply from the control perspective. The model they proposed is a choked, isothermal, lumped system. This model becomes the foundation of lumped dynamic modeling in fuel cells. They have proposed the model with the following assumptions.

Assumption 3.3.1.

- *The gasses are ideal.*
- *The stack is fed with hydrogen and air.*
- *The gas transport channels have a fixed volume, but their lengths are small.*
- *The temperature is stable.*
- *The only loss in the fuel cells is ohmic.*
- *The Nernst equation can be applied.*

The partial pressure of H_2 can be modeled as follows [57]

$$\frac{d}{dt}P_{H_2} = \frac{RT}{V_{an}}\left(q_{H_2}^{in} - q_{H_2}^{out} - q_{H_2}^{r}\right) \tag{3.8}$$

where $q_{H_2}^{in}$, $q_{H_2}^{out}$, and $q_{H_2}^{r}$ are input flow, output flow, and hydrogen flow that react [$\text{kmol} \cdot \text{s}^{-1}$], respectively.

We can extend the result to the other chemical reactions. Under the assumption of the ideal gas law

$$PV = nRT \tag{3.9}$$

where P is pressure, V is the volume, n is the number of moles, R is the universal gas constant, and T is the temperature, the reaction between the pressure change rate and the molar flow can be found as follows

$$\frac{d}{dt}P = \frac{RT}{V}N \tag{3.10}$$

where $N = \frac{d}{dt}n$ represents the molar flow [kmol/s]. We get three differential equations, for hydrogen at the anode side,

$$\frac{d}{dt}P_{H_2} = \frac{RT}{V_a}\left(N_{H_2}^{in} - N_{H_2}^{out} + N_{H_2}^{react}\right) \tag{3.11}$$

for water vapor at the anode side,

$$\frac{d}{dt}P_{H_2O} = \frac{RT}{V_a}\left(- N_{H_2O}^{out} + N_{H_2O}^{react}\right) \tag{3.12}$$

and for oxygen at the cathode side,

$$\frac{d}{dt}P_{O_2} = \frac{RT}{V_c}\left(N_{O_2}^{in} - N_{O_2}^{out} + N_{O_2}^{react}\right) \tag{3.13}$$

Equations (3.11) - (3.13) can be expressed as follows

$$\begin{aligned}
\frac{d}{dt}P_{H_2} &= \frac{RT}{V_a}\left(N_{H_2}^{in} - N_{H_2}^{out} + 2K_r I_{fc}(t)\right) \\
\frac{d}{dt}P_{H_2O} &= \frac{RT}{V_a}\left(- N_{H_2O}^{out} + 2K_r I_{fc}(t)\right) \\
\frac{d}{dt}P_{O_2} &= \frac{RT}{V_c}\left(N_{O_2}^{in} - N_{O_2}^{out} + K_r I_{fc}(t)\right)
\end{aligned} \tag{3.14}$$

where $K_r = \frac{N_0}{4F}$ is a constant defined for modeling purpose [$\text{kmol} \cdot \text{s}^{-1} \cdot \text{A}^{-1}$] calculated via the basic electrochemical relationship where N_0 is the number of cells, F is the Faraday's constant, and I is the stack current.

For fuel cell stack protection, cell utilization (u_f), which should be kept between 0.7 and 0.9, is defined as follows [76, 88]

$$u_f = \frac{N_{H_2}^{in} - N_{H_2}^{out}}{N_{H_2}^{in}} = \frac{N_{H_2}^{react}}{N_{H_2}^{in}} \tag{3.15}$$

If $u_f < 0.7$ (underused fuel), the fuel cell voltage would rise rapidly, and if $u_f > 0.9$ (overused fuel), there exists a permanent damage to the cells because of fuel starvation.

3.3.3 Energy Balance: Thermal Model

Sedghisigarchi and Feliachi [76] have considered temperature dynamics as well as the species dynamics. The model set-up is similar to that of Padulles et al [57], but in addition they introduced the energy balance equation for the stack temperature as follows

$$M_p C_p \frac{dT}{dt} = \Sigma Q_i = Q_{fuel} + Q_{air} + Q_{rad} + Q_{gen} \tag{3.16}$$

where M_p is the mass of the cell unit, C_p is the heat capacity of the cell unit, T is the stack temperature, V_e is the volume of the cell unit, Q_{fuel} is the convective heat transfer to fuel, Q_{air} is the convective heat transfer to air, Q_{rad} is the radiation heat between cell unit and separators, and Q_{gen} is the generated electric power.

The convective heat transfers for fuel and air are calculated as follows based on thermal models of the dynamic models in [88–91]

$$\begin{aligned} Q_{fuel} &= A_{fuel} h_{fuel} (T - T_{an}) \\ Q_{air} &= A_{air} h_{air} (T - T_{ca}) \end{aligned} \tag{3.17}$$

where the heat transfer coefficients h are functions of the Nusselt factor [89] as

$$h = \frac{K_c N_u}{D_h} \tag{3.18}$$

T_{an} and T_{ca} represent the anode and cathode cell temperatures, respectively, and K_c is the gas conductivity, N_u is set to 4 according to [92], and D_h is the hydraulic diameter. The radiation heat transfer is defined in [88–91]

$$Q_{rad} = F_v \sigma (T^4 - T_s^4) \tag{3.19}$$

where F_v is the radiation view factor and σ is the Stefan-Boltzmann constant. In equations (3.17) and (3.19), T_{an}, T_{ca}, and T_s are calculated as [88, 89, 91]

$$\begin{aligned} M_{an}C_{an}\frac{dT_{an}}{dt} &= \Sigma Q_{an} \\ M_{ca}C_{ca}\frac{dT_{ca}}{dt} &= \Sigma Q_{ca} \\ M_sC_s\frac{dT_s}{dt} &= \Sigma Q_s \end{aligned} \tag{3.20}$$

In [80], Jurado has improved the thermal model in [75] as follows,

$$\begin{aligned} M_pC_P\frac{dT}{dt} =& N_{ta}^{in}\left[\sum_i^{\xi} x_{ai}^{in}\left(\bar{h}_{ai}^{in}-\bar{h}_i\right)\right]-\sum_i^{\xi}\bar{h}_iR_{ai} \\ &+ N_{tc}^{in}\left[\sum_i^{\xi} x_{ci}^{in}\left(\bar{h}_{ci}^{in}-\bar{h}_i\right)\right]-\sum_i^{\xi}\bar{h}_iR_{ci}-P_{dc} \end{aligned} \tag{3.21}$$

where M and C_P are the mass and heat capacities of the cell unit, N_{ta}^{in} and N_{tc}^{in} are anode and cathode total inlet molar flows, x_{ai}^{in} and x_{ci}^{in} are anode and cathode inlet mole fractions, $\bar{h}_{ai}^{in}$ and $\bar{h}_{ai}^{in}$ are anode and cathode inlet partial molar enthalpies, $\bar{h}_i$ is the partial molar enthalpy at stack temperature, R_{ai} and R_{ci} are anode and cathode total rates of production of species, ξ is total gas components in anode or cathode, and P_{dc} is stack dc power. The partial molar enthalpy under the ideal gas supposition is calculated using

$$\bar{h}_i = \bar{h}_i^{ref} + \int_{T_{ref}}^{T} c_{p,i}(u)du \tag{3.22}$$

and the coefficients of the specific heats $c_{p,i}$ are encountered in standard reference tables.

3.3.4 Operation Voltage - Nernst's Equation

In the previous section, the stack voltage is obtained like in (3.5) [68]

$$V = E - V_{activation} - V_{ohmic} - V_{concentration} \tag{3.23}$$

The activation loss $V_{activation}$ is the voltage loss due to the rate of reactions on the surface of the electrodes. Using Butler-Volmer equation [93], the activation loss is described as follows,

$$i = i_0\left\{\exp\left(\beta\frac{nF\eta_{act}}{RT}\right)-\exp\left[-\left(1-\beta\right)\frac{nF\eta_{act}}{RT}\right]\right\} \tag{3.24}$$

The stack voltage of (3.5), considering only the static response, can be written as follows [68]

$$\begin{aligned} V =& E - V_{activation} - V_{ohmic} - V_{concentration} \\ =& E - iR_{in} - A\ln\left(\frac{i}{i_0}\right) - B\ln\left(1 - \frac{i}{i_l}\right) \end{aligned} \tag{3.25}$$

where i is the cell current, R_{in} is the inheritance resistance of the fuel cell, i_0 is the exchange current, i_l is the limiting current, and A and B are coefficients. The exchange current i_0 is important for weighing the activity of catalyst reaction and the limiting current i_l is used up at a rate equal to its maximum supply rate.

The ohmic loss V_{ohmic} is the voltage drop from the internal resistances in the electrolyte. The dynamics was modeled using an equivalent RC circuit proposed in [68]. In 2005, Qi et al. [94] modeled the ohmic loss by considering the effect of duoble layer capacitance and inherent resistance.

The concentration loss $V_{concentration}$ is the voltage loss from the reduction in concentration gases or the transport of mass of oxygen and hydrogen. This voltage drop occurs at the triple phase boundary (tbp), which is the interface between the electrode and the electrolyte. In [57], Padulles et al. showed the impact of current and fuel supply on partial pressures on tpb by treating current as a dynamic model input. In [94], Qi et al. adopted Fick's Law [95] and proposed a dynamic model using a partial differential equation.

3.4 SOFC Control

The objectives of SOFC control can be defined as follows [57, 75, 96]

- Maintain the required power output to its desired level
- Keep the maximum cell temperature below the upper bound
- Keep the fuel utilization within optimal operating limits for all power outputs

To achieve the above objectives, power can be controlled by controlling the fuel and air flow rates. An override temperature controller also can be used to keep the cell

temperature under the maximum limit. Depending on the objective, current density or temperature can be considered as disturbances.

Mainly, two controllers, Model Predictive Controller and PID controller, are used for a SOFC system.

Several literatures have focused on using the Model Predictive Controller (MPC) for SOFC [69, 70, 79, 80, 84, 85, 96–100] since MPC has good features for process control. The main objective is to control the output power, fuel utilization and temperature by manipulating the current, fuel and air flow rates. Jurado [79, 80] has presented a method for identification of the SOFC model based on the model of Padulles et al. [57] using a Hammerstein model and applied a predictive controller using fuzzy Hammerstein models which are special kinds of nonlinear systems where the nonlinear block is static and is followed by a linear system. Wang et al. [97] have developed a data driven MPC. Wu et al. [69] applied a fuzzy model to build MPC and Wu et al. [70] used MPC to control the voltage and keep the fuel utilization within a certain range. In [84], Hue et al. have proposed model predictive control for the model of [83]. Wu et al. [69] have presented a nonlinear predictive controller based on a GA-RBF neural network model to track the voltage of the SOFC to guarantee the fuel utilization to operate within a safe range.

The other controller, PID controller, is used to handle the abrupt voltage changes in the transient operation and to reach the target load efficiently. In [101], Aguiar et al. have considered two controllers, which are for fuel and air flow rates proportional to the current density disturbance and another and for temperature using a typical feedback PID. The model implemented in [102] is used considering mass and energy balances, electrochemical reaction, and temperature. Inui et al. [103] have proposed a cell temperature control method by optimizing the parameters of the air utilization and the inlet gas temperature fore each average current density. Li et al. [77] have designed a constant utilization controller for controlling the input hydrogen fuel in proportion to the stack current then designed a constant voltage controller adding external voltage-control loop. Kaneko et al. [104] have considered two controllers for a fluctuating biomass gas fueled SOFC and a micro gas turbine hybrid system.

The first one is to control power output by manipulating the flow rate of biomass gas and the second one is to control the temperature adjusting a bypass valve around the recuperator. Kandepu et al. [105] have developed a lumped dynamic SOFC model and designed controllers for the fuel flow rate and the temperature with the current density treated as a disturbance. The nonlinear model is linearized with its nominal values and decentralized PI controllers are applied. In [106], the authors have proposed a special control strategy developed for rapid load following and applied the result to the system in [107]. Stiller et al. [108] have implemented the stable region of a SOFC-GT system and controllers for fuel utilization, fir flow, temperature to provide safe operation of the system, quick load-following and high efficiency, long lifetime of the fuel cell, and governing external influence. Sorrentino et al. [109] have developed a control-oriented model considering electrochemical reaction, electric potential balance, material balance, and energy balance and proposed a PI controller for a planar SOFC. Hajimolana and Soroush have designed a controller to keep the average stack temperature as constant as possible and maintain a constant fuel cell outlet voltage, [73].

There exist other kinds of dynamic models and controllers. In 2005, Magistri et al. [110] have presented models developed for analysis of the Rolls-Royce Integrated Planar SOFC and studied the performance of the SOFC stack and the turbomachinery and the auxiliaries. In 2006, Wachter et al. [111] have modeled a SOFC-GT hybrid system and studied its dynamics. They have proposed a nonlinear system to analyze the transient behavior and a linear system from the nonlinear system to predict the behavior at the steady state. Lu et al. [112] have addressed dynamic modeling for a stand alone SOFC auxiliary power unit. Huo et al. [83] have proposed a dynamic modeling of SOFC stack using a Hammerstein mode. It is an advanced model since the model of Jurado [80] using a Hammerstein mode need prior information of the system. Chakraborty [86] has presented a genetic programming to static and dynamic modeling and simulation of SOFC. The model is based on the model of [57]. In 2011, Chakraborty [87] has presented the error in the model of [57]. In [113], an ultra capacitor is used to avoid sudden loss in voltage and to avoid possible damage to electrical equipment.

3.5 Control Strategies for the SOFCs

3.5.1 Sliding Mode Control for Fuel Cell Stacks

In this section, we combine the material balance model and the temperature model, and then apply the sliding mode control technique to the model of the planar SOFCs. The material balance model and the temperature model are rewritten from (3.14) and (3.16) considering the mass balance of N_2 as

$$\begin{aligned}
\frac{d}{dt}P_{H_2} &= \frac{RT_{fc}}{V_a}\left(N_{H_2}^{in} - N_{H_2}^{out} - \frac{N_0}{2F}A_c I_{fc}(t)\right) \\
\frac{d}{dt}P_{H_2O} &= \frac{RT_{fc}}{V_a}\left(-N_{H_2O}^{out} + \frac{N_0}{2F}A_c I_{fc}(t)\right) \\
\frac{d}{dt}P_{O_2} &= \frac{RT_{fc}}{V_c}\left(N_{O_2}^{in} - N_{O_2}^{out} - \frac{N_0}{4F}A_c I_{fc}(t)\right) \\
\frac{d}{dt}P_{N_2} &= \frac{RT_{fc}}{V_c}\left(N_{N_2}^{in} - N_{N_2}^{out}\right) \\
\beta\frac{dT_{fc}}{dt} + T_{fc} &= v
\end{aligned} \tag{3.26}$$

$N_{H_2}^{out}$, $N_{H_2O}^{out}$, and $N_{O_2}^{out}$ are related to the output current $I_{fc}(t)$ as follows [2, 3]

$$\begin{aligned}
N_{H_2}^{out} &= \left(Anode_{in} - \frac{N_0}{2F}A_c I_{fc}(t)\right)F_{H_2} \\
N_{H_2O}^{out} &= \left(Anode_{in} + \frac{N_0}{2F}A_c I_{fc}(t)\right)F_{H_2O} \\
N_{O_2}^{out} &= \left(Cathode_{in} - \frac{N_0}{4F}A_c I_{fc}(t)\right)F_{O_2} \\
N_{N_2}^{out} &= Cathode_{in}F_{N_2}
\end{aligned} \tag{3.27}$$

where $F_{H_2} = \frac{p_{H_2}}{p_{H_2}+p_{H_2O}}$, $F_{H_2O} = \frac{p_{H_2O}}{p_{H_2}+p_{H_2O}}$, $F_{O_2} = \frac{p_{O_2}}{p_{O_2}+p_{N_2}}$, and $F_{N_2} = \frac{p_{N_2}}{p_{O_2}+p_{N_2}}$ are the pressure fractions of hydrogen, water vapor, and oxygen, respectively. $N_{H_2}^{in}$ and $N_{O_2}^{in}$ can be represented using the molar fraction of H_2 and O_2, which are $\gamma_{H_2} = N_{H_2}^{in}/Anode_{in}$ and $\gamma_{O_2} = N_{O_2}^{in}/Cathode_{in}$, respectively.

Using $Anode_{in} = u_a k_a$ and $Cathode_{in} = u_c k_c$ where k_a and k_c are the conversion factor on each side, which are converted from standard liters per minute (slpm) to

mol/s, the model in (3.26) can be rewritten as

$$\begin{aligned}
\frac{d}{dt}P_{H_2} &= \frac{R}{V_a}T_{fc}\bigg(Y_{H_2}u_ak_a - \bigg(u_ak_a - \frac{N_0}{2F}A_cI_{fc}(t)\bigg)\frac{p_{H_2}}{p_{H_2}+p_{H_2O}} - \frac{N_0}{2F}A_cI_{fc}(t)\bigg)\\
\frac{d}{dt}P_{H_2O} &= \frac{R}{V_a}T_{fc}\bigg(-\bigg(u_ak_a + \frac{N_0}{2F}A_cI_{fc}(t)\bigg)\frac{p_{H_2O}}{p_{H_2}+p_{H_2O}} + \frac{N_0}{2F}A_cI_{fc}(t)\bigg)\\
\frac{d}{dt}P_{O_2} &= \frac{R}{V_c}T_{fc}\bigg(Y_{O_2}u_ck_c - \bigg(u_ck_c - \frac{N_0}{4F}A_cI_{fc}(t)\bigg)\frac{p_{O_2}}{p_{O_2}+p_{N_2}} - \frac{N_0}{4F}A_cI_{fc}(t)\bigg)\\
\frac{d}{dt}P_{N_2} &= \frac{R}{V_c}T_{fc}\bigg(Y_{N_2}u_ck_c - u_ck_c\frac{p_{N_2}}{p_{O_2}+p_{N_2}}\bigg)\\
\beta\frac{dT_{fc}}{dt} &+ T_{fc} = v
\end{aligned} \tag{3.28}$$

The model of (3.29) can be represented in state space as follows

$$\begin{aligned}
\dot{x}_1(t) &= \frac{R}{V_a}x_5(t)\bigg(\Big(Y_{H_2} - \frac{x_1(t)}{x_1(t)+x_2(t)}\Big)k_au_a - \frac{x_2(t)}{x_1(t)+x_2(t)}\frac{N_0}{2F}A_cI_{fc}(t)\bigg)\\
\dot{x}_2(t) &= \frac{R}{V_a}x_5(t)\bigg(-\frac{x_2(t)}{x_1(t)+x_2(t)}k_au_a + \frac{x_1(t)}{x_1(t)+x_2(t)}\frac{N_0}{2F}A_cI_{fc}(t)\bigg)\\
\dot{x}_3(t) &= \frac{R}{V_c}x_5(t)\bigg(\Big(Y_{O_2} - \frac{x_3(t)}{x_3(t)+x_4(t)}\Big)k_cu_c - \frac{x_4(t)}{x_3(t)+x_4(t)}\frac{N_0}{4F}A_cI_{fc}(t)\bigg)\\
\dot{x}_4(t) &= \frac{R}{V_c}x_5(t)\bigg(\Big(Y_{N_2} - \frac{x_4(t)}{x_3(t)+x_4(t)}\Big)k_cu_c\bigg)\\
\dot{x}_5(t) &= \frac{1}{\beta}\Big(v - x_5(t)\Big)
\end{aligned} \tag{3.29}$$

where

$$\begin{aligned}
x(t) &= \begin{bmatrix}x_1(t) & x_2(t) & x_3(t) & x_4(t) & x_5(t)\end{bmatrix}^T\\
&= \begin{bmatrix}P_{H_2}(t) & P_{H_2O}(t) & P_{O_2}(t) & P_{N_2}(t) & T_{fc}(t)\end{bmatrix}^T
\end{aligned} \tag{3.30}$$

The output equation is

$$y(t) = \begin{bmatrix}x_1(t) & x_3(t) & x_5(t)\end{bmatrix}^T = \begin{bmatrix}P_{H_2}(t) & P_{O_2}(t) & T_{fc}(t)\end{bmatrix}^T \tag{3.31}$$

and the control input is

$$u(t) = \begin{bmatrix}u_a(t) & u_c(t) & v(t)\end{bmatrix}^T \tag{3.32}$$

Similarly to control of PEMFCs, we consider same control objective that is to keep the pressure difference between hydrogen and oxygen small. We design the anode sliding surface ($s_1(t)$) as follows,

$$s_1(t) = y_1(t) - y_{1ref} = 0 \tag{3.33}$$

and the cathode sliding surface can be designed to force $x_2(t)$ to follow $x_1(t)$, which means

$$s_2(t) = y_2(t) - y_1(t) = 0 \tag{3.34}$$

With the sliding surfaces defined in (3.33) and (3.34), we can find

$$\begin{aligned} \dot{s}_1(t) &= \dot{y}_1(t) = \dot{x}_1(t) \\ &= \frac{R}{V_a} x_5(t) \Bigg(\Big(Y_{H_2} - \frac{x_1(t)}{x_1(t)+x_2(t)} \Big) k_a u_a - \frac{x_2(t)}{x_1(t)+x_2(t)} \frac{N_0}{2F} A_c I_{fc}(t) \Bigg) \end{aligned} \tag{3.35}$$

and

$$\begin{aligned} \dot{s}_2(t) =& \dot{y}_2(t) - \dot{y}_1(t) = \dot{x}_3(t) - \dot{x}_1(t) \\ =& \frac{R}{V_c} x_5(t) \Bigg(\Big(Y_{O_2} - \frac{x_3(t)}{x_3(t)+x_4(t)} \Big) k_c u_c - \frac{x_4(t)}{x_3(t)+x_4(t)} \frac{N_0}{4F} A_c I_{fc}(t) \Bigg) \\ & - \frac{R}{V_a} x_5(t) \Bigg(\Big(Y_{H_2} - \frac{x_1(t)}{x_1(t)+x_2(t)} \Big) k_a u_a - \frac{x_2(t)}{x_1(t)+x_2(t)} \frac{N_0}{2F} A_c I_{fc}(t) \Bigg) \end{aligned} \tag{3.36}$$

Note that

$$\begin{aligned} Y_{H_2} - \frac{x_1(t)}{x_1(t)+x_2(t)} > 0 \\ Y_{O_2} - \frac{x_3(t)}{x_3(t)+x_4(t)} > 0 \end{aligned} \tag{3.37}$$

since H_2 and O_2 are used for reactions. We assume that the current change is in the region

$$0 < I_{min} < I(t) < I_{max} \tag{3.38}$$

Similarly to the PEMFCs model in Chapter 2, $u_a(t)$ can be designed

$$u_a(t) = \begin{cases} \dfrac{C_1 \frac{x_1(t)}{x_1(t)+x_2(t)} I_{min}}{\big(Y_{H_2} - \frac{x_1(t)}{x_1(t)+x_2(t)} \big) k_a} - \sigma_1 \mathrm{sat}\big(s_1(t)\big) & \text{if } s_1(t) > 0 \\ \dfrac{C_1 \frac{x_1(t)}{x_1(t)+x_2(t)} I_{max}}{\big(Y_{H_2} - \frac{x_1(t)}{x_1(t)+x_2(t)} \big) k_a} - \sigma_2 \mathrm{sat}\big(s_1(t)\big) & \text{if } s_1(t) < 0 \end{cases} \tag{3.39}$$

where $C_1 = \frac{N_0}{2F} A_c I_{fc}(t)$. With this input we have

$$\dot{s}_1(t) = \begin{cases} \frac{R}{V_a} x_5(t) \Bigg(C_1 \frac{x_1(t)}{x_1(t)+x_2(t)} \big(I_{min} - I_{fc}(t) \big) \\ \qquad - \big(Y_{H_2} - \frac{x_1(t)}{x_1(t)+x_2(t)} \big) k_a \sigma_1 \mathrm{sat}\big(s_1(t)\big) \Bigg) < 0 & \text{if } s_1(t) > 0 \\ \frac{R}{V_a} x_5(t) \Bigg(C_1 \frac{x_1(t)}{x_1(t)+x_2(t)} \big(I_{max} - I_{fc}(t) \big) \\ \qquad - \big(Y_{H_2} - \frac{x_1(t)}{x_1(t)+x_2(t)} \big) k_a \sigma_2 \mathrm{sat}\big(s_1(t)\big) \Bigg) > 0 & \text{if } s_1(t) < 0 \end{cases} \tag{3.40}$$

For the cathode input $u_c(t)$, it is more complicated because we have to consider $s_1(t)$ in equation (3.36). When $s_2(t) > 0$, $\dot{s}_2(t) < 0$ which implies

$$\begin{aligned}\dot{s}_2(t) =& \frac{R}{V_c}x_5(t)\bigg(\Big(Y_{O_2} - \frac{x_3(t)}{x_3(t)+x_4(t)}\Big)k_c u_c - \frac{x_4(t)}{x_3(t)+x_4(t)}\frac{N_0}{4F}A_c I_{fc}(t)\bigg) \\ &- \frac{R}{V_a}x_5(t)\bigg(\Big(Y_{H_2} - \frac{x_1(t)}{x_1(t)+x_2(t)}\Big)k_a u_a - \frac{x_2(t)}{x_1(t)+x_2(t)}\frac{N_0}{2F}A_c I_{fc}(t)\bigg) < 0\end{aligned} \tag{3.41}$$

If the second term in (3.41) is greater than zero, it is enough to design $u_c(t)$ such that it satisfies

$$\frac{R}{V_c}x_5(t)\bigg(\Big(Y_{O_2} - \frac{x_3(t)}{x_3(t)+x_4(t)}\Big)k_c u_c - \frac{x_4(t)}{x_3(t)+x_4(t)}\frac{N_0}{4F}A_c I_{fc}(t)\bigg) < 0 \tag{3.42}$$

which produces

$$u_c(t) = \frac{C_2\frac{x_3(t)}{x_3(t)+x_4(t)}I_{min}}{\big(Y_{O_2} - \frac{x_3(t)}{x_3(t)+x_4(t)}\big)k_c} - \sigma_3\mathrm{sat}\big(s_2(t)\big) \tag{3.43}$$

where $C_2 = \frac{N_0}{4F}A_c I_{fc}(t)$. But if the second term in (3.41) is smaller than zero, we have to check the minimum value of the second term. Since the minimum of $-\mathrm{sat}\big(s_1(t)\big)$ is -1 and that of $I_{min} - I_{fc}(t)$ is $I_{min} - I_{max}$, the minimum value of the second term in (3.41) is

$$\frac{R}{V_a}x_5(t)\bigg(C_1\frac{x_1(t)}{x_1(t)+x_2(t)}\big(I_{min} - I_{max}\big) - \sigma_1\bigg) \tag{3.44}$$

which is smaller than zero. Therefore, $u_c(t)$ can be designed as follows

$$u_c(t) = \frac{C_2\frac{x_3(t)}{x_3(t)+x_4(t)}I_{min} + \frac{V_c}{V_a}\bigg(C_1\frac{x_1(t)}{x_1(t)+x_2(t)}\big(I_{min} - I_{max}\big) - \sigma_1\bigg)}{\big(Y_{O_2} - \frac{x_3(t)}{x_3(t)+x_4(t)}\big)k_c} - \sigma_3\mathrm{sat}\big(s_2(t)\big) \tag{3.45}$$

and (3.41) can be written as

$$\begin{aligned}\dot{s}_2(t) =& \frac{R}{V_c}x_5(t)\bigg(C_1\frac{x_3(t)}{x_3(t)+x_4(t)}\big(I_{min} - I_{fc}(t)\big) - \big(Y_{O_2} - \frac{x_3(t)}{x_3(t)+x_4(t)}\big)k_c\sigma_3\mathrm{sat}\big(s_2(t)\big)\bigg) \\ &+ \frac{R}{V_a}x_5(t)\bigg(C_1\frac{x_1(t)}{x_1(t)+x_2(t)}\big(I_{min} - I_{max}\big) - \sigma_1\bigg) \\ &- \frac{R}{V_a}x_5(t)\bigg(\Big(Y_{H_2} - \frac{x_1(t)}{x_1(t)+x_2(t)}\Big)k_a u_a - \frac{x_2(t)}{x_1(t)+x_2(t)}\frac{N_0}{2F}A_c I_{fc}(t)\bigg) < 0\end{aligned} \tag{3.46}$$

Similarly, in the case of $s_2(t) < 0$, the maximum value of (3.41) is

$$\frac{R}{V_a}x_5(t)\bigg(C_1\frac{x_1(t)}{x_1(t)+x_2(t)}\big(I_{max} - I_{min}\big) + \sigma_2\bigg) \tag{3.47}$$

and $u_c(t)$ is chosen as follows

$$u_c(t) = \frac{C_2 \frac{x_3(t)}{x_3(t)+x_4(t)} I_{max} + \frac{V_c}{V_a} x_5(t) \Big(C_1 \frac{x_1(t)}{x_1(t)+x_2(t)} \big(I_{max} - I_{min}\big) + \sigma_2 \Big)}{\big(Y_{O_2} - \frac{x_3(t)}{x_3(t)+x_4(t)}\big) k_c} - \sigma_4 \text{sat}\big(s_2(t)\big) \tag{3.48}$$

We can check that

$$\begin{aligned} \dot{s}_2(t) =& \frac{R}{V_c} x_5(t) \Big(C_1 \frac{x_3(t)}{x_3(t)+x_4(t)} \big(I_{max} - I_{fc}(t)\big) - \big(Y_{O_2} - \frac{x_3(t)}{x_3(t)+x_4(t)}\big) k_c \sigma_4 \text{sat}\big(s_2(t)\big) \Big) \\ &+ \frac{R}{V_a} x_5(t) \Big(C_1 \frac{x_1(t)}{x_1(t)+x_2(t)} \big(I_{max} - I_{min}\big) + \sigma_2 \Big) \\ &- \frac{R}{V_a} x_5(t) \Big(\Big(Y_{H_2} - \frac{x_1(t)}{x_1(t)+x_2(t)}\Big) k_a u_a - \frac{x_2(t)}{x_1(t)+x_2(t)} \frac{N_0}{2F} A_c I_{fc}(t) \Big) > 0 \end{aligned} \tag{3.49}$$

Note that $\sigma_i > 0,\ i = 1, 2, 3, 4.$

In summary, the control input is defined by

$$u_a(t) = \begin{cases} \frac{C_1 \frac{x_1(t)}{x_1(t)+x_2(t)} I_{min}}{\big(Y_{H_2} - \frac{x_1(t)}{x_1(t)+x_2(t)}\big) k_a} - \sigma_1 \text{sat}\big(s_1(t)\big) & \text{if } s_1(t) > 0 \\ \frac{C_1 \frac{x_1(t)}{x_1(t)+x_2(t)} I_{max}}{\big(Y_{H_2} - \frac{x_1(t)}{x_1(t)+x_2(t)}\big) k_a} - \sigma_2 \text{sat}\big(s_1(t)\big) & \text{if } s_1(t) < 0 \end{cases} \tag{3.50}$$

and

$$u_c(t) = \begin{cases} \frac{C_2 \frac{x_3(t)}{x_3(t)+x_4(t)} I_{min} + \frac{V_c}{V_a} \Big(C_1 \frac{x_1(t)}{x_1(t)+x_2(t)} \big(I_{min} - I_{max}\big) - \sigma_1 \Big)}{\big(Y_{O_2} - \frac{x_3(t)}{x_3(t)+x_4(t)}\big) k_c} - \sigma_3 \text{sat}\big(s_2(t)\big) & \text{if } s_2(t) > 0 \\ \frac{C_2 \frac{x_3(t)}{x_3(t)+x_4(t)} I_{max} + \frac{V_c}{V_a} \Big(C_1 \frac{x_1(t)}{x_1(t)+x_2(t)} \big(I_{max} - I_{min}\big) + \sigma_2 \Big)}{\big(Y_{O_2} - \frac{x_3(t)}{x_3(t)+x_4(t)}\big) k_c} - \sigma_4 \text{sat}\big(s_2(t)\big) & \text{if } s_2(t) < 0 \end{cases} \tag{3.51}$$

Using the fact,

$$L_1 \leq \frac{\frac{x_1(t)}{x_1(t)+x_2(t)}}{Y_{H_2} - \frac{x_1(t)}{x_1(t)+x_2(t)}} \leq L_2 \tag{3.52}$$

and

$$L_3 \leq \frac{\frac{x_3(t)}{x_3(t)+x_4(t)}}{Y_{O_2} - \frac{x_3(t)}{x_3(t)+x_4(t)}} \leq L_4 \tag{3.53}$$

we can also design a simplified control law as

$$u_a(t) = \begin{cases} L_1 C_1 I_{min} - \sigma_1 \text{sat}\big(s_1(t)\big) & \text{if } s_1(t) > 0 \\ L_2 C_1 I_{max} - \sigma_2 \text{sat}\big(s_1(t)\big) & \text{if } s_1(t) < 0 \end{cases} \tag{3.54}$$

and

$$u_c(t) = \begin{cases} L_3C_2I_{min} - \sigma_3\text{sat}\big(s_2(t)\big) + \frac{V_c}{V_a}\Big(L_2C_1\big(I_{min} - I_{max}\big) - \sigma_1\Big) & \text{if } s_2(t) > 0 \\ L_4C_2I_{max} - \sigma_4\text{sat}\big(s_2(t)\big) + \frac{V_c}{V_a}\Big(L_2C_1\big(I_{max} - I_{min}\big) + \sigma_2\Big) & \text{if } s_2(t) < 0 \end{cases} \tag{3.55}$$

Note that $x(t)$ does not appear on the control inputs $u_a(t)$ and $u_c(t)$, but control inputs $u_a(t)$ and $u_c(t)$ are coupled. In the following section, we have simulated the system assuming that the temperature stays in a given range.

3.6 Numerical Example Without Temperature Control

The numerical data taken from [88], used in this chapter, are presented in Table 3.1.

Table 3.1: Parameters Of Fuel Cell

Symbol	Parameter	Value [Unit]
R	Gas constant	0.08205 [L atm mol^{-1} K^{-1}]
T	Operating cell temperature	1153 [K]
N	Number of cells	200
V_A	Anode volume	0.005 [m^3]
V_C	Cathode volume	0.010 [m^3]
k_a	Anode conversion factor	7.034×10^{-4} [mol s^{-1}]
k_c	Cathode conversion factor	7.036×10^{-4} [mol s^{-1}]
A	Fuel cell active area	0.01 [m^2]
F	Faraday constant	96,485 [A s mol^{-1}]
Y_{O_2}	O_2 reactant factor	0.2095
Y_{N_2}	N_2 reactant factor	0.7808
Y_{H_2}	H_2 reactant factor	0.9999
$C1$	$N \cdot A/2F$	4.21×10^{-6} [m^2 mol A^{-1} s^{-1}]
$C2$	$1.2684N \cdot A/F$	1.07×10^{-5} [m^2 mol A^{-1} s^{-1}]

Assuming that the state variables are available at all times, using the control inputs in (3.50) and (3.51) with $\sigma_1 = \sigma_2 = \sigma_3 = \sigma_4 = 100$, the results are shown in Figures 3.5 and 3.6.

In this simulation, the current density changes are assumed as in Figure 3.7 and T_{fc} is assumed to change as in Figure 3.8. Even though, T_{fc} is a parameter that should be controlled, we assumed that the variation of T is between $1150 - 1156K$. Figures 3.5 and 3.6 show that after 20 seconds the output $y_2(t)$ follows $y_1(t)$, which means we can keep the pressure difference between hydrogen and oxygen in a small range after

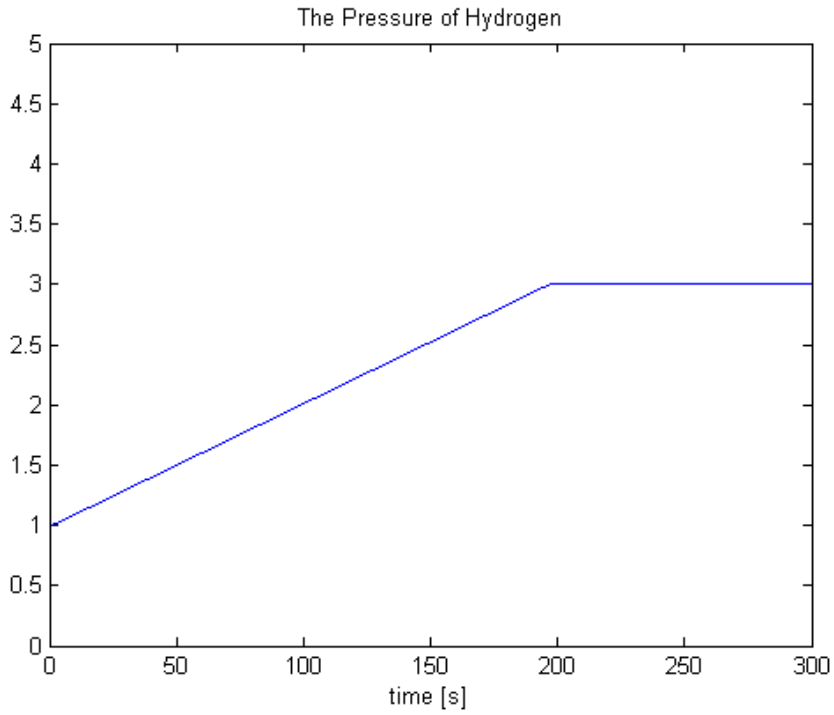

Figure 3.5: Pressure of hydrogen for the nonlinear system using (3.50)

20 seconds.

If we use the same sliding mode technique as in Chapter 2 ($s_i(t) = y_i(t) - Y_{i_{desrired}}$), the outputs are shown in Figures 3.9 and 3.10. The pressures reach at 3 atm finally, but in transient state, there exists some difference between hydrogen and oxygen pressures. When the sliding mode control technique proposed in this chapter is used, no ripples appear as evident and the pressure between outputs $y_1(t)$ and $y_2(t)$ stays in a small range after some time.

3.7 Conclusion

We have applied the sliding mode strategy for the nonlinear SOFC model using the same objective as in Chapter 2. The proposed sliding mode controller copes very well with the cell current changes $I(t)$, and keeps hydrogen and oxygen pressure difference small in the transient mode as well as keeps very precisely the pressures of hydrogen and oxygen at the desired (required) values as at steady state.

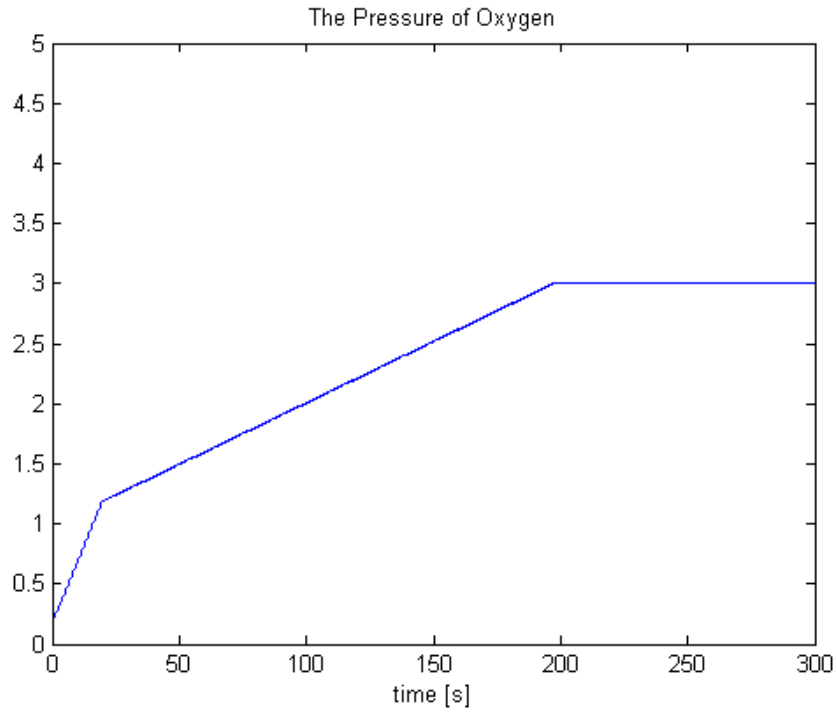

Figure 3.6: Pressure of oxygen for the nonlinear system using (3.51)

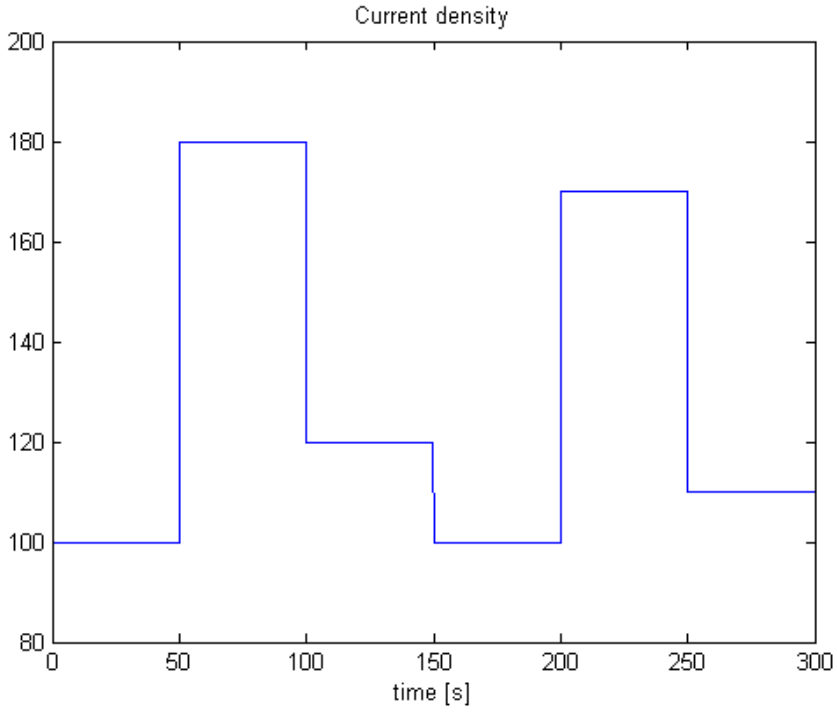

Figure 3.7: Current density changes

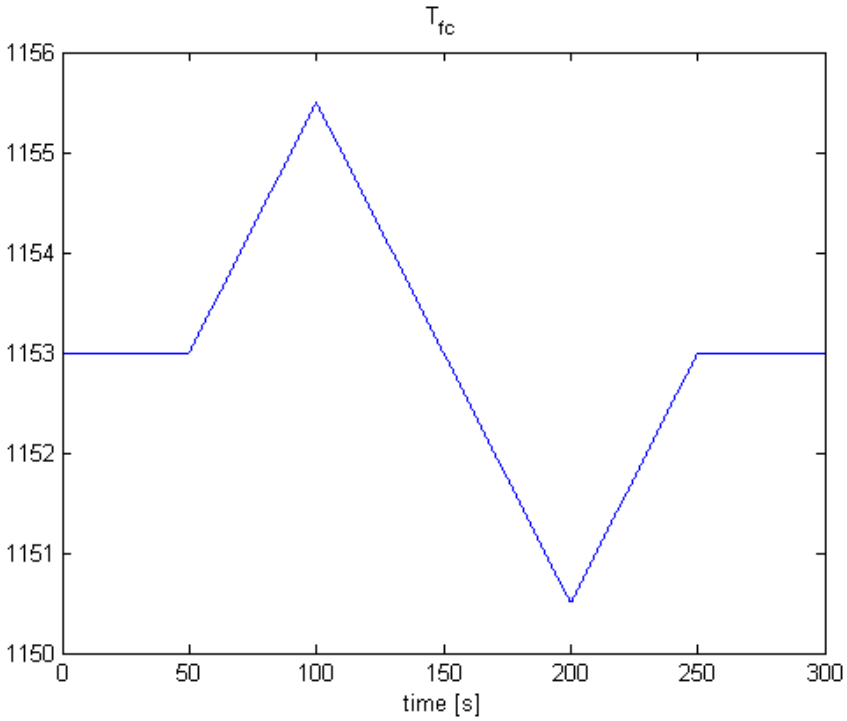

Figure 3.8: Temperature (T_{fc}) changes

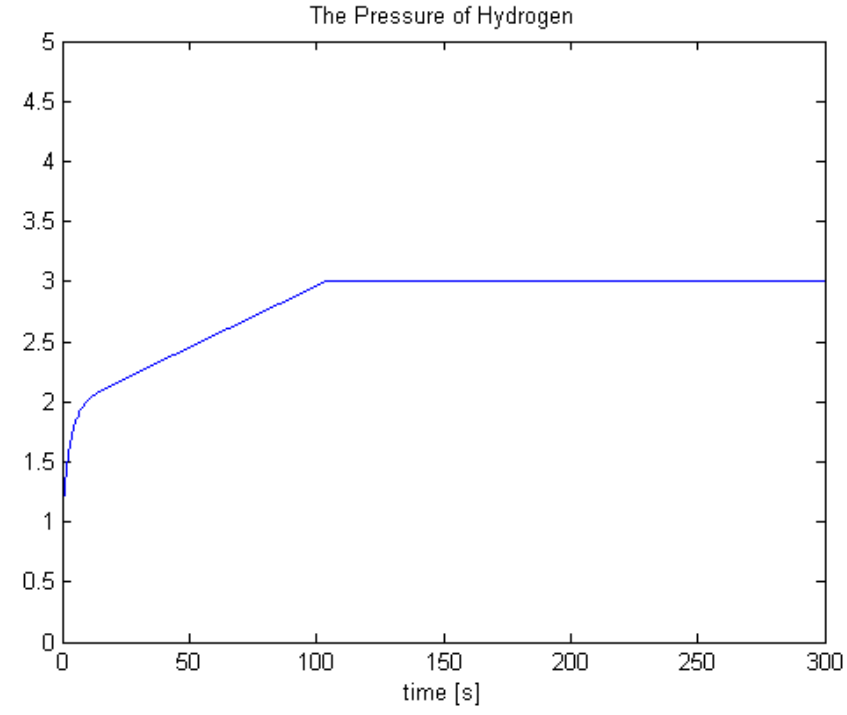

Figure 3.9: Pressure of hydrogen

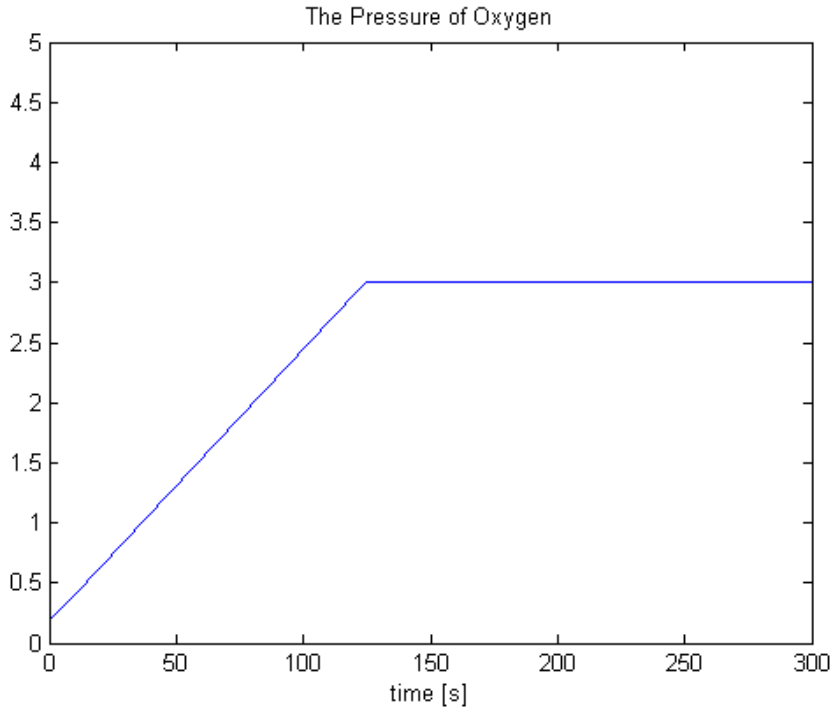

Figure 3.10: Pressure of oxygen

Chapter 4

Control of Processes of Solar Cells

4.1 Introduction

Jump parameter linear systems have mode switches governed by a Markov stochastic process. This class of systems has been studied in different set-ups by many researchers [55, 114, 115]. Optimal control of jump parameter linear systems has been considered in several papers [55, 116–118]. In [116], the authors presented the linear-quadratic optimal regulator for the linearized process dynamics of a steam boiler in a solar-powered central receiver, whose dynamics depends on clouds interfering with the Sun. In this chapter, we will use linear-quadratic optimal control to study the switching phenomena in the Cuk converter used in solar cells (photovoltaic systems).

Maximum power point tracking (MPPT) is one of most important objectives for photovoltaic (PV) systems, [119–123]. Its schematic is presented in Figure 4.1. By

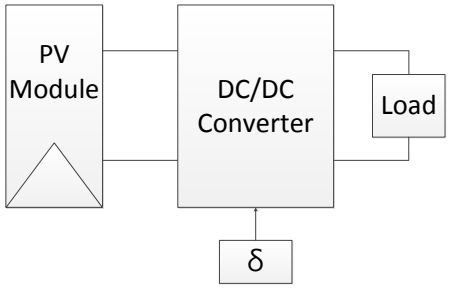

Figure 4.1: Block diagram of a stand-alone PV system for MPPT and a DC/DC converter

adjusting the duty cycle δ in Figure 4.1 for the DC/DC converter, maximum power point tracking can be achieved. The relationship between the output power and voltage is shown in Figure 4.2 parameterized by the value of the duty cycle.

The DC/DC converter (buck, boost, buck-boost, or Cuk converter) has two modes

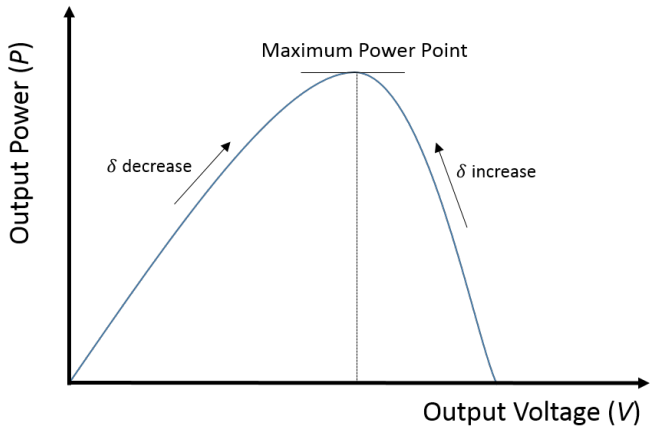

Figure 4.2: Output power versus output voltage parameterized by the duty cycle δ

through a switch therefore, it could be considered as a jump parameter linear system. Control of DC/DC converters has been studied by many well-respected researchers, for example [122, 124–126]. Especially, the switched systems in power electronics, with an emphasis on DC/DC converters, have been researched in recent years, for example [127–130]. Even though, the optimal control techniques for the Cuk converter have been studied in some papers [131–133], the jump parameter optimal control technique has not been considered so far.

The Cuk converter uses capacitive energy transfer, and analysis can be based on the current balance of the capacitor (although inductor voltage-balance analysis is also possible). The Cuk converter combines the functionality of buck and boost converters, i.e. it can either increase or decrease the output voltage with respect to the input voltage. It uses a capacitor as its main energy-storage component, which increases its efficiency. Input and output currents are smoothed by inductors. Control of the Cuk converter has been studied in a series of papers, see for example [134–136], but none of them used the technique proposed in this chapter.

In this chapter, we have considered the Cuk converter and studied the two modes for the converter using theory of jump parameter linear systems. We have applied the linear-quadratic optimal controller for the obtained jump parameter linear system using a modified version of the algorithm of [55] and presented the optimal quadratic performance values with respect to the change of δ. In the following section, the Cuk

converter circuit and its state-space model are described. In Section 4.3, optimal control for the jump parameter linear system of the Cuk converter is considered and the modified (accelerated) version algorithm of [55] is derived. Simulation results are presented in Section 4.4. The simulation results show the efficiency of the proposed technique despite of the presence of disturbances.

4.2 Cuk Converter in State Space

The Cuk converter is based on a switching boost-buck topology. Its schematic is presented in Figure 4.3. Depending on the switch Q_1, there exist "ON-STATE" (see Figure

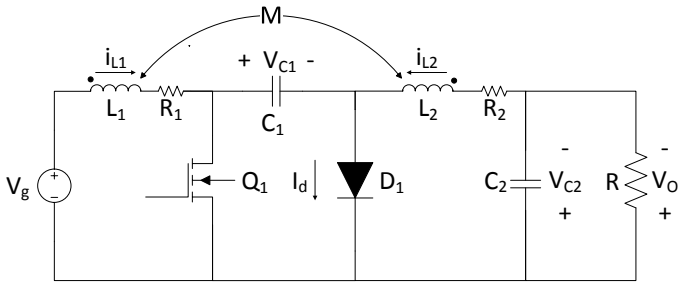

Figure 4.3: Cuk converter schematic

4.4) and "OFF-STATE" (see Figure 4.5).

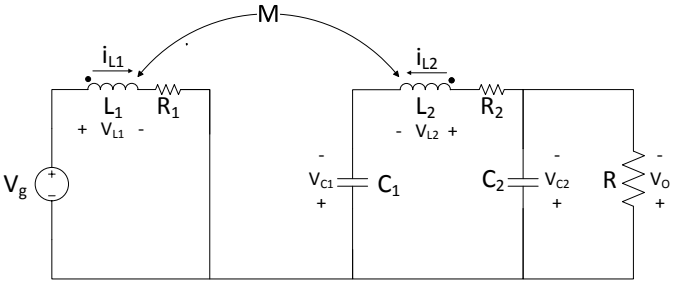

Figure 4.4: Cuk converter with the switch Q_1 in "ON-STATE"

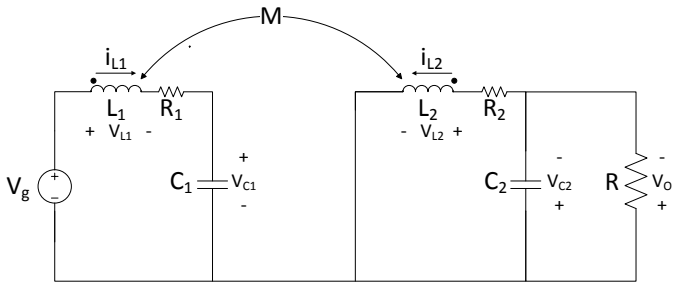

Figure 4.5: Cuk converter with the switch Q_1 in "OFF-STATE"

The input voltage V_g is fed into the circuit through L_1. In mode 1 (when Q_1 is on), current i_1 flows through L_1 and the diode D_1 is reverse biased. The energy dissipated from the storage elements in the output stage with L_2 and C_2 acting as a smoothing filter. In mode 2 (when $Q1$ is off), L_1 reverses to maintain the current flow and source current as its magnetic filed collapses. The energy in the output stage is provided via C_1. In the steady state, the average values of V_{L1} and V_{L2} (with the duty cycle δ of the switch, $0 < \delta < 1$) are

$$\begin{aligned} V_{L_1} &= \delta V_g + (1-\delta)(V_g - V_{C_1}) \\ V_{L_2} &= \delta(V_{C_1} - V_{C_2}) + (1-\delta)(-V_{C_2}) \end{aligned} \tag{4.1}$$

since $V_{L_2} = V_{C_1} - V_{C_2}$ when Q_1 is on and $V_{L_2} = -V_{C_2}$ when Q_1 is off [137]. By letting the both voltages to go to zeros in the steady state, since the voltage across the capacitor cannot change instantaneously when the switching speed is high, we can find

$$\frac{V_O}{V_g} = \frac{V_{C_2}}{V_g} = \frac{\delta}{1-\delta} \tag{4.2}$$

In the state space, with the state variables $\begin{bmatrix} x_1 & x_2 & x_3 & x_4 \end{bmatrix}^T = \begin{bmatrix} i_{L_1} & i_{L_2} & V_{C_1} & V_{C_2} \end{bmatrix}^T$, the model can be expressed as follows.

In mode 1

$$\begin{aligned}
\frac{\mathrm{d}i_{L_1}}{\mathrm{dt}} =& \frac{-L_2R_1}{L_1L_2-M^2}i_{L_1} + \frac{MR_2}{L_1L_2-M^2}i_{L_2} \\
&+ \frac{-M}{L_1L_2-M^2}V_{C_1} + \frac{M}{L_1L_2-M^2}V_{C_2} + \frac{L_2}{L_1L_2-M^2}V_g \\
\frac{\mathrm{d}V_{C_1}}{\mathrm{dt}} =& \frac{MR_1}{L_1L_2-M^2}i_{L_1} + \frac{-L_1R_2}{L_1L_2-M^2}i_{L_2} \\
&+ \frac{L_1}{L_1L_2-M^2}V_{C_1} + \frac{-L_1}{L_1L_2-M^2}V_{C_2} + \frac{-M}{L_1L_2-M^2}V_g \\
\frac{\mathrm{d}i_{L_2}}{\mathrm{dt}} =& \frac{-1}{C_1}i_{L_2} \\
\frac{\mathrm{d}V_{C_2}}{\mathrm{dt}} =& \frac{1}{C_2}i_{L_2} + \frac{-1}{RC_2}V_{C_2} \\
V_O =& V_{C_2}
\end{aligned} \tag{4.3}$$

and, the equations in the state space are represented as follows

$$\begin{aligned}
\dot{x} =& \begin{bmatrix} \frac{-L_2R_1}{L_1L_2-M^2} & \frac{MR_2}{L_1L_2-M^2} & \frac{-M}{L_1L_2-M^2} & \frac{M}{L_1L_2-M^2} \\ \frac{MR_1}{L_1L_2-M^2} & \frac{-L_1R_2}{L_1L_2-M^2} & \frac{L_1}{L_1L_2-M^2} & \frac{-L_1}{L_1L_2-M^2} \\ 0 & \frac{-1}{C_1} & 0 & 0 \\ 0 & \frac{1}{C_2} & 0 & \frac{-1}{RC_2} \end{bmatrix} x + \begin{bmatrix} \frac{L_2}{L_1L_2-M^2} \\ \frac{-M}{L_1L_2-M^2} \\ 0 \\ 0 \end{bmatrix} V_g \\
=& A_1x + B_1V_g \\
y =& [0 \quad 0 \quad 0 \quad 1]x = C_1x
\end{aligned} \tag{4.4}$$

In mode 2, we have

$$\begin{aligned}
\frac{\mathrm{d}i_{L_1}}{\mathrm{dt}} =& \frac{-L_2R_1}{L_1L_2-M^2}i_{L_1} + \frac{MR_2}{L_1L_2-M^2}i_{L_2} \\
&+ \frac{-L_2}{L_1L_2-M^2}V_{C_1} + \frac{M}{L_1L_2-M^2}V_{C_2} + \frac{L_2}{L_1L_2-M^2}V_g \\
\frac{\mathrm{d}V_{C_1}}{\mathrm{dt}} =& \frac{MR_1}{L_1L_2-M^2}i_{L_1} + \frac{-L_1R_2}{L_1L_2-M^2}i_{L_2} \\
&+ \frac{M}{L_1L_2-M^2}V_{C_1} + \frac{-L_1}{L_1L_2-M^2}V_{C_2} + \frac{-M}{L_1L_2-M^2}V_g \\
\frac{\mathrm{d}i_{L_2}}{\mathrm{dt}} =& \frac{-1}{C_1}i_{L_1} \\
\frac{\mathrm{d}V_{C_2}}{\mathrm{dt}} =& \frac{1}{C_2}i_{L_2} + \frac{-1}{RC_2}V_{C_2} \\
V_O =& V_{C_2}
\end{aligned} \tag{4.5}$$

and, the state space equations are shown as follows

$$\begin{aligned}\dot{x} &= \begin{bmatrix} \frac{-L_2R_1}{L_1L_2-M^2} & \frac{MR_2}{L_1L_2-M^2} & \frac{-L_2}{L_1L_2-M^2} & \frac{M}{L_1L_2-M^2} \\ \frac{MR_1}{L_1L_2-M^2} & \frac{-L_1R_2}{L_1L_2-M^2} & \frac{M}{L_1L_2-M^2} & \frac{-L_1}{L_1L_2-M^2} \\ \frac{-1}{C_1} & 0 & 0 & 0 \\ 0 & \frac{1}{C_2} & 0 & \frac{-1}{RC_2} \end{bmatrix} x + \begin{bmatrix} \frac{L_2}{L_1L_2-M^2} \\ \frac{-M}{L_1L_2-M^2} \\ 0 \\ 0 \end{bmatrix} V_g \\ &= A_2x + B_2V_g \\ y &= [0 \quad 0 \quad 0 \quad 1]x = C_2x \end{aligned} \tag{4.6}$$

The averaged state space method as defined in [134] is well-known method used in modeling switching converters.

$$\begin{aligned}\dot{x} &= Ax + BV_g \\ y &= Gx \end{aligned} \tag{4.7}$$

with

$$\begin{aligned} A &= \delta A_1 + (1-\delta)A_2 = \begin{bmatrix} 0 & 0 & -\frac{1-\delta}{L_1} & 0 \\ 0 & 0 & \frac{\delta}{L_2} & -\frac{1}{L_2} \\ \frac{1-\delta}{C_1} & -\frac{\delta}{C_1} & 0 & 0 \\ 0 & \frac{1}{C_2} & 0 & -\frac{1}{RC_2} \end{bmatrix} \\ B &= \delta B_1 + (1-\delta)B_2 = [\tfrac{1}{L_1} \quad 0 \quad 0 \quad 0]^T \\ G &= \delta G_1 + (1-\delta)G_2 = [0 \quad 0 \quad 0 \quad 1] \end{aligned} \tag{4.8}$$

4.3 Jump Parameter Linear Optimal Control Systems

This section is based on applying the jump parameter linear system theory and a modified version of the algorithm [55] to the Cuk converter. The idea to use the jump parameter linear optimal controller for the Cuk converter was for the first time presented in [137]. The results are farther developed where a new, accelerated algorithm of [55] was derived.

The Cuk converter's switch Q_1 will change from mode 1 to mode 2 and vice versa and this is considered that this change between those systems is governed by a Markov chain. The Cuk converter is assumed to have two states with the transition matrix [114] (see Figure 4.6)

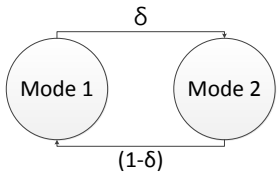

Figure 4.6: Two state Markov chain in MPPT

$$\Pi = \begin{bmatrix} -\delta & \delta \\ (1-\delta) & -(1-\delta) \end{bmatrix} \tag{4.9}$$

Consider a general linear dynamic system described by

$$\dot{x}(t) = A(r)x(t) + B(r)u(t), \quad x(t_0) = x_0 \tag{4.10}$$

where $x(t)$ is the state vector of dimension n, $u(t)$ is a control input of dimension m, A and B are mode-dependent matrices of appropriate dimensions, and r is a Markovian process that represents the mode of the system and takes on values in a discrete set $\Psi = 1, 2, \cdots, N$.

In general, the stationary transition probabilities of the system modes are determined by a Markov chain, whose transition rate matrix given by [114]:

$$\Pi = \begin{bmatrix} \pi_{11} & \pi_{12} & \cdots & \pi_{1N} \\ \pi_{21} & \pi_{22} & \cdots & \pi_{2N} \\ \vdots & \vdots & \ddots & \vdots \\ \pi_{N1} & \pi_{N2} & \cdots & \pi_{NN} \end{bmatrix} \tag{4.11}$$

This matrix has the property that $\pi_{ij} \geq 0, i \neq j$ and $\pi_{ii} = -\sum_{j \neq i} \pi_{ij}$. The performance of the linear dynamic system (4.10), is measured by the following criterion:

$$J = E\left\{ \int_0^\infty \left[x^T(t)Q(r)x(t) + u^T(t)R(r)u(t) \right] \mathrm{d}t | t_0, x(t_0), r(t_0) \right\} \tag{4.12}$$

where $Q(r) \geq 0$ and $R(r) > 0$ for every r.

The optimal feedback controls are then given by [116]

$$u_{opt} = -R_k^{-1} B_k^T P_k x(t), \quad k = 1, 2, \cdots, N \tag{4.13}$$

where k indicates the mode of the system ($A(r = k) = A_k, B(r = k) = B_k, Q(r = k) = Q_k, R(r = k) = R_k$) and the P_k's are the positive semi-definite stabilizing solutions of

a set of the coupled algebraic Riccati equations defined by

$$A_k^T P_k - P_k S_k P_k + P_k A_k + Q_k + \sum_{j=1, j\neq k}^{N} \pi_{kj} P_j = 0, \qquad k = 1, 2, \cdots, N \tag{4.14}$$

where $A_k = A_k + 1/2\pi_{kk} I$ and $S_k = B_k R_k^{-1} B_k^T$. Equations (4.13) and (4.14) are non-linear algebraic. The existence of positive semi-definite stabilizing solutions (stabilizable with respect to A_k) of these equations under the control oriented assumptions (controllability-observability and their weaker conditions - stabilizability and detectability) given in [55].

The following modified and accelerated algorithm of the algorithm from [55], for solving the set of coupled algebraic Riccati equation (4.14) in terms of decoupled linear Lyapunov algebraic equations was proposed as

$$\begin{aligned} (\mathbf{A_k} - S_k P_k^{(i)})^T P_k^{(i+1)} + P_k^{(i+1)} (\mathbf{A_k} - S_k P_k^{(i)}) \\ = -P_k^{(i)} S_k P_k^{(i)} - Q_k^{(i)} \\ P_k^{(0)} \geq 0, \ k = 1, 2, \cdots, N \end{aligned} \tag{4.15}$$

where

$$Q_k^{(i)} = Q_k + \sum_{j=1}^{k-1} \pi_{kj} P_j^{(i+1)} + \sum_{j=k+1}^{N} \pi_{kj} P_j^{(i)} \geq 0 \tag{4.16}$$

The convergence proof of this algorithm can be done similarly to the proof of [55]. In the next section we will specialize this general algorithm for the Cuk converter used in solar cells for MPPT.

4.4 Simulation Results

A typical solar panel converts only around 15 percent of the incident solar irradiation into energy. In order to increase the efficiency of the solar panel we should use the Maximum Power Point Tracking technique (MPPT). According to the maximum power transfer theorem, the power delivered to the load has a maximum value when the source internal impedance (Thevenin impedance) matches the load impedance. So in other words, we need to match each time the impedance seen from the converter input side

with the internal impedance of the solar panel if the system is required to operate at the MPP of the solar array.

In this chapter, we are using, at the source side, the Cuk converter connected to the solar panel and this is a converter technique to enhance the solar array output voltage. Now by simply changing the duty cycle of the Cuk converter's switch with a smart control, we can match the source impedance with the load impedance and reach our goal. The solar panel will be then more efficient, less costly and applicable for different purposes from basic loads to non linear loads.

The numerical values for the Cuk converter connected to a solar panel are taken from [137]. The numerical values $L_1 = 0.5\text{mH},\ L_2 = 7.5\text{mH},\ M = 0\text{mH},\ C_1 = 2.0\mu\text{F},\ C_2 = 20\mu\text{F},\ R_1 = R_2 = 0\Omega,\ R = 30\Omega$ produce

$$A_1 = \begin{bmatrix} 0 & 0 & 0 & 0 \\ 0 & 0 & 1.3 \times 10^2 & -1.3 \times 10^2 \\ 0 & -5 \times 10^5 & 0 & 0 \\ 0 & 5 \times 10^4 & 0 & -1.67 \times 10^3 \end{bmatrix}$$

$$A_2 = \begin{bmatrix} 0 & 0 & -2 \times 10^3 & 0 \\ 0 & 0 & 0 & -1.33 \times 10^2 \\ 5 \times 10^5 & 0 & 0 & 0 \\ 0 & 5 \times 10^4 & 0 & -1.67 \times 10^3 \end{bmatrix}$$

$$B_1 = B_2 = [2 \times 10^3 \quad 0 \quad 0 \quad 0]^T$$

The transition matrix is

$$\Pi = \begin{bmatrix} -\delta & \delta \\ (1-\delta) & -(1-\delta) \end{bmatrix}$$

where the duty cycle δ is dictated by the maximum power point tracking (MPPT). Using algorithm of (4.15)-(4.16) for $N = 2$, matrices $\mathbf{A_1}$ and $\mathbf{A_2}$, and $Q_1 = Q_2 = I_4,\ R_1 = R_2 = 1$, we have obtained the optimal values for J_1^{opt} and J_2^{opt} for different values of δ and presented them in Table 4.1.

It can be observed from Table 4.1 that the optimal criteria hardly change with the value of the duty cycle δ. This facilitates that the duty cycle value δ can be

Table 4.1: Optimal Performance Criterion as functions of δ

δ	J_1^{opt}	J_2^{opt}
0.1	11.840565	0.120935
0.2	11.839769	0.120884
0.3	11.838972	0.120833
0.4	11.838176	0.120783
0.5	11.837380	0.120732
0.6	11.836584	0.120682
0.7	11.835788	0.120631
0.8	11.834993	0.120581
0.9	11.834197	0.120530

independently chosen to achieve the maximum power of PV as dictated by MPPT. These optimal performance criterion results show that it is preferable for the converter to be in mode 2, since it will spend less energy in this mode. Note that the quadratic performance chosen in fact represents an energy measure ("square" of the state variables plus "square" of the control variables).

In the following we show that the proposed technique is more general and not specific only for solar cells. To that end, we simulate the Cuk converter using MATLAB under the proposed optimal switching control law for a standard control problem (independent of a particular application of the Cuk converter) to eliminate tracking errors. Our goal is that the output of the Cuk converter follows a constant value, for example $V_o = 24V$, despite of switching of the feedback gains, and potential disturbances. It is well known in standard control books [59] that an integrator has to be inserted in the feedback loop to cope with constant or slow varying disturbances, see also [131]. According to [131], "the switching dc-dc converter is inevitable subjected to disturbances for a lot of reasons." After adding the integrator, we have applied the optimal control technique for the corresponding jump parameter linear system. The feedback system with the Cuk converter is shown in Figure 4.7 and its Simulink implementation is found in Figure 4.8.

With the same system matrices as in Section 4.3, the augmented system state vector is defined $[x \quad \epsilon]$ where $\epsilon = \int e\mathrm{dt}$, where e is the tracking error [59]. The corresponding

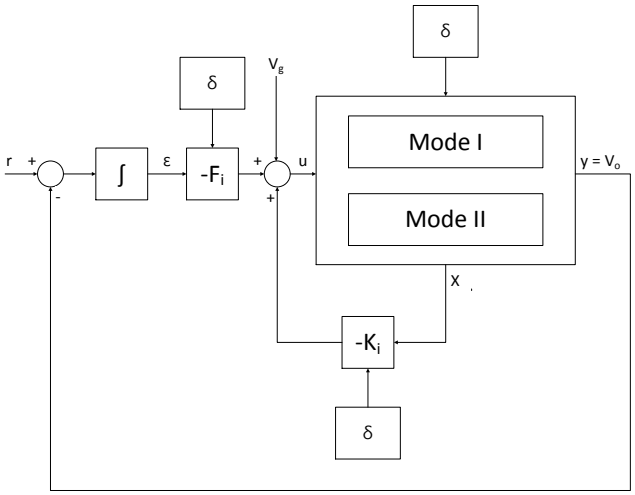

Figure 4.7: Cuk converter schematic in a feedback loop with an integrator

state space matrices are given as follows

$$\bar{A}_1 = \begin{bmatrix} A_1 & 0 \\ -C_1 & 0 \end{bmatrix},\ \bar{B}_1 = \begin{bmatrix} B_1 \\ 0 \end{bmatrix},\ \bar{C}_1 = [C_1 \quad 0], \bar{D}_1 = 0$$

$$\bar{A}_2 = \begin{bmatrix} A_2 & 0 \\ -C_2 & 0 \end{bmatrix},\ \bar{B}_2 = \begin{bmatrix} B_2 \\ 0 \end{bmatrix},\ \bar{C}_2 = [C_2 \quad 0], \bar{D}_2 = 0$$

The overall control law is [59]

$$u_i = -[K_i \quad F_i] \begin{bmatrix} x \\ \epsilon \end{bmatrix},\ i = 1, 2$$

where K_i and F_i are found via the jump parameter technique. The objective is to keep the output voltage V_O at $24V$ with the nominal input equal to $12V$ even if there exists a disturbance on the input. In our simulation, the disturbance is caused by constant changes of the duty cycle, but there are many sources of disturbances in the switched systems like the Cuk converter, as previously indicated in [131]. With the duty cycle given by $\delta = \frac{V_O}{V_g + V_O}$, we have assumed a disturbance for $V_g = \frac{1-\delta}{\delta} V_o$ as shown in Figure 4.9. The outputs of the averaged system and the jump parameter optimal controlled system are shown in Figures 4.10 and 4.11, respectively. For the jump parameter controlled system, in order to find the optimal feedback gains, we have used R and Q as follows, $R = 1$, $Q = \text{diag}\{10, 10, 10, 10, 1000\}$. Comparing with the

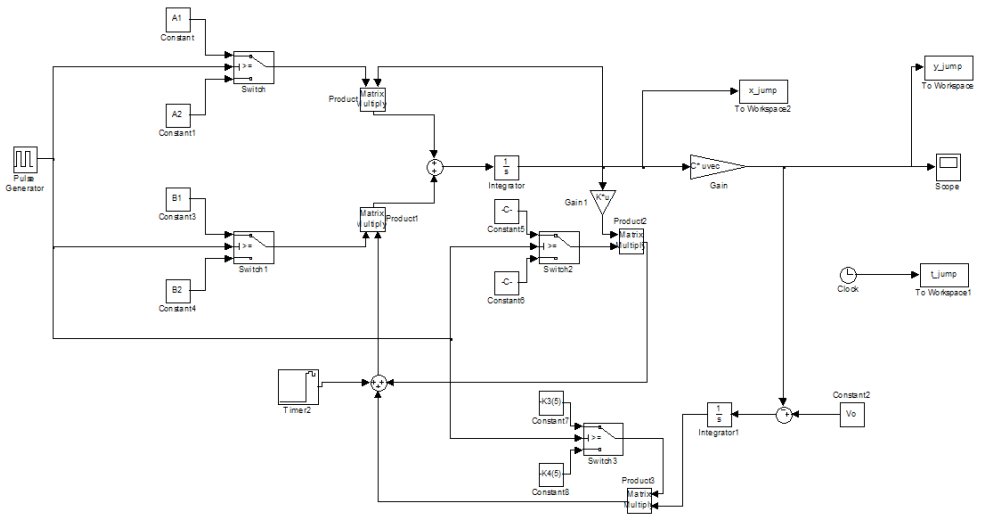

Figure 4.8: Simulink implementation for the Cuk converter schematic in a feedback loop with an integrator

output of the averaged system and the jump parameter optimally controlled system, we see that for the method proposed in this chapter the output shows relatively small ripples whenever V_g is changed. These ripples are considerable smaller than 1.5 and 3 ripples seen in Figure 4.10 for the averaged Cuk converter system.

4.5 Conclusion

In this chapter, we have applied the optimal jump parameter control technique to the Cuk converter used in solar cells. The simulation results obtained sustain the efficiency of the proposed technique even in the case with constant disturbances caused by changes of the duty cycle. The optimal performance criterion results obtained by changing the duty cycle, indicate that the optimal values are almost insensitive to the value of the duty cycle δ, which gives complete freedom in adjusting δ while performing circuit operations in an optimal manner from the system (circuit) energy stand point of view.

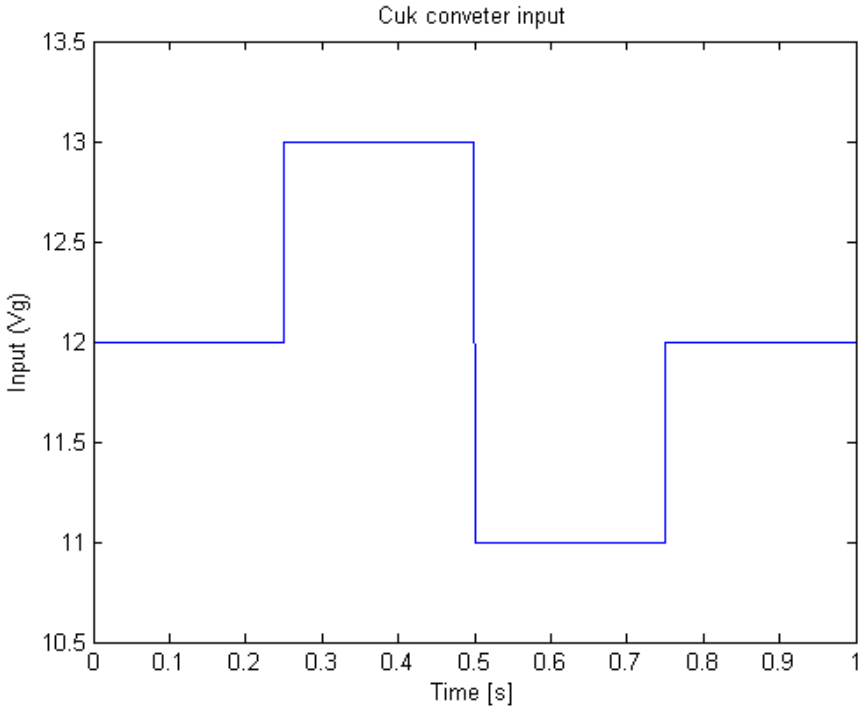

Figure 4.9: Input V_g with a disturbance

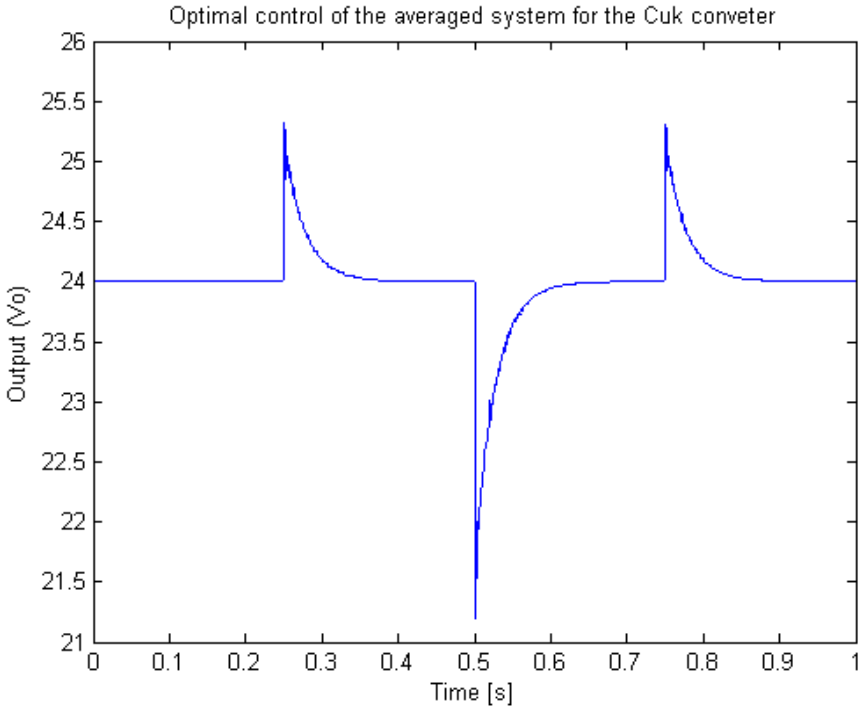

Figure 4.10: Output V_o for the averaged system

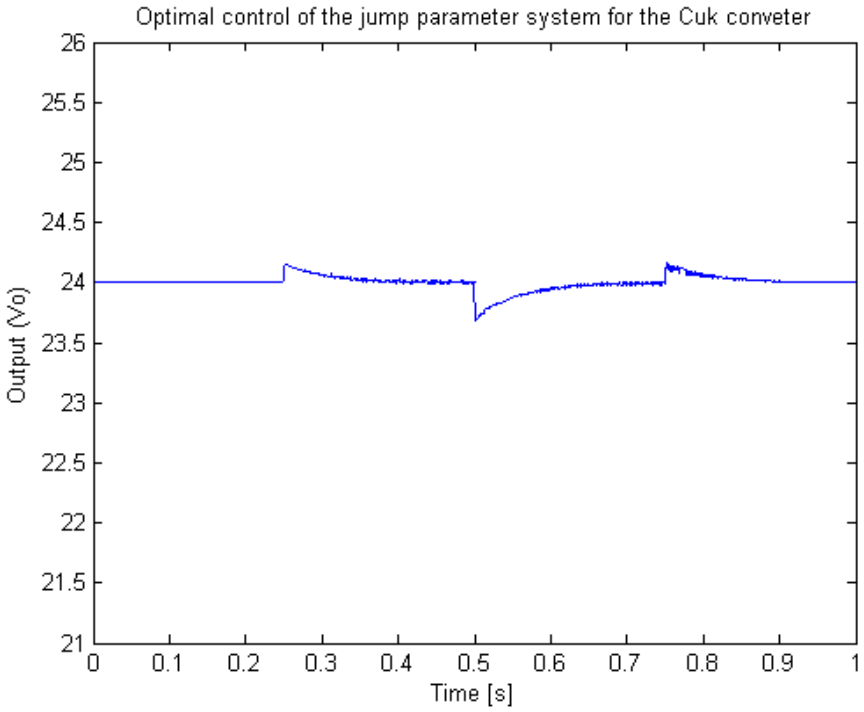

Figure 4.11: Output V_o for the jump parameter optimally controlled system

Chapter 5

Conclusions and Future Work

5.1 Conclusions

The study of control techniques for fuel cells and solar cells are investigated in this dissertation. Using sliding mode control, the pressures are kept at the desired values in PEMFCs and SOFCs despite the abrupt cell current change. We have also applied the jump parameter linear system control technique to the Cuk converter to find the optimal value and to reduce a constant disturbance with the integral action.

For PEMFCs model, we have applied the sliding mode strategy for the linearized model as well as nonlinear model in Chapter 2. In Chapter 3, a similar technique is used for SOFCs. The sliding mode technique is robust with respect to the disturbance, which in this case is the fuel cell current $I(t)$. The proposed controller keeps very precisely the pressures of hydrogen and oxygen at the desired (required) values. Especially, the proposed control technique for SOFCs makes the pressure difference between hydrogen and oxygen very small in both the transient mode and at steady state.

For the jump parameter linear system control technique applied to the Cuk converter, we have found a modified and accelerated algorithm of the algorithm from [55]. We have applied the technique with the integral action to keep the output at the desired value with a constant disturbance.

5.2 Future Work

In the future, more accurate stack models of fuel cells could be and should be developed since "the chemical kinetics in PEMFCs is fast, and the limiting factors in PEMFCs

are water and heat transport." And, in the state space modeling in [4], the electrochemical reactions in the catalysts layers and the species transport in the membrane electrolyte assembly are not considered. In modeling of SOFCs, we need to consider the temperature controller. The temperature is one of the most important factors in SOFCs. We can combine our result to the fuel cell systems with reformer, burner, heat exchangers, and etc.

The reaching time using sliding mode control technique for both cases (PEMFCs and SOFCs) need to be estimated. The reaching time to the boundary layer of sliding surfaces should converge exponentially.

Since the fuel cells are very complex systems, they may be studied and corresponding controllers may be designed in the future using multiple time scales [138] and/or weak coupling among subsystems of fuel cells and gas reformers. Sliding mode control for weakly coupled linear systems has been recently considered in [139].

The effect of ON/OFF dynamics in the Cuk converter should be studied in more detail since it is faster than the cell dynamics. The result of the jump parameter linear system for the Cuk converter can be extended to buck, boost, or buck-boost converters. Also, the accelerated algorithm can be used for any jump parameter linear systems for fast convergence.

Appendix A

Elements for Section 2

A.1 Functions φ_{ij} in (2.6)

$$
\begin{aligned}
\varphi_{11} =& C_1^2 I^2 - 2\lambda_{H_2} C_1 I\big(Y_{H_2}-1\big)k_a u_a + \lambda_{H_2}^2 Y_{H_2}\big(Y_{H_2}-2\big)k_a^2 u_a^2 \\
\varphi_{12} =& C_1^2 I^2 - \lambda_{H_2} C_1 I Y_{H_2} k_a u_a + \lambda_{H_2}^2 \big(Y_{H_2}-1\big)k_a^2 u_a^2 \\
\varphi_{21} =& \lambda_{H_2} C_1 I\big(Y_{H_2}-1\big)k_a u_a - \lambda_{H_2}^2\big(Y_{H_2}^2 - 3Y_{H_2}+2\big)k_a^2 u_a^2 \\
\varphi_{22} =& C_1^2 I^2 - \lambda_{H_2} C_1 I Y_{H_2} k_a u_a + \lambda_{H_2}^2 \big(Y_{H_2}-1\big)k_a^2 u_a^2 \\
\varphi_{31} =& I^3 C_1^2\big(-C_1 + C_2 + (C_1+C_2)Y_{N_2}\big) + \lambda_{air} I^2 C_1\big(3C_1 - (C_1+2C_2)Y_{N_2}\big)k_c u_c \\
&+ \lambda_{air} I^2 C_1\big(-4C_2 Y_{O_2} - 2(C_1+C_2)Y_{N_2}Y_{O_2}\big)k_c u_c \\
&+ 2\lambda_{air}^2 I\big(2C_1 - C_1 Y_{N_2} - 4C_1 Y_{O_2} + 2(C_1+C_2)Y_{O_2}^2 + (C_1+2C_2)Y_{N_2}Y_{O_2}\big)k_c^2 u_c^2 \\
&+ 4\lambda_{air}^3\big(Y_{N_2}+Y_{O_2}-2\big)Y_{O_2}k_c^2 u_c^2 Y_{O_2} \\
\varphi_{32} =& I^3 C_1^2\big(-C_1 + C_2 + (C_1+C_2)Y_{N_2}\big) \\
&+ \lambda_{air} I^2 C_1\big(-2(3C_1 - C_2) + (3C_1+4C_2)Y_{N_2} + 2(C_1+C_2)Y_{O_2}\big)k_c u_c \\
&+ 2\lambda_{air}^2 I\big(2C_2 Y_{N_2} + (C_1+2C_2)Y_{O_2} - 3C_1\big)k_c^2 u_c^2 + 4\lambda_{air}^3\big(Y_{N_2}+Y_{O_2}-1\big)k_c^3 u_c^3
\end{aligned}
$$

$$
\begin{aligned}
\varphi_{41} =& I^2 C_1 Y_{N_2}\big((C_1 - C_2) - (C_1 + C_2)Y_{N_2}\big) + \lambda_{air} I Y_{N_2}\big(- 3C_1 + (C_1 + 2C_2)Y_{N_2}\big)k_c u_c \\
&+ \lambda_{air} I Y_{N_2}\big(2(C_1 + C_2)Y_{O_2}\big)k_c u_c + 2\lambda_{air}^2\big(- 2 + Y_{N_2} + Y_{O_2}\big)Y_{N_2} k_c^2 u_c^2 \\
\varphi_{42} =& I^2 C_1\big((C_1 - C_2) - (C_1 + C_2)Y_{N_2}\big) + \lambda_{air} I Y_{N_2}\big(- 4C_1 + (C_1 + 2C_2)Y_{N_2}\big)k_c u_c \\
&+ \lambda_{air} I Y_{N_2}\big(2(C_1 + C_2)Y_{O_2}\big)k_c u_c + 2\lambda_{air}^2\big(- 1 + Y_{N_2} + Y_{O_2}\big)k_c^2 u_c^2 \\
\varphi_{51} =& I^3 C_1^2 Y_{N_2}\big(C_1 - C_2 - (C_1 + C_2)Y_{N_2}\big) + \lambda_{air} I^2 C_1\big(B_1 + B_2 + B_3 + B_4\big)k_c u_c \\
&- 2\lambda_{air}^2 I\big(B_5 + B_6 + B_7\big)k_c^2 u_c^2 - 4\lambda_{air}^3\big(2 + Y_{N_2} + Y_{O_2}\big)\big(1 + Y_{N_2} + Y_{O_2}\big)k_c^3 u_c^3 \\
& B_1 = 2(C_1 - C_2) - 7C_1 Y_{N_2}; \quad B_2 = -2(C_1 - C_2)Y_{O_2} \\
& B_3 = 4(C_1 + C_2)Y_{N_2} Y_{O_2}; \qquad B_4 = (3C_1 + 4C_2)Y_{N_2}^2 \\
& B_5 = 3C_1 + 2(C_1 - C_2)Y_{N_2}; \quad B_6 = -(5C_1 + 2C_2)Y_{O_2} + 2C_2 Y_{N_2}^2 \\
& B_7 = 2(C_1 + C_2)Y_{O_2}^2 + 2(C_1 + 2C_2)Y_{N_2} Y_{O_2} \\
\varphi_{52} =& I^3 C_1^2\big(- C_1 + C_2 + (C_1 + C_2)Y_{N_2}\big) \\
&+ \lambda_{air} I^2 C_1\big(- 2(3C_1 - C_2) + (3C_1 + 4C_2)Y_{N_2} + 2(C_1 + C_2)Y_{O_2}\big)k_c u_c \\
&+ 2\lambda_{air}^2 I\big(2C_2 Y_{N_2} + (C_1 + 2C_2)Y_{O_2} - 3C_1\big)k_c^2 u_c^2 + 4\lambda_{air}^3\big(Y_{N_2} + Y_{O_2} - 1\big)k_c^3 u_c^3
\end{aligned}
$$

A.2 Elements a_{ij} in (2.12)

$$
\begin{aligned}
a_{11} =& \frac{RT}{V_A}\big(- \lambda_{H_2} k_a \bar{u}_a + C_1 \bar{I}\big)\frac{\bar{x}_2}{(\bar{x}_1 + \bar{x}_2)^2} \\
a_{12} =& \frac{RT}{V_A}\big(\lambda_{H_2} k_a \bar{u}_a - C_1 \bar{I}\big)\frac{\bar{x}_1}{(\bar{x}_1 + \bar{x}_2)^2} \\
a_{21} =& \frac{RT}{V_A}\lambda_{H_2}\left(\frac{-\varphi_a P_{vs}}{(\bar{x}_1 + \bar{x}_2 - \varphi_a P_{vs})^2} + \frac{\bar{x}_2}{(\bar{x}_1 + \bar{x}_2)^2}\right)k_a \bar{u}_a - \frac{RT}{V_A}\left(C_1 \bar{I}\frac{\bar{x}_2}{(\bar{x}_1 + \bar{x}_2)^2}\right) \\
a_{22} =& \frac{RT}{V_A}\lambda_{H_2}\left(\frac{-\varphi_a P_{vs}}{(\bar{x}_1 + \bar{x}_2 - \varphi_a P_{vs})^2} - \frac{\bar{x}_1}{(\bar{x}_1 + \bar{x}_2)^2}\right)k_a \bar{u}_a + \frac{RT}{V_A}\left(C_1 \bar{I}\frac{\bar{x}_1}{(\bar{x}_1 + \bar{x}_2)^2}\right)
\end{aligned}
$$

$$
\begin{aligned}
a_{33} =& \frac{RT}{V_C}\big(-\lambda_{air}k_c\bar{u}_c + \frac{C_1}{2}\bar{I}\big)\frac{\bar{x}_4+\bar{x}_5}{(\bar{x}_3+\bar{x}_4+\bar{x}_5)^2}\\
a_{34} =& \frac{RT}{V_C}\big(\lambda_{air}k_c\bar{u}_c - \frac{C_1}{2}\bar{I}\big)\frac{\bar{x}_3}{(\bar{x}_3+\bar{x}_4+\bar{x}_5)^2}\\
a_{43} =& \frac{RT}{V_C}\lambda_{air}k_c\bar{u}_c\frac{\bar{x}_4}{(\bar{x}_3+\bar{x}_4+\bar{x}_5)^2}\\
a_{44} =& \frac{RT}{V_C}\lambda_{air}k_c\bar{u}_c\frac{\bar{x}_3+\bar{x}_5}{(\bar{x}_3+\bar{x}_4+\bar{x}_5)^2}\\
a_{53} =& \frac{RT}{V_C}\lambda_{air}\left(\frac{-\varphi_c P_{vs}}{(\bar{x}_3+\bar{x}_4+\bar{x}_5-\varphi_c P_{vs})^2} + \frac{\bar{x}_5}{(\bar{x}_3+\bar{x}_4+\bar{x}_5)^2}\right)k_c\bar{u}_c\\
&+ \frac{RT}{V_C}(C_1+C_2)\bar{I}\frac{\bar{x}_5}{(\bar{x}_3+\bar{x}_4+\bar{x}_5)^2}\\
a_{55} =& \frac{RT}{V_C}\lambda_{air}\left(\frac{-\varphi_c P_{vs}}{(\bar{x}_3+\bar{x}_4+\bar{x}_5-\varphi_c P_{vs})^2} - \frac{\bar{x}_3+\bar{x}_4}{(\bar{x}_3+\bar{x}_4+\bar{x}_5)^2}\right)k_c\bar{u}_c\\
&- \frac{RT}{V_C}(C_1+C_2)\bar{I}\frac{\bar{x}_3+\bar{x}_4}{(\bar{x}_3+\bar{x}_4+\bar{x}_5)^2}
\end{aligned}
$$

A.3 Elements b_{ij} in (2.13)

$$
\begin{aligned}
b_{11} &= \frac{RT}{V_A}\lambda_{H_2}\left(Y_{H_2} - \frac{\bar{x}_1}{\bar{x}_1+\bar{x}_2}\right)k_a\\
b_{21} &= \frac{RT}{V_A}\lambda_{H_2}\left(\frac{\varphi_a P_{vs}}{\bar{x}_1+\bar{x}_2-\varphi_a P_{vs}} - \frac{\bar{x}_2}{\bar{x}_1+\bar{x}_2}\right)k_a\\
b_{32} &= \frac{RT}{V_C}\lambda_{air}\left(Y_{O_2} - \frac{\bar{x}_3}{\bar{x}_3+\bar{x}_4+\bar{x}_5}\right)k_c\\
b_{42} &= \frac{RT}{V_C}\lambda_{air}\left(Y_{N_2} - \frac{\bar{x}_4}{\bar{x}_3+\bar{x}_4+\bar{x}_5}\right)k_c\\
b_{52} &= \frac{RT}{V_C}\lambda_{air}\left(\frac{\varphi_c P_{vs}}{\bar{x}_3+\bar{x}_4+\bar{x}_5-\varphi_a P_{vs}} - \frac{\bar{x}_5}{\bar{x}_3+\bar{x}_4+\bar{x}_5}\right)k_c
\end{aligned}
$$

Bibliography

[1] M. El-Sharkh, A. Rahman, M. Alam, P. Byrne, A. Sakla, T. Thomas, A dynamic model for a stand-alone PEM fuel cell power plant for residential applications, Journal of Power Sources 138 (1-2) (2004) 199–204.

[2] R. S. Gemmen, Analysis for the effect of inverter ripple current on fuel cell operating condition, Journal of Fluids Engineering 125 (3) (2003) 576–585.

[3] L.-Y. Chiu, B. Diong, R. Gemmen, An improved small-signal model of the dynamic behavior of PEM fuel cells, Industry Applications, IEEE Transactions on 40 (4) (2004) 970–977.

[4] W. Na, B. Gou, Feedback linearization-based nonlinear control for PEM fuel cells, Energy Conversion, IEEE Transactions on 23 (2008) 179–190.

[5] Y. Qi, B. Huang, J. Luo, Dynamic modeling of a finite volume of solid oxide fuel cell: The effect of transport dynamics, Chemical Engineering Science 61 (18) (2006) 6057–6076.

[6] B. Gou, W. Na, B. Diong, Fuel Cells: Modeling, Control, and Applications, CRC Press / Taylor and Francis Group, Boca Raton, Florida, USA, 2010.

[7] J. T. Pukrushpan, A. G. Stefanopoulou, H. Peng, Control of Fuel Cell Power Systems, Springer, USA, 2004.

[8] C.-C. Chu, C.-L. Chen, Robust maximum power point tracking method for photovoltaic cells: A sliding mode control approach, Solar Energy 83 (8) (2009) 1370 – 1378.

[9] R. Talj, D. Hissel, R. Ortega, M. Becherif, Experimental validation of a PEM fuell-cell reduced-order model and a motor-compressor higher order sliding mode control, Industrial Electronics, IEEE Transactions on 57 (2010) 1906–1913.

[10] C. Kunusch, P. Puleston, M. Mayosky, J. Riera, Sliding mode strategy for PEM

fuel cells stacks breathing control using a super-twisting algorithm, Control Systems Technology, IEEE Transactions on 17 (1) (2009) 167–174.

[11] F. Zenith, S. Skogestad, Control of fuel cell power output, Journal of Process Control 17 (4) (2007) 333–347.

[12] A. Hajizadeh, M. Golkar, Intelligent robust control of hybrid distributed generation system under voltage sag, Expert Systems with Applications 37 (2010) 7627–7638.

[13] A. Hajizadeh, M. Golkar, A. Feliachi, Voltage control and active power management of hybrid fuel-cell/energy-storage power conversion system under unbalanced voltage sag conditions, IEEE Transaction on Energy Conversion 25 (2010) 1195–1208.

[14] W. Garcia-Gaban, F. Dorado, C. Bordons, Real-time implementation of a sliding mode controller for air supply on a PEM fuel cell, Journal of Process Control, 20 (2010) 325–336.

[15] G. Wang, Y. Wang, J. Shi, H. Shao, Coordinating IMC-PID and adaptive SMC controllers for PEM, ISA Transactions 49 (2010) 87–94.

[16] J.-K. Kuo, C.-F. Wang, An integrated simulation model for PEM fuel cell power systems with a buck DC-DC converter, International Journal of Hydrogen Energy 36 (18) (2011) 11846–11855.

[17] X. Li, Z.-H. Deng, D. Wei, C.-S. Xu, G.-Y. Cao, Novel variable structure control for the temperature of PEM fuel cell stack based on the dynamic thermal affine model, Energy Conversion and Management 52 (11) (2011) 3265–3274.

[18] W. Garcia-Gabin, D. Zambrano, E. F. Camacho, Sliding mode predictive control of a solar air conditioning plant, Control Engineering Practice 17 (6) (2009) 652 – 663.

[19] M. Ellouze, R. Gamoudi, , A. Mami, Sliding mode control applied to a photovoltaic water-pumping system, International Journal of Physical Sciences 5 (4) (2010) 334 – 344.

[20] M. de la Parte, C. Cirre, E. Camacho, M. Berenguel, Application of predictive sliding mode controllers to a solar plant, Control Systems Technology, IEEE

Transactions on 16 (4) (2008) 819 –825.

[21] F. Valenciaga, P. Puleston, P. Battaiotto, Power control of a solar/wind generation system without wind measurement: a passivity/sliding mode approach, Energy Conversion, IEEE Transactions on 18 (4) (2003) 501 – 507.

[22] F. Valenciaga, P. Puleston, P. Battaiotto, Power control of a photovoltaic array in a hybrid electric generation system using sliding mode techniques, IEE Proceedings - Control Theory and Applications 148 (6) (2001) 448 –455.

[23] R.-J. Wai, W.-H. Wang, C.-Y. Lin, High-performance stand-alone photovoltaic generation system, Industrial Electronics, IEEE Transactions on 55 (1) (2008) 240 –250.

[24] I.-S. Kim, Robust maximum power point tracker using sliding mode controller for the three-phase grid-connected photovoltaic system, Solar Energy 81 (3) (2007) 405 – 414.

[25] J. Knight, S. Shirsavar, W. Holderbaum, An improved reliability cuk based solar inverter with sliding mode control, Power Electronics, IEEE Transactions on 21 (4) (2006) 1107 – 1115.

[26] H. De Battista, P. Puleston, R. Mantz, C. Christiansen, Sliding mode control of wind energy systems with doig-power efficiency and torsional dynamics optimization, Power Systems, IEEE Transactions on 15 (2) (2000) 728 –734.

[27] C. Evangelista, P. Puleston, F. Valenciaga, A simple robust controller for power maximization of a variable-speed wind turbine, International Journal of Energy Research 34 (10) (2010) 924–932.

[28] P. Camocardi, P. Battaiotto, R. Mantz, Autonomous bdfig-wind generator with torque and pitch control for maximum efficiency in a water pumping system, International Journal of Hydrogen Energy 35 (11) (2010) 5778 – 5785.

[29] C. Evangelista, P. Puleston, F. Valenciaga, Wind turbine efficiency optimization. comparative study of controllers based on second order sliding modes, International Journal of Hydrogen Energy 35 (11) (2010) 5934 – 5939.

[30] N.-C. Tsai, C.-W. Chiang, Spindle position regulation for wind power generators, Mechanical Systems and Signal Processing 24 (3) (2010) 873 – 889.

[31] J.Hu, H. Nian, B. Hu, Y. He, Z. Zhu, Direct active and reactive power regulation of dfig using sliding-mode control approach, Energy Conversion, IEEE Transactions on 25 (4) (2010) 1028 –1039.

[32] W.-M. Lin, C.-M. Hong, F.-S. Cheng, On-line designed hybrid controller with adaptive observer for variable-speed wind generation system, Energy 35 (7) (2010) 3022 – 3030.

[33] S. Benelghali, M. El Hachemi Benbouzid, J. Charpentier, T. Ahmed-Ali, I. Munteanu, Experimental validation of a marine current turbine simulator: Application to a permanent magnet synchronous generator-based system second-order sliding mode control, Industrial Electronics, IEEE Transactions on 58 (1) (2011) 118 –126.

[34] S. Benelghali, M. El Hachemi Benbouzid, T. Ahmed-Ali, J. Charpentier, High-order sliding mode control of a marine current turbine driven doubly-fed induction generator, IEEE Journal of Oceanic Engineering 35 (2) (2010) 402 –411.

[35] K. Vrdoljak, N. Peric, M. Mehmedovic, Sliding mode based load-frequency control in power systems, Electric Power Systems Research 80 (5) (2010) 514 –527.

[36] J. Cabrera-Vazquez, A. G. Loukianov, J. M. Canedo, V. I. Utkin, Robust controller for synchronous generator with local load via vsc, International Journal of Electrical Power & Energy Systems 29 (4) (2007) 348 – 359.

[37] F. Valenciaga, Second order sliding power control for a variable speed-constant frequency energy conversion system, Energy Conversion and Management 51 (12) (2010) 3000 – 3008.

[38] J. Hu, L. Shang, Y. He, Z. Zhu, Direct active and reactive power regulation of grid-connected dc/ac converters using sliding mode control approach, Power Electronics, IEEE Transactions on 26 (1) (2011) 210 –222.

[39] B. Allaoua, A. Laoufi, Application of a robust fuzzy sliding mode controller synthesis on a buck-boost dc-dc converter power supply for an electric vehicle propulsion system, Journal of Electrical Engineering and Technology 6 (2011) 67 – 75.

[40] G. Sziebig, B. Takarics, P. Korondi, Control of an embedded system via internet, Industrial Electronics, IEEE Transactions on 57 (10) (2010) 3324 –3333.

[41] J. Gamazo-Real, E. Vazquez-Sanchez, J. Gomez-Gill, Position and speed control of brushless dc motors using sensorless techniques and application trends, Sensors 10 (2010) 6901–6947.

[42] M. Hajian, G. Markadeh, J. Soltani, S. Hoseinnia, Energy optimized sliding-mode control of sensorless induction motor drives, Energy Conversion and Management 50 (9) (2009) 2296 – 2306.

[43] G. Chu, C. Tse, S. C. Wong, S.-C. Tan, A unified approach for the derivation of robust control for boost pfc converters, Power Electronics, IEEE Transactions on 24 (11) (2009) 2531 –2544.

[44] J. Matas, L. de Vicuna, J. Miret, J. Guerrero, M. Castilla, Feedback linearization of a single-phase active power filter via sliding mode control, Power Electronics, IEEE Transactions on 23 (1) (2008) 116 –125.

[45] J. Matas, M. Castilla, J. Guerrero, L. Garcia de Vicuna, J. Miret, Feedback linearization of direct-drive synchronous wind-turbines via a sliding mode approach, Power Electronics, IEEE Transactions on 23 (3) (2008) 1093 –1103.

[46] R.-J. Wai, C.-Y. Lin, Active low-frequency ripple control for clean-energy power-conditioning mechanism, Industrial Electronics, IEEE Transactions on 57 (11) (2010) 3780–3792.

[47] G. Park, Z. Gajic, W.-C. Su, Applications of sliding mode control to energy and power systems, in: The International Conference on Sustainable Systems and the Environment, 2011.

[48] A. Sinha, Linear Systems, CRC Press, Inc., Boca Raton, FL, 2007.

[49] V. Utkin, Variable structure systems with sliding modes, Automatic Control, IEEE Transactions on 22 (2) (1977) 212–222.

[50] K. Young, Controller design for a manipulator using theory of variable structure systems, Systems, Man and Cybernetics, IEEE Transactions on 8 (2) (1978) 101–109.

[51] V. I. Utkin, K. D. Young, Methods for constructing discontinuity planes in multidimensional variable structure systems, Automation and Remote Control 39 (10) (1978) 1466–1470.

[52] C.-T. Chen, Linear System Theory and Design, Oxford University Press, Inc., New York, NY, USA, 1999.

[53] W.-C. Su, T. Nguyen, Introduction to Sliding Mode Control, Lecture Notes, Department of Electrical and Computer Engineering, Rutgers University, Piscataway, New Jersey, 2009.

[54] B. Drazenovic, The invariance conditions in variable structure systems, Automatica 5 (3) (1969) 287–295.

[55] Z. Gajic, I. Borno, Lyapunov iterations for optimal control of jump linear systems at steady state, Automatic Control, IEEE Transactions on 40 (11) (1995) 1971–1975.

[56] J. Larminie, A. Dicks, Fuel Cell Systems Explained, John Wiley & Sons, Chichester, 2000.

[57] J. Padulles, G. Ault, J. McDonald, An integrated sofc plant dynamic model for power systems simulation, Journal of Power Resources 86 (2000) 495–500.

[58] Z. Gajic, Linear Dynamic Systems and Signals, Prentice Hall, 2003.

[59] H. Khalil, Nonlinear Systems, Prentice Hall, Upper Saddle River, NJ, 2002.

[60] W.-C. Su, S. V. Drakunov, Ü. Özgüner, Constructing discontinuity surfaces for variable structure systems: a Lyapunov approach, Automatica 32 (6) (1996) 925–928.

[61] S. Laghrouche, F. Plestan, A. Glumineau, Higher order sliding mode control based on integral sliding mode, Automatica 43 (3) (2007) 531–537.

[62] J. E. Slotine, W. Li, Applied Nonlinear Control, Prentice Hall, Englewood Cliffs, New Jersey, 1991.

[63] V. I. Utkin, J. Guldner, J. Shi, Sliding Mode Control in Electromechanical Systems, Taylor & Francis, London, 1999.

[64] Z. Gajic, M. Lelic, Modern Control Systems Engineering, Prentice Hall, 1996.

[65] W.-C. Su, Sliding surface design for singularly perturbed systems, International Journal of Control 72 (11) (1999) 990–995.

[66] G. Park, Z. Gajic, Sliding mode control of a linearized polymer electrolyte membrane fuel cell model, Journal of Power Sources 212 (2012) 226–232.

[67] G. Park, Z. Gajic, A simple sliding mode controller of a fifth-order nonlinear PEM fuel cell model, Energy Conversion, IEEE Transactions on in press (2014).

[68] J. Larminie, A. Dicks, Fuel Cell Systems Explained, John Wiley & Sons Inc., Chichester, West Sussex, 2003.

[69] X.-J. Wu, X.-J. Zhu, G.-Y. Cao, H.-Y. Tu, Predictive control of sofc based on a ga-rbf neural network model, Journal of Power Sources 179 (1) (2008) 232–239.

[70] X.-J. Wu, X.-J. Zhu, G.-Y. Cao, H.-Y. Tu, Dynamic modeling of sofc based on a T-S fuzzy model, Simulation Modelling Practice and Theory 16 (5) (2008) 494–504.

[71] Y.-W. Kang, J. Li, G.-Y. Cao, H.-Y. Tu, J. Li, J. Yang, A reduced 1d dynamic model of a planar direct internal reforming solid oxide fuel cell for system research, Journal of Power Sources 188 (1) (2009) 170–176.

[72] H. Xi, J. Sun, Dynamic analysis of planar solid oxide fuel cell models with different assumptions of temperature layers, Journal of Fuel Cell Science and Technology 6 (1) (2009) 011011.

[73] S. A. Hajimolana, M. Soroush, Dynamics and control of a tubular solid-oxide fuel cell, Computers & Chemical Engineering 48 (13) (2009) 6112–6125.

[74] D. Hall, R. Colclaser, Transient modeling and simulation of a tubular solid oxide fuel cell, Energy Conversion, IEEE Transactions on 14 (3) (1999) 749–753.

[75] Y. Zhu, K. Tomsovic, Development of models for analyzing the load-following performance of microturbines and fuel cells, Electric Power Systems Research 62 (1) (2002) 1–11.

[76] K. Sedghisigarchi, A. Feliachi, Dynamic and transient analysis of power distribution systems with fuel cells-part i: fuel-cell dynamic model, Energy Conversion, IEEE Transactions on 19 (2) (2004) 423–428.

[77] Y. Li, S. Choi, S. Rajakaruna, An analysis of the control and operation of a solid oxide fuel-cell power plant in an isolated system, Energy Conversion, IEEE Transactions on 20 (2) (2005) 381–387.

[78] F. Jurado, M. Valverde, Genetic fuzzy control applied to the inverter of solid oxide fuel cell for power quality improvement, Electric Power Systems Research

76 (1-3) (2005) 93–105.

[79] F. Jurado, A method for the identification of solid oxide fuel cells using a hammerstein model, Journal of Power Sources 154 (1) (2006) 145–152.

[80] F. Jurado, Predictive control of solid oxide fuel cells using fuzzy hammerstein models, Journal of Power Sources 158 (1) (2006) 245–253.

[81] K. Sedghisigarchi, A. Feliachi, Impact of fuel cells on load-frequency control in power distribution systems, Energy Conversion, IEEE Transactions on 21 (1) (2006) 250–256.

[82] Y. Li, S. Rajakaruna, S. Choi, Control of a solid oxide fuel cell power plant in a grid-connected system, Energy Conversion, IEEE Transactions on 22 (2) (2007) 405–413.

[83] H.-B. Huo, Z.-D. Zhong, X.-J. Zhu, H.-Y. Tu, Nonlinear dynamic modeling for a sofc stack by using a hammerstein model, Journal of Power Sources 175 (1) (2008) 441–446.

[84] H.-B. Huo, X.-J. Zhu, W.-Q. Hu, H.-Y. Tu, J. Li, J. Yang, Nonlinear model predictive control of sofc based on a hammerstein model, Journal of Power Sources 185 (1) (2008) 338–344.

[85] T. Zhang, G. Feng, Rapid load following of an sofc power system via stable fuzzy predictive tracking controller, Fuzzy Systems, IEEE Transactions on 17 (2) (2009) 357–371.

[86] U. K. Chakraborty, Static and dynamic modeling of solid oxide fuel cell using genetic programming, Energy 34 (6) (2009) 740–751.

[87] U. K. Chakraborty, An error in solid oxide fuel cell stack modeling, Energy 36 (2) (2011) 801–802.

[88] K. Sedghisigarchi, A. Feliachi, Dynamic modeling of fuel cells, in: A. Keyhani, M. Marwali (Eds.), Smart Power Grids 2011, Springer-Verlag, 2011, pp. 625–653.

[89] W. Jiang, R. Fang, R. A. Dougal, J. A. Khan, hermoelectric model of a tubular sofc for dynamic simulation, Journal of Energy Resources Technoloty 130 (2008) 022601–1 – 022601–10.

[90] R. Gemmen, Dynamic modeling of fuel cells, in: R. Bove, S. Ubertini (Eds.),

Modeling Solid Oxide Fuel Cells: Methods, Procedures and Techniques, Springer Science Business, 2008, pp. 269–322.

[91] B.-G. San, P.-L. Zhou, D. Clealand, Dynamic modeling of tubular SOFC for marine power system, Journal of Marine Science and Application 9 (2010) 231–240.

[92] M. Rokni, J. Yuan, The development of heat transfer and gas flow modeling in the solid oxide fuel cells (sofc), in: Electrochemical Society, SOFC-VI, 1999, pp. 1099–1108.

[93] R. O'Hayre, S.-W. Cha, W. Colella, F. B. Prinz, Fuel Cell Fundamentals, 2nd Edition, John Wiley & Sons, Hoboken, NJ, 2009.

[94] Y. Qi, B. Huang, K. T. Chuang, Dynamic modeling of solid oxide fuel cell: The effect of diffusion and inherent impedance, Journal of Power Sources 150 (0) (2005) 32–47.

[95] R. P. Iczkowski, M. B. Cutlip, Voltage losses in fuel cell cathodes, Journal of The Electrochemical Society 127 (7) (1980) 1433–1440.

[96] X. W. Zhang, S. H. Chan, H. K. Ho, J. Li, G. Li, Z. Feng, Nonlinear model predictive control based on the moving horizon state estimation for the solid oxide fuel cell, International Journal of Hydrogen Energy 33 (9) (2008) 2355–2366.

[97] X. Wang, B. Huang, T. Chen, Data-driven predictive control for solid oxide fuel cells, Journal of Process Control 17 (2) (2007) 103–114.

[98] L. Wang, H. Zhang, S. Weng, Modeling and simulation of solid oxide fuel cell based on the volume-resistance characteristic modeling technique, Journal of Power Sources 177 (2) (2008) 579–589.

[99] P. Vijay, A. Samantaray, A. Mukherjee, A bond graph model-based evaluation of a control scheme to improve the dynamic performance of a solid oxide fuel cell, Mechatronics 19 (4) (2009) 489–502.

[100] J. Yang, X. Li, H.-G. Mou, L. Jian, Predictive control of solid oxide fuel cell based on an improved Takagi-Sugeno fuzzy model, Journal of Power Sources 193 (2) (2009) 699–705.

[101] P. Aguiar, C. Adjiman, N. Brandon, Anode-supported intermediate-temperature

direct internal reforming solid oxide fuel cell: Ii. model-based dynamic performance and control, Journal of Power Sources 147 (1-2) (2005) 136–147.

[102] P. Aguiar, C. Adjiman, N. Brandon, Anode-supported intermediate temperature direct internal reforming solid oxide fuel cell. i: model-based steady-state performance, Journal of Power Sources 138 (1-2) (2004) 120–136.

[103] Y. Inui, N. Ito, T. Nakajima, A. Urata, Analytical investigation on cell temperature control method of planar solid oxide fuel cell, Energy Conversion and Management 47 (15-16) (2006) 2319–2328.

[104] T. Kaneko, J. Brouwer, G. Samuelsen, Power and temperature control of fluctuating biomass gas fueled solid oxide fuel cell and micro gas turbine hybrid system, Journal of Power Sources 160 (1) (2006) 316–325.

[105] R. Kandepu, L. Imsland, B. A. Foss, C. Stiller, B. Thorud, O. Bolland, Modeling and control of a sofc-gt-based autonomous power system, Energy 32 (4) (2007) 406–417.

[106] F. Mueller, F. Jabbari, R. Gaynor, J. Brouwer, Novel solid oxide fuel cell system controller for rapid load following, Journal of Power Sources 172 (1) (2007) 308–323.

[107] F. Mueller, F. Jabbari, J. Brouwer, R. Roberts, T. Junker, H. Ghezel-Ayagh, Control design for a bottoming solid oxide fuel cell gas turbine hybrid system, Journal of Fuel Cell Science and Technology 4 (3) (2007) 221–230.

[108] C. Stiller, B. Thorud, O. Bolland, R. Kandepu, L. Imsland, Control strategy for a solid oxide fuel cell and gas turbine hybrid system, Journal of Power Sources 158 (1) (2006) 303–315.

[109] M. Sorrentino, C. Pianese, Y. G. Guezennec, A hierarchical modeling approach to the simulation and control of planar solid oxide fuel cells, Journal of Power Sources 180 (1) (2008) 380–392.

[110] L. Magistri, A. Traverso, F. C. adn M. Bozzolo, P. Costamagna, A. F. Massardo, Modelling of pressurised hybrid systems based on integrated planar solid oxide fuel cell(ip-sofc) technology, Full Cells 5 (1) (2005) 80–96.

[111] C. Wächter, R. Lunderstädt, F. Joos, The modeling of a standalone solid-oxide

fuel cell auxiliary power unit, Journal of Power Sources 161 (2) (2006) 938–948.

[112] N. Lu, Q. Li, X. Sun, M. Khaleel, The modeling of a standalone solid-oxide fuel cell auxiliary power unit, Journal of Power Sources 161 (2) (2006) 938–948.

[113] A. M. Murshed, B. Huang, K. Nandakumar, Estimation and control of solid oxide fuel cell system, Computers & Chemical Engineering 34 (1) (2010) 96–111.

[114] M. Mariton, Jump Linear Systems in Automatic Control, Marcer Dekker, Inc., New York, NY, 1990.

[115] L. Zhang, E.-K. Boukas, Stability and stabilization of Markovian jump linear systems with partly unknown transition probabilities, Automatica 45 (2) (2009) 463 – 468.

[116] D. Sworder, R. Rogers, An LQ-solution to a control problem associated with a solar thermal central receiver, Automatic Control, IEEE Transactions on 28 (10) (1983) 971–978.

[117] M. Branicky, V. Borkar, S. Mitter, A unified framework for hybrid control: model and optimal control theory, Automatic Control, IEEE Transactions on 43 (1) (1998) 31 –45.

[118] O. Costa, R. Okimura, Discrete-time mean variance optimal control of linear systems with Markovian jumps and multiplicative noise, International Journal of Control 82 (2) (2009) 256–267.

[119] O. Lopez-Lapena, M. Penella, M. Gasulla, A closed-loop maximum power point tracker for subwatt photovoltaic panels, Industrial Electronics, IEEE Transactions on 59 (3) (2012) 1588–1596.

[120] O. Lopez-Lapena, M. Penella, M. Gasulla, A new MPPT method for low-power solar energy harvesting, Industrial Electronics, IEEE Transactions on 57 (9) (2010) 3129 –3138.

[121] A. Safari, S. Mekhilef, Simulation and hardware implementation of incremental conductance MPPT with direct control method using Cuk converter, Industrial Electronics, IEEE Transactions on 58 (4) (2011) 1154–1161.

[122] Y.-C. Chang, C.-L. Kuo, K.-H. Sun, T.-C. Li, Development and operational control of two-string maximum power point trackers in DC distribution systems,

Power Electronics, IEEE Transactions on 28 (4) (2013) 1852–1861.

[123] B. Subudhi, R. Pradhan, A comparative study on maximum power point tracking techniques for photovoltaic power systems, Sustainable Energy, IEEE Transactions on 4 (1) (2013) 89–98.

[124] E. Bianconi, J. Calvente, R. Giral, E. Mamarelis, G. Petrone, C. Ramos-Paja, G. Spagnuolo, M. Vitelli, A fast current-based MPPT technique employing sliding mode control, Industrial Electronics, IEEE Transactions on 60 (3) (2013) 1168–1178.

[125] B. Alajmi, K. Ahmed, S. Finney, B. Williams, A maximum power point tracking technique for partially shaded photovoltaic systems in microgrids, Industrial Electronics, IEEE Transactions on 60 (4) (2013) 1596–1606.

[126] M. de Brito, L. Galotto, L. Sampaio, G. de Azevedo e Melo, C. Canesin, Evaluation of the main MPPT techniques for photovoltaic applications, Industrial Electronics, IEEE Transactions on 60 (3) (2013) 1156–1167.

[127] R. Cardim, M. C. M. Teixeira, E. Assuncao, M. Covacic, Variable-structure control design of switched systems with an application to a DC/DC power converter, Industrial Electronics, IEEE Transactions on 56 (9) (2009) 3505–3513.

[128] G. Deaecto, J. Geromel, F. Garcia, J. Pomilio, Switched affine systems control design with application to DC/DC converters, Control Theory Applications, IET 4 (7) (2010) 1201–1210.

[129] P. Karamanakos, T. Geyer, S. Manias, Direct voltage control of DC-DC boost converters using enumeration-based model predictive control, Power Electronics, IEEE Transactions on.

[130] T. Hashemi, A. Farnam, R. M. Esfanjani, H. M. Kojabadi, A new approach to design switching strategy for the buck converters, in: 4th Power Electronics, Drive Systems and Technologies Conference (PEDSTC), 2013, pp. 301–305.

[131] F. H. F. Leung, P.-S. Tam, C. K. Li, The control of switching DC-DC converters-a general LQR problem, Industrial Electronics, IEEE Transactions on 38 (1) (1991) 65–71.

[132] F. Garofalo, P. Marino, S. Scala, F. Vasca, Control of DC-DC converters with linear optimal feedback and nonlinear feedforward, Power Electronics, IEEE Transactions on 9 (6) (1994) 607–615.

[133] A. Zaeri, M. Bayati Poodeh, S. Eshtehardiha, Improvement of Cuk converter performance with optimum LQR controller based on genetic algorithm, in: Intelligent and Advanced Systems, 2007. ICIAS 2007. International Conference on, 2007, pp. 917–922.

[134] S. Cuk, R. D. Middlebrook, Advances in switched-mode power conversion Part I, Industrial Electronics, IEEE Transactions on IE-30 (1) (1983) 10–19.

[135] S. Cuk, R. D. Middlebrook, Advances in switched-mode power conversion Part II, Industrial Electronics, IEEE Transactions on IE-30 (1) (1983) 19–29.

[136] Z. Chen, PI and sliding mode control of a Cuk converter, Power Electronics, IEEE Transactions on 27 (8) (2012) 3695–3703.

[137] E. Selwan, Control Strategies for Power Converters Used on Solar Cells, Master Thesis, Rutgers University, 2012.

[138] M. Skataric, Z. Gajic, Slow and fast dynamics of a natural gas gydrogen reformer, International Journal of Hydrogen Energy in press.

[139] G. Park, Z. Gajic, Sliding mode control of continuous-time weakly coupled linear systems with external disturbances, Automatica 49 (2) (2013) 676–680.

[140] F. Barbir, PEM Fuel Cells: Theory and Practice, Elsevier Academic Press, New York, 2005.

[141] Q. Li, W. Chen, Y. Wang, J. Jia, M. Han, Nonlinear robust control of proton exchange membrane fuel cell by state feedback exact linearization, Journal of Power Sources 194 (2009) 338–348.

[142] C. Kunusch, A. Husar, P. Puleston, M. Mayosky, J. More, Linear identification and model adjustment of a PEM fuel cell stack, International Journal of Hydrogen Energy 33 (2008) 3581–3587.

[143] M. Meiler, O. Schid, M. Schudy, E. Hofer, Dynamic fuel cell stack model for real-time simulation based on system identification, Journal of Power Sources 176 (2008) 523–528.

[144] C. Milosavljevic, General conditions for the existence of quasi-sliding mode on the switching hyperplane in discrete variable structure systems, Automatiion and Remote Control 46 (1985) 307–314.

[145] G. Golo, C. Milosavljevic, Robust discretetime chattering free sliding mode control, Systems & Control Letters 41 (2000) 19–28.

[146] K. Furuta, Sliding mode control of a discrete system, Systems & Control Letters 14 (1990) 142–145.

[147] C. Chan, Servo-systems with discrete-variable structure control, Systems & Control Letters 17 (1991) 321–325.

[148] R. Pots, X. Yu, Discrete variable structure system with pseudo-sliding mode, International Journal of Australian Mathematical Society 14 (1990) 142–145.

[149] X. Yu, P. R, Computer controlled variable structure systems, International Journal of Australian Mathematical Society 34 (1992) 1–17.

[150] W. Gao, D. Wang, A. Homaifa, Discrete-time variable structure control systems, IEEE Transaction on Industrial Electronics 42 (1995) 117–122.

[151] G. Bartolini, A. Ferrara, V. Utkin, Adaptive sliding-mode control in discrete-time systems, Automatica 31 (1995) 769–773.

[152] A. Bartoszewitz, Discrete-time quasi-sliding mode control strategies, Industrial Electronics, IEEE Transactions on 45 (1998) 633–637.

[153] K. Furuta, Y. Pan, Variable structure control with sliding sector, Automatica 36 (2000) 211–228.

[154] Č. Milosavljević, B. Peruničić-Draženović, B. Veselić, D. Mitić, A new design of servo mechanisms with digital sliding mode, Electrical Engineering 89 (3) (2005) 233–244.

[155] T. Nguyen, W.-C. Su, Z. Gajic, Sliding mode control for singularly perturbed linear continuous time systems: Composite control approaches, Dynamics of Continuous, Discrete and Impulsive Systems: Series B 17 (2010) 1001–1018.

[156] D. M. Boskovic, M. Krstic, W. Liu, Boundary control of an unstable heat equation via measurement of domain-averaged temperature, Automatic Control, IEEE Transactions on 46 (12) (2001) 2022–2028.

[157] C. Edwards, S. K. Spurgeon, Sliding mode control: theory and applications, CRC Press, 1998.

[158] M.-B. Cheng, V. Radisavljevic, W.-C. Su, Sliding mode boundary control of a parabolic {PDE} system with parameter variations and boundary uncertainties, Automatica 47 (2) (2011) 381 – 387.

[159] D. Georgis, S. Jogwar, A. Almansoori, P. Daoutidis, Control of an energy integrated solid oxide fuel cell system, in: American Control Conference (ACC), 2011, pp. 1518–1523.

[160] I. Matraji, S. Laghrouche, M. Wack, Pressure control in a PEM fuel cell via second order sliding mode, International Journal of Hydrogen Energy 37 (21) (2012) 16104–16116.

[161] J. VanderSteen, B. Kenney, J. Pharoah, K. Karan, Mathematical modelling of the transport phenomena and the chemical/electrochemical reactions in solid oxide fuel cells: a review, in: In Canadian Hydrogen and Fuel Cells Conference, 2004.

[162] A. M. Murshed, B. Huang, K. Nandakumar, Control relevant modeling of planer solid oxide fuel cell system, Journal of Power Sources 163 (2) (2007) 830–845.

[163] A. Chaisantikulwat, C. Diaz-Goano, E. Meadows, Dynamic modelling and control of planar anode-supported solid oxide fuel cell, Computers & Chemical Engineering 32 (10) (2008) 2365–2381.

[164] B. Huang, Y. Qi, A. M. Murshed, Dynamic Modeling and Predictive Control in Solid Oxide Fuel Cells: First Principle and Data-based Approaches, John Wiley & Sons Ltd., Chichester, UK, 2012.

[165] R. W. Erickson, D. Maksimovic, Fundamentals of Power Electronics, Kluwer Academic/Plenum Publishers, New York, NY, 2001.

[166] X. Feng, K. Loparo, Y. Ji, H. Chizeck, Stochastic stability properties of jump linear systems, Automatic Control, IEEE Transactions on 37 (1) (1992) 38 –53.

[167] O. Costa, M. Fragoso, R. Marques, Discrete-time Markovian Jump Linear Systems, Springer-Verlag, London, 2004.

[168] D. de Farias, J. Geromel, J. do Val, O. Costa, Output feedback control of Markov jump linear systems in continuous-time, Automatic Control, IEEE Transactions

on 45 (5) (2000) 944 –949.

[169] Z. Sun, S. Ge, Analysis and synthesis of switched linear control systems, Automatica 41 (2) (2005) 181 – 195.

[170] E.-K. Boukas, Z.-K. Liu, Robust H-infinity control of discrete-time Markovian jump linear systems with mode-dependent time-delays, Automatic Control, IEEE Transactions on 46 (12) (2001) 1918 –1924.

[171] L. Zhang, E.-K. Boukas, J. Lam, Analysis and synthesis of Markov jump linear systems with time-varying delays and partially known transition probabilities, Automatic Control, IEEE Transactions on 53 (10) (2008) 2458 –2464.

[172] Y. Ji, H. Chizeck, Controllability, stabilizability, and continuous-time Markovian jump linear quadratic control, Automatic Control, IEEE Transactions on 35 (7) (1990) 777 –788.

[173] H. J. Chizeck, A. S. Willsky, D. Castanon, Discrete-time Markovian-jump linear quadratic optimal control, International Journal of Control 43 (1) (1986) 213–231.

[174] J. He, Y. W. Li, Hybrid voltage and current control approach for DG-grid interfacing converters with LCL filters, Industrial Electronics, IEEE Transactions on 60 (5) (2013) 1797–1809.

[175] M. Qin, J. Xu, Improved pulse regulation control technique for switching DC/DC converters operating in DCM, Industrial Electronics, IEEE Transactions on 60 (5) (2013) 1819–1830.

[176] X. Wang, F. Zhuo, J. Li, L. Wang, S. Ni, Modeling and control of dual-stage high-power multifunctional PV system in d-q-o coordinate, Industrial Electronics, IEEE Transactions on 60 (4) (2013) 1556–1570.

[177] M. Sechilariu, B. Wang, F. Locment, Building integrated photovoltaic system with energy storage and smart grid communication, Industrial Electronics, IEEE Transactions on 60 (4) (2013) 1607–1618.

[178] A. Vidal, F. Freijedo, A. Yepes, P. Fernandez-Comesana, J. Malvar, O. Lopez, J. Doval-Gandoy, Assessment and optimization of the transient response of proportional-resonant current controllers for distributed power generation systems, Industrial Electronics, IEEE Transactions on 60 (4) (2013) 1367–1383.

[179] S.-J. Cheng, Y.-K. Lo, H.-J. Chiu, S.-W. Kuo, High-efficiency digital-controlled interleaved power converter for high-power PEM fuel-cell applications, Industrial Electronics, IEEE Transactions on 60 (2) (2013) 773–780.

[180] Y.-F. Liu, P. Sen, S.-P. Huang, Function control-a novel strategy to achieve improved performance of the DC-to-DC switching regulators, Industrial Electronics, IEEE Transactions on 42 (2) (1995) 186–191.

[181] M. Umamaheswari, G. Uma, K. Vijayalakshmi, Design and implementation of reduced-order sliding mode controller for higher-order power factor correction converters, Power Electronics, IET 4 (9) (2011) 984–992.

[182] F. Amato, C. Cosentino, A. Fiorillo, A. Merola, Stabilization of bilinear systems via linear state-feedback control, Circuits and Systems II: Express Briefs, IEEE Transactions on 56 (1) (2009) 76–80.

[183] C.-T. Pan, C.-M. Lai, A high-efficiency high step-up converter with low switch voltage stress for fuel-cell system applications, Industrial Electronics, IEEE Transactions on 57 (6) (2010) 1998–2006.